UNIVERSITÄT PADERBORN
Die Universität der Informationsgesellschaft

Stimuli-Responsive Backbone-Degradable (Co-)Polymers for Drug Delivery

by Tarik Rust, M. Sc.

born on November 27th, 1992 in Bielefeld

Dissertation

submitted to the Department of Chemistry at Paderborn University for the degree of

Doctor rerum naturalium

(Dr. rer. nat.)

Reviewer: Prof. Dr. Dirk Kuckling
Prof. Dr. Klaus Langer

Submitted: 4/16/2021
Thesis disputation: 6/4/2021

To all the people believing in me and supporting me.

Especially to my family and friends.

Abstract

In modern therapy, applying highly potent drugs while cutting side effects for patients is one of the core challenges. One possible strategy is delivering a drug to a specific target site by encapsulation into a polymeric matrix. Especially light-responsive polymers are regarded as promising materials due to, e.g., the capability of tailored on-demand release in illuminated areas. In this work, several light-responsive diol monomers were prepared to synthesize a series of different novel light-responsive backbone-degradable (co-)polymers by polycondensation and polyaddition. Upon exposure with UV light, the obtained light-responsive polymers showed successful degradation in solution as observed by SEC and UV/Vis spectroscopy. Additionally, light induced decomposition of films and aqueous suspensions was confirmed by SEC, UV/Vis, SPR, and profilometry measurements. Depending on the incorporated comonomers, the functional co-polyurethanes exhibited either enhanced hydrophilicity or dual-responsiveness to light as well as redox or acidic environments, which was detected by SEC after treatment with a reducing agent or acid, respectively. Ultimately, particulate carriers were formulated from the polymers by typical methods like nanoprecipitation or single emulsion solvent evaporation. Triggered decomposition as well as cargo release of the carriers was confirmed by DLS, fluorescence spectroscopy and microscopy.

Kurzzusammenfassung

Eine der zentralen Herausforderungen in modernen therapeutischen Anwendungen ist das Verabreichen hochwirksamer Medikamente bei simultaner Verringerung der Nebenwirkungen. Eine mögliche Strategie hierfür ist der Transport eines Wirkstoffes zu einem spezifischen Ziel durch Einkapseln in eine polymere Matrix. Besonders lichtresponsive Polymere werden als vielversprechende Materialien angesehen, unter anderem aufgrund der Möglichkeit einer maßgeschneiderten schaltbaren Freisetzung. Im Rahmen dieser Arbeit wurden verschiedene lichtresponsive Monomere hergestellt, um eine Serie unterschiedlicher lichtresponsiver rückgratspaltbarer (Co-)Polymere durch Polykondensation oder Polyaddition zu synthetisieren. Untersuchungen via GPC und UV/Vis-Spektroskopie zeigten die erfolgreiche Zersetzung der erhaltenen Polymere in Lösung unter Bestrahlung mit UV-Licht. Zusätzlich wurde die lichtinduzierte Zersetzung von Filmen und wässrigen Suspensionen durch GPC-, UV/Vis-, SPR- und Profilometriemessungen bestätigt. Die funktionellen Copolyurethane zeigten abhängig von den eingebauten Comonomeren, entweder erhöhte Hydrophilie oder Doppelresponsivität auf Licht sowie auf Redox oder saure Umgebungen, was nach Behandlung mit einem Reduktionsmittel beziehungsweise einer Säure via GPC ermittelt wurde. Abschließend wurden typische Methoden wie Nanofällung oder Einzelemulsionslösungsmittelverdampfung verwendet, um partikuläre Trägersysteme aus den Polymeren herzustellen. Die gezielte Zersetzung der Trägersysteme sowie die Freisetzung eingekapselter Fracht wurden mittels DLS, Fluoreszenzspektroskopie und Mikroskopie bestätigt.

Contents

1. Motivation

Polymers exhibiting a change in polarity, solubility or structure as a response to internal or external stimuli, like pH,[1],[2] temperature,[3] redox conditions,[4],[5] or light[6],[7],[8] have been of great interest in recent years. One reason for this interest is the broad field of possible applications for such polymers, which include catalyst immobilization,[9] sensors[10],[11] and patterning[12],[13] as well as tissue engineering,[14],[15] drug delivery,[16],[17],[18] and tissue adhesives.[19] Recently, light as a stimulus gained tremendous attention since this trigger can be applied both remotely and accurately by adjusting the parameters of irradiation, such as wavelength, irradiation time or intensity.[20],[21] Thus light-responsive polymers show high potential as efficient and targeted controlled release systems, which reduce side effects compared to conventional therapy.[22],[23] Photocleavable moieties employed most commonly in such systems are coumarin[24],[25] and *ortho*-nitrobenzyl[26],[27],[28] (oNB) derivatives. The combination of different stimuli-responsive units in one polymer is regarded especially useful for controlling release profiles or enhancing release rates of the drug delivery system (DDS).[29],[30],[31] For example, Kalva *et al.* developed a photo and pH dual-responsive polycarbonate block copolymer conjugated with doxorubicin via an imine linkage to pendant groups that also contain oNB functions.[32] Upon cleavage of the pendant groups by irradiation or pH decrease the drug was released successfully, while the disintegration of the micelles due to hydrophilic/hydrophobic imbalance was observed. Polymeric nano- and microparticles are a typical platform for drug delivery systems and a promising therapeutic strategy for pharmaceutically challenging drugs.[22],[33] Especially nanoparticles (NP) are of great interest, e.g. for cancer treatment, because of their passive targeting ability due to the enhanced permeability and retention (EPR) effect.[34],[35] Polycarbonates[36],[37],[38] (PC) and polyurethanes[39],[40],[41] (PU) are generally considered excellent materials for biomedical applications because of their biodegradability, low toxicity and biocompatibility. A versatile route for the synthesis of polyurethanes is the polyaddition of diols and diisocyanates using organotin catalysts which also enables end-group functionalization.[7],[42] Common approaches for the synthesis of polycarbonates are the ring-opening polymerization (ROP) of cyclic carbonates, like trimethylenecarbonate,[36],[43] and the polycondensation of diol monomers.[37],[44] While ROP typically leads to PC with narrow dispersity and defined architecture, synthesis of

the cyclic carbonate monomers is often expensive and due to the polymerization mechanism restricted to diols of certain carbon chain length.[45] On the contrary, numerous different diols can be utilized for polycondensation with, e.g., dimethylcarbonate (DMC) or diphenylcarbonate (DPC) employing organocatalysts or alkali-metal catalysts, even in large-scale approaches.[44],[45],[46] The Kuckling group and the Langer group reported the synthesis of polycarbonates with light-cleavable pendant groups for the application as photosensitizer loaded controlled release systems for the photodynamic therapy (PDT) of gastrointestinal tumors.[17],[26],[47],[48] Upon irradiation, the polymers showed degradation by a nucleophilic “backbiting” of the liberated amine groups which led to an increased release of photosensitizer compared to standard polylactic-*co*-glycolic acid (PLGA) nanoparticles. In order to enhance the degradation, the number of steps of the degradation process could be decreased by direct integration of the stimuli-degradable moiety into the polymer backbone.

The aim of this work was a thorough study of the applicability of stimuli-responsive backbone-degradable polymers for drug delivery applications with special emphasis on light as a trigger. Therefore, a series of different monomers, homopolymers as well as copolymers that respond to light, but also to redox or acidic environments, with decomposition of the main chain should be synthesized. Step-growth polymerization techniques, namely polycondensation and polyaddition, should be employed for synthesis of polycarbonates and polyurethanes due to the good biocompatibility of these polymers. Besides the characterization of the products with typical methods like size exclusion chromatography (SEC) or nuclear magnetic resonance (NMR) spectroscopy, the degradation behavior of the synthesized polymers should be investigated using various analysis methods like UV/Vis spectroscopy, infrared (IR) spectroscopy or mass spectrometry (MS). Ultimately, micro- and nanoparticles should be formulated from the polymers and the particle degradability should be investigated in order to test their applicability as nanoparticulate drug delivery systems. For the analysis of particle formation, degradation as well as cargo release, methods like dynamic light scattering (DLS), fluorescence spectroscopy and microscopy should be employed.

2. Theoretical Background

2.1. Step-Growth Polymerization

Typically, the step-growth polymerization is defined by three characteristic properties. Firstly, no initiator is needed to start the polymerization as, e.g., the elimination of small molecules can drive the reaction. Secondly, all species participating in the polymerization are equal in reactivity and especially no less stable active chains are formed during the process, as it is known for radical chain-growth polymerization. Thus, the reaction of the functional units occurs under strictly statistical terms without any preference. Thirdly, high molar masses can only be achieved at very high conversions which can be derived from the correlation of number average degree of polymerization (P_n) and conversion (p) as can be seen in *Figure 2-1*.[49]

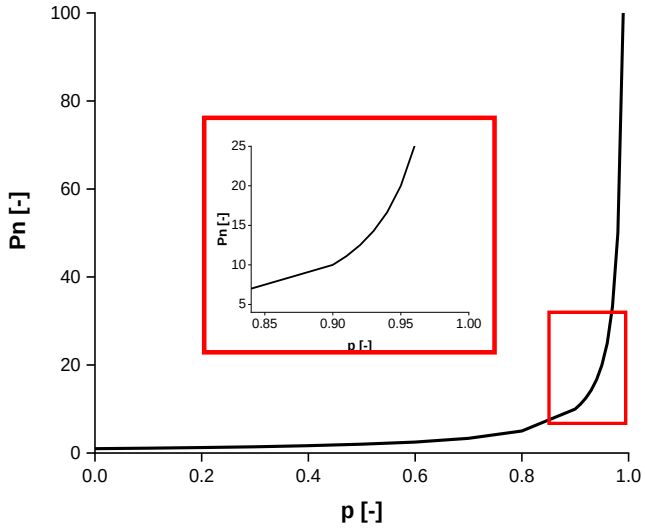

Figure 2-1: General correlation of p and P_n for step-growth polymerization.

In general, compounds bearing functional groups capable of forming covalent bonds can be used as monomers for these reactions. Typical examples are carboxy and hydroxyl functions, which form ester groups under elimination of water. On the one hand, it is possible to combine both of these functions in one monomer, a so-called AB-type monomer. On the other hand, two bifunctional monomers can be used for the polymerization, which are then referred to as AA and BB type. The use of multifunctional compounds leads to the formation of branched or crosslinked polymers by the same reaction pathway. In case of the AA/BB type monomers, an exact

stoichiometry is necessary to reach high P_n as can be seen in *Figure 2-2*.[49],[50]

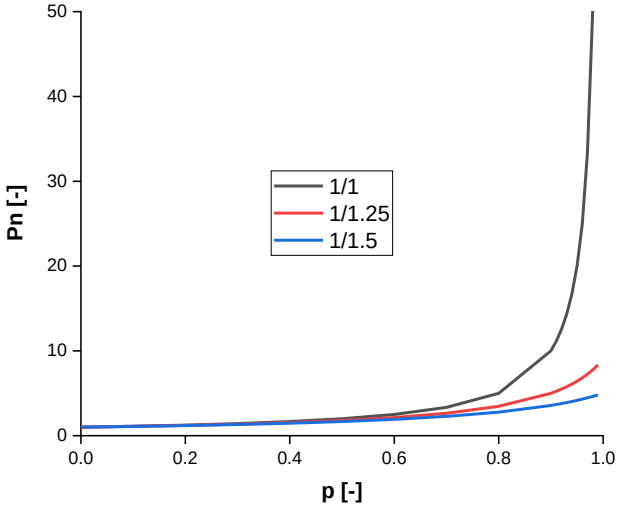

Figure 2-2: Correlation of p and P_n for step-growth polymerization using AA/BB type monomers in different stoichiometry.

The reason for this is that the polymerization is stopped after full conversion of the lacking monomer due to termination of all formed chains with the excess compound. Carothers was the first to describe this relation of P_n and p mathematically by the Carothers equation introducing the factor of stoichiometric ratio (r) (2-1).

$$P_n = \frac{r+1}{r-2rp+1} \tag{2-1}$$

In general, r is defined by the number of functional groups A (n_A) divided by the number of functional groups B (n_B) (2-2).

$$r = \frac{n_A}{n_B} \tag{2-2}$$

P_n is equal to the initial number of monomers (n_0) divided by the number of monomers after a certain reaction time (n_t) (2-3).

$$P_n = \frac{n_0}{n_t} = \frac{n_A + n_B}{n_{A,t} + n_{B,t}} \tag{2-3}$$

Assuming an excess of functional groups A compared to B, the equations 2-5 and 2-6 for the conversion of both functional groups can be derived from the general expression for p (2-4).

$$p = 1 - \frac{n_t}{n_0} \Leftrightarrow n_t = (1-p)n_0 \tag{2-4}$$

$$n_{A,t} = (1-p)\, n_A \tag{2-5}$$

$$n_{B,t} = (1-p \cdot r)\, n_B \tag{2-6}$$

Insertion of equations 2-5 and 2-6 for the sum of remaining functional groups after reaction time (t) in 2-3 yields equation 2-7, which can be simplified to the Carothers equation (2-1).

$$P_n = \frac{n_A + \frac{n_A}{r}}{\frac{n_A}{r} \cdot (r - 2rp + 1)} = \frac{r+1}{r-2rp+1} \tag{2-7}$$

Besides P_n, and thus the number average molar mass (M_n), the polydispersity (Đ) is considered as one of the most important values to characterize polymers. Đ is defined by the ratio of weight average molar mass (M_w) and M_n (2-8). Since P_n is proportional to M_n and the weight average degree of polymerization (P_w) is proportional to M_w, Đ of step-growth polymerization is also dependent from p (2-9).

$$Đ = \frac{M_w}{M_n} = \frac{P_w}{P_n} \tag{2-8}$$

$$Đ = \frac{\frac{1+p}{1-p}}{\frac{1}{1-p}} = 1 + p \tag{2-9}$$

In case of full conversion (p = 1), Đ of an ideal step-growth polymerization is 2, assuming no side-reactions occurred.[49]

Typical types of step-growth polymerizations are the polycondensation under elimination of small molecules, e.g. water, and the polyaddition. Both reactions show high similarities from a mechanistic point of view, which is in each case identical to the conventional organic reaction.[51] The most prominent polymers obtained by these reactions are polyesters, polyamides and polycarbonates from polycondensation as well as polyurethanes from polyaddition.[50] Regarding the scope of this work, the

polycondensation reaction will be discussed with emphasis on the formation of polycarbonates.

2.1.1. Polycondensation

The formation of polycarbonates by polycondensation typically involves a diol monomer as well as a carbonate source where the diol acts as a nucleophile and the carbonate source as an electrophile (*Scheme 2-1*).

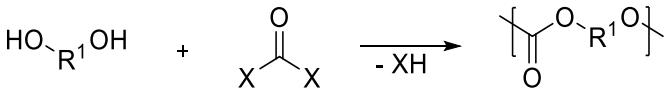

Scheme 2-1: General reaction scheme of polycarbonate formation by polycondensation.

While conventionally phosgene is employed as a carbonate source, alternatives like DMC and DPC, which are less toxic as well as less harmful to the environment, can also be used.[52],[53] Though the process using DPC was discovered early on for the production of bisphenol-A (BPA) based polycarbonates, the available experimental setups limited the commercial use. Thus, one of the first systems that could be used on a big scale was the synthesis of poly(BPA) based on phosgene employing pyridine as both, solvent and base, for scavenging the HCl produced during synthesis.[54],[55] However, the challenging isolation and purification of the product led to the development of the well-known interfacial polycondensation between phosgene in an organic phase, typically dichloromethane (DCM), and BPA as a sodium adduct in a basic aqueous phase (*Scheme 2-2*).[50],[54],[55]

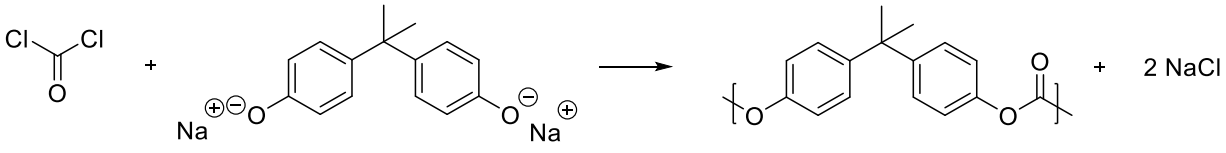

Scheme 2-2: General reaction scheme of the interfacial polycondensation of BPA with phosgene.

While the process involving phosgene can be carried out at room temperature, due to the high reactivity of phosgene, higher temperatures are usually needed for DMC and DPC. Especially the polymerization employing DPC as a carbonate source is carried

out under high temperatures as a polycondensation in the melt. In general, this procedure consists of two steps. At first the initial condensation of the molten reaction mixture is carried out until equilibrium between hydroxyl-terminated oligomers and phenyl carbonate-terminated oligomers is reached. In a second step transesterification is performed under vacuum and further increased temperature to remove the phenol side product and shift the equilibrium to the product side in order to achieve high M_n (*Scheme 2-3*).[54],[56]

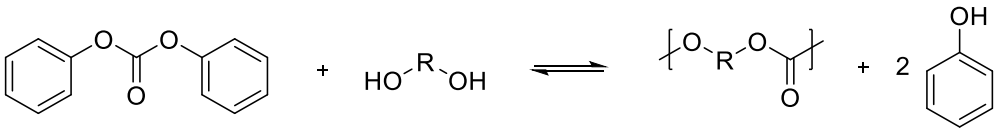

Scheme 2-3: General reaction scheme of the polycondensation in the melt using DPC.

Despite the higher experimental challenges compared to interfacial phosgenation, processes based on alternate carbonate sources faced a renaissance due to the possibilities of modern experimental setups and the general urge for more environmental-friendly production like the reduction of volatile corrosive byproducts.[52],[54],[55] Furthermore, the use of transesterification catalysts additionally increased the utility of these reactions by accelerating the reaction significantly. Among the variety of different catalysts investigated for the synthesis, like alkaline- and alkaline-earth-metal hydroxides or 4-dimethylaminopyridine (DMAP),[57],[58] alkaline- and alkaline-earth-metal-based acetylacetonates (Acac) proved to be very efficient.[59] Especially LiAcac was confirmed to significantly promote the polycondensation of various monomers with both, DPC and DMC.[17],[60] In recent years also enzyme-catalyzed procedures have been reported, which provide advantages like milder reaction conditions and high tolerance for functional groups. On the downside, these systems require long reaction times and high catalyst loading, while yielding only relatively low M_n.[56],[61],[62]

2.1.2. Polyaddition

In both, research and industry, polyurethanes are typically synthesized by stepwise polyaddition. Overall, the reaction is very similar to the polycondensation process but without the release of low molecular byproducts. Conventionally, a diol monomer is

reacted with a diisocyanate in either bulk or solution where the diol acts as a nucleophile and the diisocyanate as an electrophile (*Scheme 2-4*).[49],[50],[51]

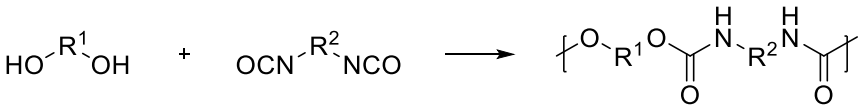

Scheme 2-4: General reaction scheme of the stepwise polyaddition.

The most prominent diisocyanates are the aliphatic 1,6-hexamethylenediisocyanate (HDI) and isophorone diisocyanate (IPDI) as well as the aromatic diphenylmethane-4,4'-diisocyanate (MDI) and toluenediisocyanate (TDI; typically in a 4/1 mixture of 2,4- and 2,6-TDI) (*Scheme 2-5*).[49],[51]

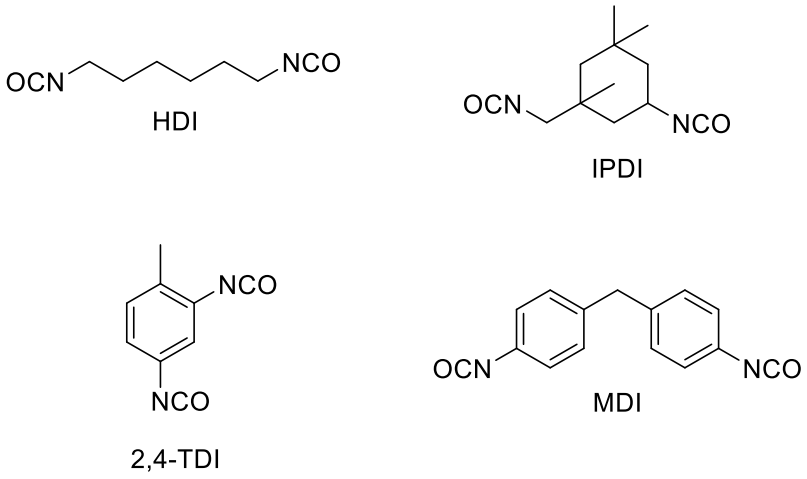

Scheme 2-5: Structures of the most prominent diisocyanates for polyaddition.

In general, aromatic diisocyanates are more reactive than aliphatic ones, while primary diisocyanates show faster reaction than the higher substituted ones.[51] This is especially important for reactions employing IPDI which bears both, a primary and a secondary isocyanate function. Most of the processes for polyurethane synthesis are carried out in solution, as only the polyaddition of 1,4-butanediol and HDI is commonly conducted in the melt.[50] Reasons for this are for example the high reaction temperature needed for the polymerization in bulk as well as the increased probability of side-reactions between diisocyanate and polyurethane. Typical examples for such side-reactions are the formation of allophanate, isocyanurate or biuret functions, which lead to crosslinking of the product and are in some cases, like certain industrial applications, even desired (*Scheme 2-6*).[51]

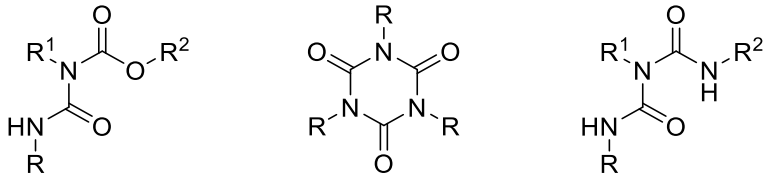

Scheme 2-6: Typical side-products of the polyurethane synthesis by polyaddition.

Besides short-chain diol monomers, also oligomers and polymers with M_n ranging from 2000-10000 g/mol are commonly used for the polyaddition, which enables tailoring of the product properties. While the use of short-chain diols leads to more rigid polyurethanes, longer chain length of the diol enhances the polyurethane flexibility. Usually, polyether or polyester diols are used as polymeric monomers for the polyurethane synthesis, which are then called polyols. Furthermore, two different approaches for conducting the polyaddition are commonly employed, a one-step and a two-step process. While in the one-step process all compounds are initially mixed and the final product is obtained after a certain reaction time, the two-step process means the formation of an isocyanate-terminated prepolymer by using excess diisocyanate in a first step. In a second step, typically low molecular weight diols or diamines are added as so-called chain extenders to obtain the final product and thereby enabling further structural modification.[63] Independent of the process, most polyadditions are carried out using catalysts which efficiently promote the formation of urethane groups. Among the most prominent catalysts are organic bases like triethylamine or 1,4-diazabicyclo [2.2.2] octane (DABCO) and organometallic compounds.[51],[63] Especially dibutyltin dilaurate (DBTDL) is a widely applied catalyst in both, academic research and industry, due to the high acceleration of the carbamate forming propagation reaction, while showing only minimal promotion of side-reactions. The reason for this is the formation of complexes with both, hydroxy and isocyanate functions, enhancing the reactivity.[64],[65]

2.2. Polymers from Step-Growth Polymerization

Among the numerous polymers synthesized by step-growth polymerization are polyesters, polyamides, polyureas, polycarbonates and polyurethanes. Many of these polymers are used for various applications in both, academic research and industry. In

the following chapter, typical properties and applications of polycarbonates and polyurethanes will be highlighted.

2.2.1. Polycarbonates

Polymers bearing repeating units that are linked by carbonate functions, in other words polyesters of carbonic acid, are called polycarbonates. Typically, polycarbonates are divided into aliphatic and aromatic polycarbonates, majorly due to the significantly different material properties. Though aliphatic polycarbonates were already synthesized in the 1930s by Carothers, they were considered inferior for the industrial applications of that time because of a low melting point (T_m) and higher susceptibility to hydrolysis.[56] Furthermore, only diols of a certain chain length were accessible as monomers for the preparation of aliphatic polycarbonates by polycondensation because of the formation of thermodynamically stable cyclic carbonates as side-products.[49] Aromatic polycarbonates on the other hand, especially BPA-based ones, which were discovered in the 1950s, gained tremendous attention due to the high transparency, relatively high glass transition temperature (T_g) as well as high impact toughness.[54] Typical applications for aromatic polycarbonates are, e.g., automotive or electronic devices where polycarbonates have been used as cheap and highly capable alternatives for materials like wood, glass or metal during the last decades.[55] With rising interest in more environment-friendly production processes and materials, aliphatic polycarbonates received renewed attention partly due to the possibility of formation by copolymerization of CO_2 and epoxides (*Scheme 2-7*).[66],[67],[68]

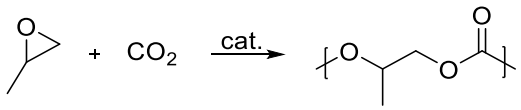

Scheme 2-7: Reaction scheme of the polymerization of propylene oxide and CO_2.

The first successful example was the polymerization of propylene oxide in the 1960s using an autoclave with 50 bar of CO_2 and a diethylzinc water mixture as a catalyst at room temperature. Since then, various cyclic monomers like oxetanes or thiiranes as well as several different catalyst systems have been investigated to improve this polymerization process and enhance its versatility.[66] Another aspect regarding green

polymer chemistry is the potential use of monomers derived from renewable sources, like vegetable oil,[37] to overcome the dependency on fossil oil and reduce the carbon footprint of polymeric products. In addition, many of these polycarbonates derived from renewable natural feedstocks are considered to be (bio-)degradable, and are thus regarded promising to solve the severe problem of plastics pollution.[69] But also in medical applications the demand for biocompatible and biodegradable materials has risen with the development of new therapies and applications, like tissue-engineering or drug delivery. As many aliphatic polycarbonates, also ones based on fossil sources, have shown good biocompatibility and biodegradability, they have emerged as a promising class of polymers in this field. Interestingly, the properties that initially appeared as disadvantageous for many conventional applications, like low T_g, proved to be a striking advantage for biomedical applications. Furthermore, the decomposition of polycarbonates does not lead to the formation of acids, which is a major advantage over conventional biodegradable polyesters, like poly(L-lactide) (PLLA),[70] as the acidification can interact with drugs or be hazardous to tissue.[36],[56] A well-known example for a biodegradable polycarbonate is poly(trimethylene carbonate), which is commonly prepared by ring-opening polymerization (*Scheme 2-8*).

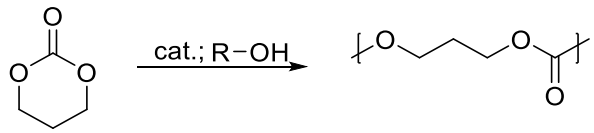

Scheme 2-8: Reaction scheme of the ROP of TMC.

ROP is a controlled polymerization technique for the preparation of aliphatic polyesters and polycarbonates from cyclic monomers, yielding low Đ and controlled end groups.[71]

2.2.2. Polyurethanes

Analogously to polycarbonates, polymers bearing repeating units linked by urethane functions, for which the term carbamate units is used more often in case of low molecular weight compounds, are called polyurethanes. Polyurethanes are a very versatile class of polymers, which led to numerous applications in fields like construction, automotive or textiles after their first synthesis in the 1930s. As a first

commercial product Perlon U was prepared by polyaddition of HDI and 1,4-butanediol in a one-step process by Otto Bayer. The incorporation of polyols instead of short-chain diols broadened the number of possible applications further due to the possibility of tailoring the product properties. Furthermore, the use of cheaper and more reactive aromatic diisocyanates instead of aliphatic diisocyanates led to a variety of products.[51],[72] However, a real commercial breakthrough was the discovery of CO_2 formation upon addition of water to the reaction mixture leading to the formation of foams, which to date are one of the most prominent fields for the industrial application of polyurethanes (*Scheme 2-9*).[63],[72]

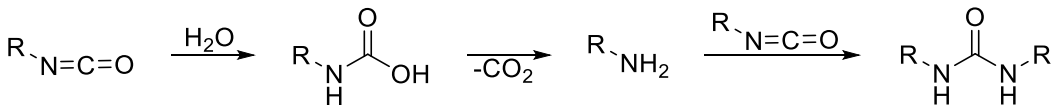

Scheme 2-9: General scheme for the reaction of isocyanate and water.

Under nucleophilic attack of water, instable carbamic acid is formed, which subsequently decomposes to CO_2 and the corresponding amine. As the amine can further react with isocyanates under formation of a urea moiety, this does not necessarily terminate the polymerization. Though in most cases these polymers are also called polyurethanes, in some cases the more proper term polyurethane/urea is used.[72] Very commonly, polyurethanes are divided into hard and soft segments where the carbamate units are typically considered as hard segments and the polyol as soft segments, because of the enhanced flexibility. Since these segments are incompatible with each other, phase-separation into soft block and hard block microdomains takes place. Thus, polyol-based polyurethanes are often referred to as biphasic multiblock copolymers.[51],[72],[73] In addition, the hard segments namely the carbamate units can form intermolecular hydrogen bonds, which leads to physical crosslinking of the polymer and further drives the segregation (*Figure 2-3*).[72]

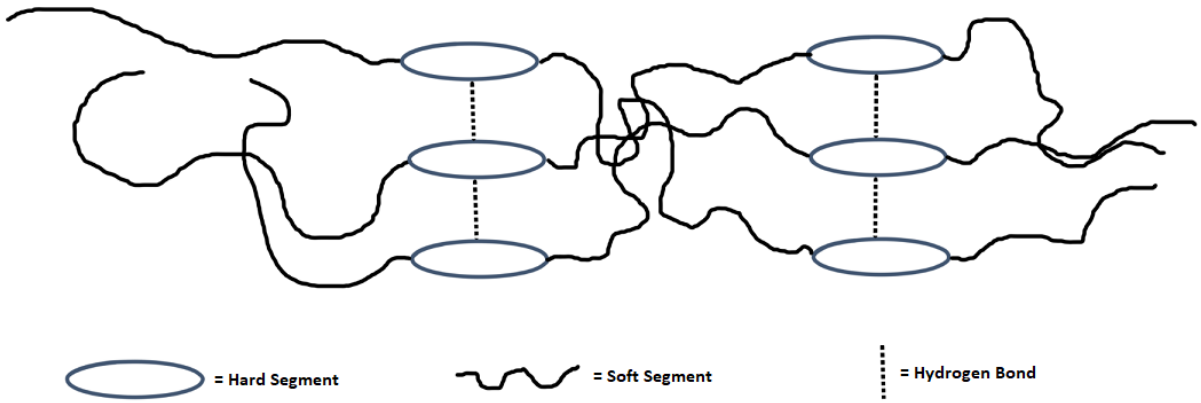

Figure 2-3: Polyurethane segment segregation and physical crosslinking.

In the biomedical field both, polyol and short-chain diol-based polyurethanes, are commonly employed depending on the type of application. In general, many polyurethanes show good biocompatibility and biodegradability, e.g., polyester-based polyurethanes undergo rapid hydrolysis after entering the human body. However, in contrast to conventional applications aromatic diisocyanates are typically not considered suitable for biomedical applications due to their toxicity.[40],[74] While linear polyurethanes prepared from low molecular weight diols are more often used in the field of nanomedicine,[75],[7] typical applications for polyol-based polyurethanes include bone engineering and vascular tissue engineering.[76],[77] Reasons for this are, e.g., the elastomeric behavior and high stability many polyol-based polyurethanes display which are necessary features for both applications.[40] Nanomedical devices, especially nanoparticulate drug delivery systems, on the other hand often require new functional, e.g. stimuli-degradable, monomers to tailor *in vivo* blood circulation times and rapid drug release with less need for long-term *in vivo* stability as is the case for implants. Thus, the functional low molecular weight compounds are often employed directly for the polyurethane synthesis instead of being incorporated into polyols first.[40],[78] Of course, exceptions can be found as this is an observed trend and no general rule.[79]

2.3. Stimuli-Degradable Polymers

Polymers that alter their properties, like solubility or charge, upon contact with a certain stimulus or trigger are commonly called stimuli-responsive. A well-known example for this behavior is poly(*N*-isopropylacrylamide), which exhibits a switch from hydrophilic to hydrophobic in aqueous environment upon increasing the solution temperature to

30-34 °C, the so-called lower critical solution temperature (LCST) behavior.[80],[81] Among these stimuli-responsive polymers, polymers bearing functions that cleave in response to the stimulus, stimuli-cleavable or stimuli-degradable polymers, have been of great interest in the last years due to their promising applicability as, e.g., drug delivery systems or patterning material.[82],[12] There are many typical examples for stimuli-degradable moieties known from low molecular weight compounds like esters, acetals or imines, which are pH-sensitive, disulfides, which are redox-sensitive, and coumarins or *ortho*-nitrobenzyl derivatives, which are light-sensitive. While light is a trigger that can be controlled externally, pH- and redox-variations are internal triggers that specifically occur at the target site.[83] Transformation of these units into polymers can be conducted by incorporation into the side-chain, backbone, block junction or as crosslinking agents (*Figure 2-4*).

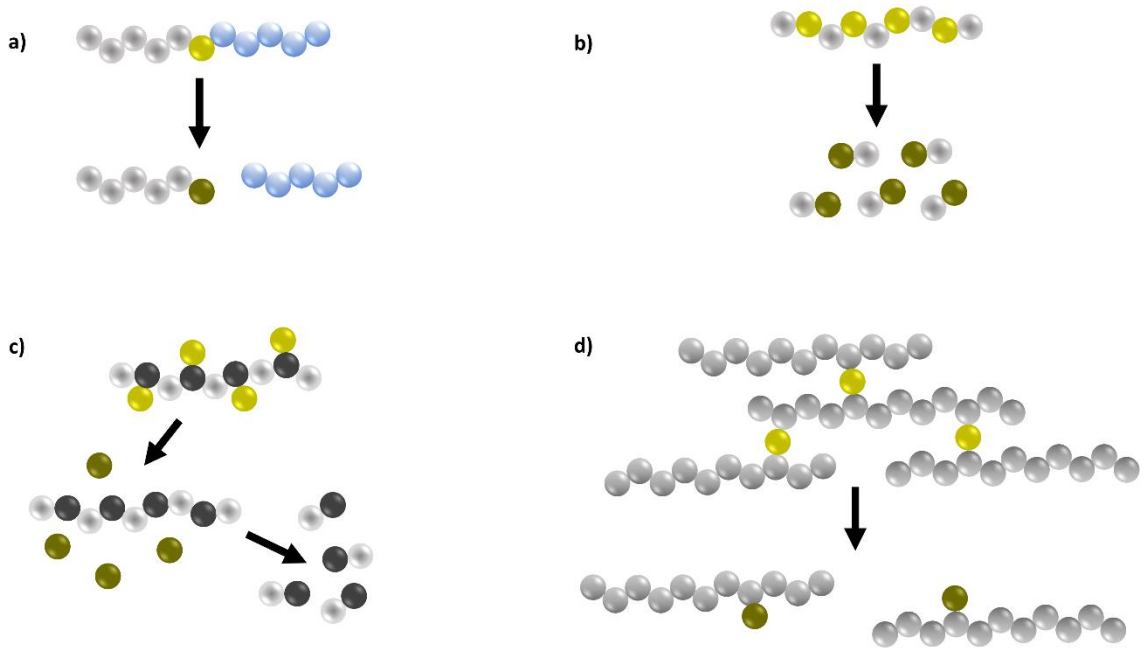

Figure 2-4: Stimuli-degradable polymers bearing the cleavable function at the block junction (a), backbone (b), side-chain (c) and crosslinking points (d).

A commonly applied concept is the synthesis of amphiphilic block copolymers with cleavable block junctions for on-demand block-cleavage. Since many amphiphilic block copolymers are capable of self-assembly into micelles or micelle-like particles, block-cleavage leads to the dissociation of these structures. If a cargo, like a drug, is encapsulated inside the micelle core, it is released upon decomposition of the matrix.[18] Polymers with cleavable side-chains do typically not lead to the direct

degradation of the polymeric chain. Instead, a nucleophilic function is released which subsequently attacks electrophilic moieties in the polymeric backbone, such as carbonate functions of polycarbonates, leading to the degradation of the polymer. The typical products of this so-called backbiting process are thermodynamically favored cyclic compounds.[26] Thus, by using these backbiting polymers as a matrix for nanoparticulate drug delivery, the particles can be disintegrated upon contact with the stimulus leading to on-demand release of the encapsulated drug.[47] As the name suggests, backbone-degradable polymers bear stimuli-cleavable moieties in the polymeric backbone. In contrast to polymers with cleavable block junctions typically each repeating unit includes a degradable function. Though the results are small fragments comparable to side-chain cleavable polymers, the degradation is typically a one-step process instead of a two-step decomposition. In contrast, the use of stimuli-degradable crosslinking agents for the formation of polymeric networks does not lead to the degradation of the polymer chains but to the dissociation of the network. While polymeric networks are regarded as insoluble, the released polymer chains can, assuming a proper solvent, be dissolved leading to the release of cargo that was previously entrapped in the network.[84] In the following chapters, the three stimuli light, pH and redox will be discussed further with special emphasis on polymers for drug delivery applications.

2.3.1. Light-Degradable Polymers

Light as a trigger has received much interest during the last years due to the high spatial and temporal control over its application as well as its tunability by wavelength and intensity adjustments. Among the different light-cleavable moieties known, like phenacyl, benzoin or coumarin derivatives, oNB derivatives are by far the most widely applied ones (*Scheme 2-10*).[85],[86],[87]

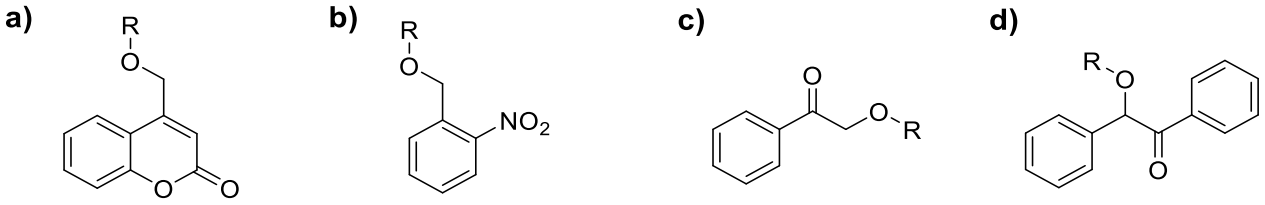

Scheme 2-10: General structure of the photocleavable protecting groups coumarin (a), oNB (b), phenacyl (c) and benzoin (d).

oNBs have long been used as photocleavable protecting groups in (bio-)chemical research, e.g., for caging adenosine triphosphate as published by Kaplan *et al.* in 1978.[88] Though the absorbance maximum of a conventional, unsubstituted oNB ester is generally about 260 nm, sufficient excitation in the UV-A region is typically achieved. Thus, the protection group is suitable for many biological applications like the investigation of force transduction in muscles by photochemical on-demand uncaging of adenosine triphosphate.[85],[89] The reason for the photodegradability of oNB derivatives is a photoisomerization process that ultimately leads to the formation of a *ortho*-nitroso benzaldehyde under cleavage of the benzylic C-O bond (*Scheme 2-11*).

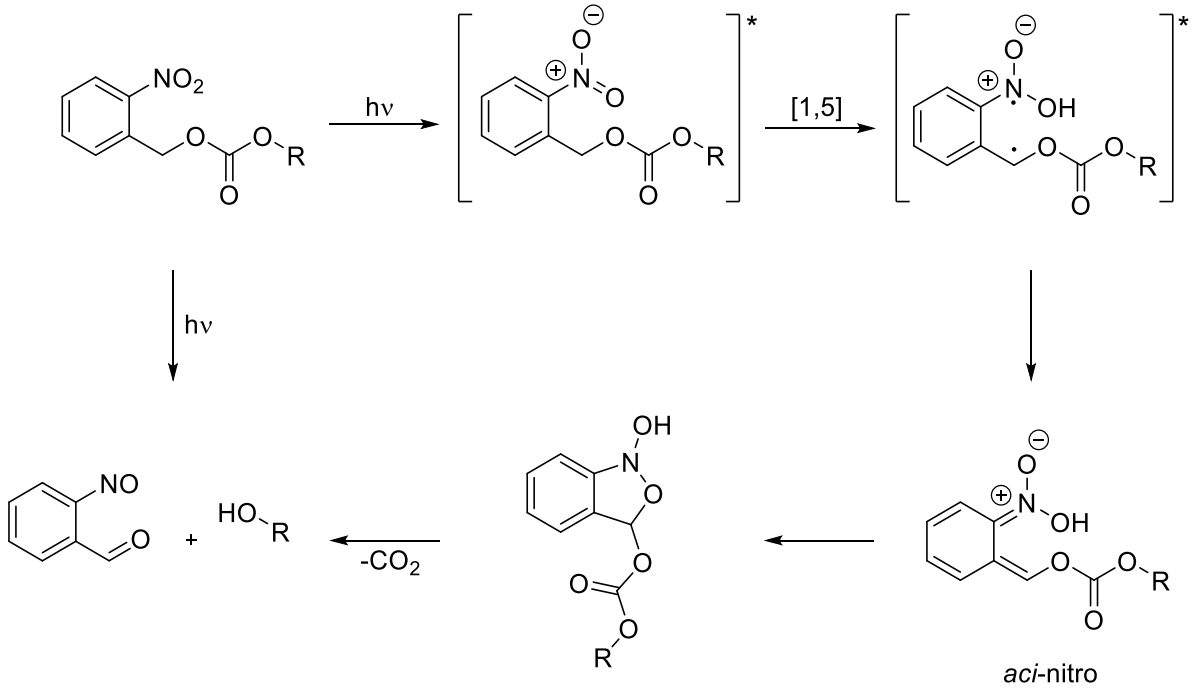

Scheme 2-11: Photoisomerization of oNB carbonate derivatives.[85],[90]

The most recent analysis of the photoisomerization process of oNB compounds was reported by Schmierer *et al.* who investigated the photo-induced reaction of *ortho*-nitrotoluene by transient absorption spectroscopy as well as femtosecond stimulated Raman spectroscopy.[91] In short, upon irradiation the oNB derivative is promoted to an excited state which leads to a [1,5]-sigmatropic rearrangement of the benzylic H-atom under formation of an *aci*-nitro compound. The *aci*-nitro compound can decay by cyclization restoring the aromaticity of the system followed by decomposition to *ortho*-nitrosobenzaldehyde and, in case of an oNB carbonate, an alcohol under CO_2 release. It was found that substitution at the benzylic site has a

significant beneficial effect on the quantum yield of such photoreactions. A very prominent example for this is the introduction of an α-methyl substituent which also leads to the formation of a less reactive *ortho*-nitrosobenzylketone instead of an aldehyde. As a possible reason for this a stabilizing effect of the intermediate benzyl radical was proposed, which would lead to an easier abstraction of the benzylic H-atom. Substitution of the aromatic core, in contrast, was found to have only minor positive effect on the quantum yield. On the opposite, while electron-donating 4-methoxy substituents were found to slightly decrease the quantum yield, 3-methoxy substituents retarded the reaction completely.[92] Nevertheless, the work regarding modifications on the aromatic ring clearly outnumbers the work regarding substitutions at the benzylic site, which is probably due to the potential increase in maximum absorbance wavelength λ_{max} that is especially useful for biochemical applications. Well-known is the bathochromic shift of electron-donating substituents like alkoxy groups, e.g., the methoxy substitution in 2-position of a typical oNB compound as depicted in *Scheme 2-11* increases λ_{max} to the less harmful UV-B region. Of course, while having no direct effects, the increase of λ_{max} also affects the quantum yield concomitantly, because many applications have a certain wavelength region for the irradiated light.[85] However, since light in the UV-A region still shows interaction with human tissue it cannot simply penetrate the body. Thus, for several biomedical applications, e.g. drug delivery, approaches like small endoscopic light sources were investigated to tackle this issue. Another possibility is the use of higher wavelength lasers with high photon density that could induce two photon absorption processes of the employed chromophores, as light of higher wavelength can penetrate deeper into the tissue. Though research regarding two photon absorption materials is growing with the interest in applications based thereon, the reported systems often vary widely, which makes a comparison of the results difficult and prevents the establishment of real trends.[85],[93] Several examples for the successful preparation of light-degradable polymers for drug delivery bearing oNB pendant groups were reported by Sun *et al.*, including biocompatible aliphatic polyester, polycarbonates and polyurethanes.[7],[17],[26] In each case the oNB compound was linked to an amine moiety via a carbamate function, which was cleaved upon irradiation liberating the nucleophilic amine group. Afterwards, the polymers were degraded by nucleophilic backbiting of the amine, yielding low molecular weight cyclic compounds. Nanoparticles formulated from these polymers showed rapid decomposition upon exposure to UV light as well as release of

the encapsulated model compounds.[48] Another approach was followed by Klinger *et al.*,[94] who used oNB containing divinyl-based crosslinkers for the preparation of light-degradable poly(methyl methacrylate) microgels. By employing a miniemulsion polymerization process the microgels were obtained as particles which revealed successful degradation upon illumination as observed by DLS and scanning electron microscopy (SEM).

2.3.2. pH-Degradable Polymers

Among stimuli-degradable and -responsive polymers a change of pH is probably one of the most applied triggers due to its versatility. Most of the published research regarding pH-responsiveness either deals with an acid-induced polarity switch, e.g. the protonation of amines in the side-chain,[95] or with acid-accelerated polymer degradation. As already explained, chain degradation induces decomposition of polymeric micelles or nanoparticles and thus releasing cargo encapsulated in the polymer matrix which can be exploited for drug delivery.[96] The basis of pH-accelerated drug delivery is on the one hand the pH-gradient in the human body, ranging from about 7.4 in the blood to about 5 in the environment of the endosomes and lysosomes.[97] On the other hand, cancer for example exhibits an acidification of the tumor microenvironment to a pH of ~6.5 because of lactate formation by glycolysis. In contrast to healthy cells, which typically employ phosphorylation, glycolysis is the main pathway of energizing cells in many tumors.[98] Furthermore, several acid-degradable functional groups with divergent degradation profiles are known, enabling the design of polymers and polymeric networks with adjusted degradability. Especially typical organic protection groups are used for the preparation of pH-accelerated polymeric release systems, including acetal/ketal, imine, hydrazone, oxime and orthoester moieties. Degradation of these units in aqueous environment occurs under mildly acidic conditions by proton-induced hydrolysis (*Scheme 2-12*).

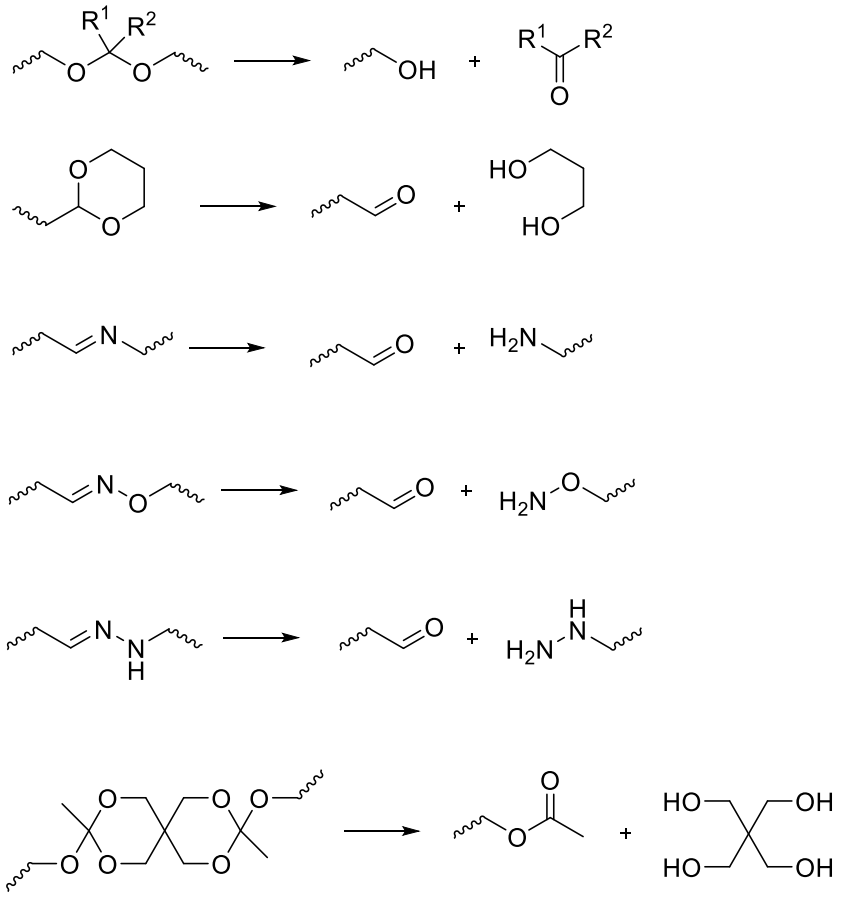

Scheme 2-12: Structures of common acid-degradable functions and their hydrolysis in acidic aqueous environment.

Besides the already discussed location of the cleavable unit, integration of these moieties into polymers can be achieved either by synthesis of functional monomers or by polymerization, e.g., polyacetals and polyorthoesters. Li *et al.* reported pH-accelerated degradation of polymeric microspheres for the controlled release of doxorubicin exhibiting enhanced antitumor efficiency.[2] Hydroxy-terminated low molecular weight PLLA was synthesized by ring-opening polymerization and used as a monomer for the acid-catalyzed polyacetal formation employing diethylene glycol divinyl ether. Upon treatment with phosphate-buffered saline (PBS) at pH 5 the resulting polymer showed decreasing molecular weight as obtained by SEC confirming the acid-accelerated degradation. Following a different approach, Huang *et al.* synthesized a diacetal containing diol monomer from 1,1,1-tris(hydroxymethyl)ethan and terephthalaldehyde.[1] Backbone-degradable polyurethanes were obtained by reaction of the monomer with lysine ethyl ester diisocyanate employing DBTDL as a catalyst. Termination with allyl alcohol enabled functionalization with thiolated polyethylene glycol (PEG) (M_n = 5000 g/mol) via radical thiol-ene reaction to form

amphiphilic triblockcopolymers with molar masses of 23200 g/mol, 18900 g/mol and 15200 g/mol, respectively. Micelles in the nanometer range were prepared showing narrow PDI and increasing size with increasing molar mass of the hydrophobic block. Treatment with PBS at pH 4, 5 and 7.4, respectively, confirmed the pH-accelerated degradation of the micelles as determined by UV/Vis spectroscopy and DLS.

As mentioned before, pH-accelerated polymer degradation is often achieved by hydrolysis reactions such as the acid-catalyzed ketal cleavage, thus leading to a dependency of degradation rates and polymer hydrophilicity. The use of comonomers to alter the properties of a polymeric material is a widely applied concept.[99] In case of pH-accelerated polymeric drug delivery systems, comonomers can be used to, e.g., adjust solubility and thus tailor the release rates of the systems. For example, Olejniczak *et al.* described the synthesis of a dual-responsive copolymer based on a ketal monomer and a lysine derived comonomer which was masked by a photolabile protecting group at the carboxylic function.[100] The protected comonomer was incorporated to accelerate degradation of the ketal moieties by liberation of the carboxylic groups upon irradiation with UV light and thereby enhancing the hydrophilicity of the polymer. Michael addition with 1,3-propanedithiol was employed to polymerize the divinyl monomers under mild conditions and ^{1}H NMR was used to confirm the degradation in mixtures of dimethyl sulfoxide (DMSO) and PBS at pH 5 and pH 7.4, respectively. Upon illumination the ketal polymers showed significantly increased hydrolysis while no notable change in pH was observed. Furthermore, the solely light-induced acceleration of the ketal hydrolysis was revealed upon photolysis in neutral PBS indicating the key role of hydrophilicity in the cleavage of ketals.

2.3.3. Redox-Degradable Polymers

Especially for drug delivery applications, redox-degradable polymers faced much attention, as the redox-cleavage of cysteine-based disulfides by, e.g., glutathione is a well-known natural process in the human body. Furthermore, they are regarded as promising candidates for tumor-targeted drug delivery since many tumors lead to glutathione overexpression in the cancer tissue as protection from oxidative cell damage. Typical redox-degradable moieties are diselenide and disulfide functions. While disulfides are by far the most common unit, diselenides are known to be more sensitive to cleavage due to the weaker bond energy compared to the disulfide

bond.[101],[102] In general, the *in vivo* reduction of disulfides occurs under formation of a mixed disulfide with the reducing agent in a first step and liberation of one corresponding thiol. Dependent on the reducing agent, the second corresponding thiol is released either by inter- or intramolecular nucleophilic attack of another thiolate under formation of a new disulfide. For example, while thioredoxin typically forms intramolecular disulfides in this process, glutaredoxin forms intermolecular disulfides with glutathione.[103] As an approach for a redox-degradable polymeric drug delivery system, Duan *et al.* employed polycondensation to synthesize amphiphilic cystamine-based polyamides with imine linked polyethylene glycol monomethylether (mPEG) (M_n = 5000 g/mol) endcaps.[104] The polymers self-assembled to micelles in aqueous environment, which showed successful degradation upon treatment with glutathione as observed by DLS. In addition, the micelles showed disruption at lowered pH due to cleavage of the acid-degradable imine linkage of the hydrophilic PEG block. An example of a diselenide-based polymer was reported by Ma *et al.* who synthesized amphiphilic polyurethanes with mPEG (M_n = 1900 g/mol) endcaps from diselenide containing low molecular weight diols.[105] Micelles loaded with the model compound rhodamine B were prepared by self-assembly in aqueous environment. Transmission electron microscopy (TEM) analysis of the micelles showed successful decomposition upon treatment with glutathione confirming the reductive degradability of the polymer. Furthermore, the oxidative degradability of the polymer was proven in the same fashion using H_2O_2 as an oxidizing agent. These results were supported by fluorescence spectroscopy measurements, which confirmed the release of the fluorescent model drug. In line with the use of disulfide and diselenide as redox-degradable moieties, the preparation of a ditelluride containing polyurethane for redox-responsive drug delivery has recently been reported by Wang *et al*.[4] Polyaddition was employed for the synthesis using ditelluride containing low molecular weight diols and PEG (M_n = 1000 g/mol) as monomers. Doxorubicin loaded nanoparticles were formulated from the random copolymer and TEM as well as DLS revealed successful decomposition upon treatment with glutathione. In addition, the glutathione induced release of doxorubicin was observed employing UV/Vis spectroscopy.

2.4. Drug Delivery

Common obstacles in modern therapy are the high hydrophobicity, low pharmacokinetic half-lives and adverse side-effects of many drugs.[106] Drug delivery is considered one of the most promising tools to overcome these issues. In general, drug delivery means the accumulation and release of a pharmacologically active compound at a specific target-site, e.g., the tumor tissue in case of cancer. This is in sharp contrast to the conventional administration of drugs, which typically leads to the free distribution throughout the body and thus reduces the efficiency by limiting the applicable doses.[35] Especially nanoscale systems, including liposomes, nanoparticles, micelles, and dendrimers, faced a lot of attention since the discovery of the enhanced permeability and retention (EPR) effect by Maeda *et al*.[81],[34] In short, the EPR effect consists of the accumulation of macromolecules by extravasation through fenestrated blood vessels as well as their detainment in tumors due to irregular lymphatic vessels. Thus, nanocarriers in a diameter range of 100-200 nm can passively target many solid tumors, e.g. breast cancer, due to the loose coating of the vascular endothelial cells.[35],[34] However, the requirements to exploit the EPR effect are not only met by tumors, but also by many inflammatory diseases like rheumatoid arthritis, which further emphasizes the utility of nanomedicine.[107],[108] Another striking advantage of nanocarriers, especially polymeric ones, is the ability to functionalize the surface in order to adjust circulation times and avoid accumulation in organs as well as clearance by the phagocyte system. While several methods like attaching membranes or graft peptides to the carrier surface are known, the functionalization with PEG, the so-called PEGylation, is probably the most prominent one.[109],[110] The PEG chains associate with water forming a hydrating layer on the particle surface, which prevents protein adsorption as well as clearance by phagocytes (*Figure 2-5*).[35]

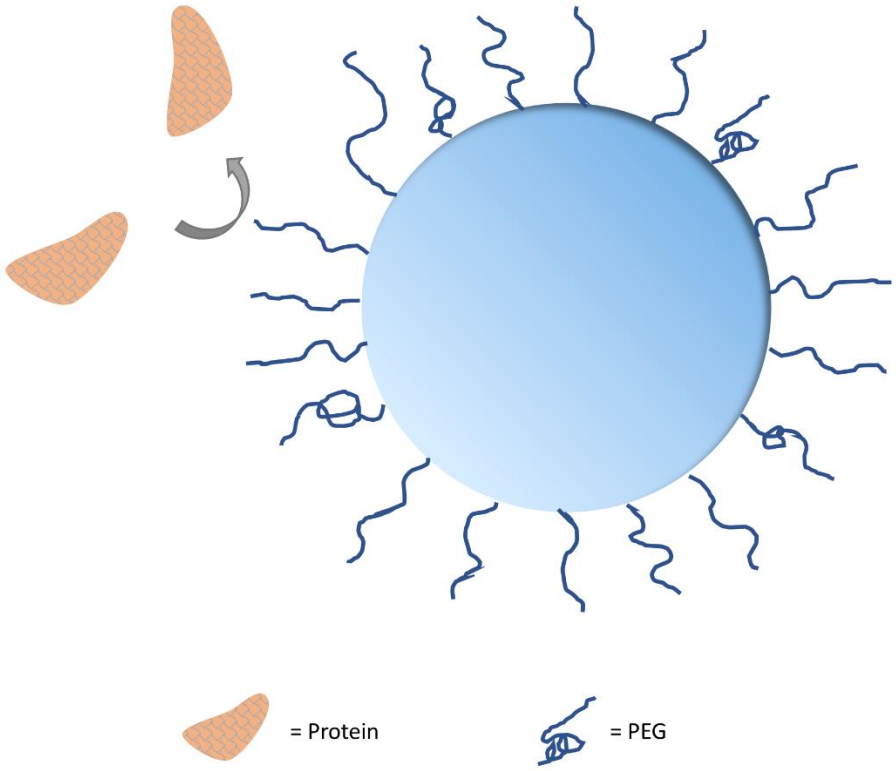

Figure 2-5: Shielding of PEGylated particle against protein adsorption.[35]

Typically, PEGylation of polymeric nanoparticles can be achieved either by using a blend of the hydrophobic matrix polymer and PEG or by using PEG containing copolymers for the particle formation. Compared to liposomes polymeric nanoparticles generally exhibit less drug leakage, higher drug encapsulation efficiency as well as a better storage stability.[111] Furthermore, the broad range of monomers, polymers and natural materials as well as methods that can be used for the formulation of nanoparticles leads to a wide variety of possible properties and structures. The most prominent preparation techniques are nanoprecipitation and emulsion solvent evaporation, which have different suitability depending on the polymer solubility and the drug to be administered.[112],[113] While nanoprecipitation is based on the diffusion of the organic solvent into the aqueous phase to form hardened nanoparticles, the emulsion solvent evaporation process yields the final particles after complete evaporation of the organic solvent. Though in both cases a surfactant is used to form stable nanodroplets in water prior to hardening, this state is only very short-lived for nanoprecipitation.[114],[115] The most common surfactant for nanoparticle formulation is poly(vinyl alcohol) (PVA). In fact only few viable alternatives, such as poloxamer, are known to be suitable as many other surfactants only yield microparticles.[116],[117] Dependent on the organic solvent being used and the amount of PVA in the aqueous

phase, it was found that small amounts of PVA, e.g. <13% for PLGA nanoparticles, remain in the particle matrix after final purification due to chain interpenetration. Even though some effects like altered cellular uptake were visible, the release of cargo was only affected minorly by residual PVA.[117] Drug loading of the nanoparticles can be achieved by chemical conjugation to the polymer or by encapsulation in the particle matrix or core, which enables the delivery of various hydrophilic or hydrophobic compounds.[112] The release of these drugs can therefore be accomplished by diffusion through the particle matrix, decomposition of the particles or cleavage of the conjugational bonds. Especially the on-demand decomposition has proven to be beneficial due to adjustable release and higher targeting by, e.g., addressing properties unique to the diseased tissue. In addition, the use of degradable polymers for this on-demand particle decomposition typically yields smaller fragments that can be cleared faster from the body. The specificity of nanoparticles can be enhanced even further by incorporation of ligands that have an affinity towards the diseased cells, which is then called active targeting.[23] A well-known example for such a compound is biotin, which can be used as a targeting ligand for tumors.[118]

3. Experimental Part

3.1. Materials and Measurements

3.1.1. Materials

All solvents used for synthesis and for analytical experiments are listed in *Table 3-1* and all chemicals used are listed in *Table 3-2*.

Table 3-1: List of the solvents used for synthesis and analysis.

Solvent	Purity	Manufacturer
Acetonitrile (MeCN)	99.9%+	Carl Roth
tert-Butanol (tBuOH)	99.5%	Acros Organics
Chloroform	dest.	Stockmeier
Dichloromethane (DCM)	HPLC grade	Carl Roth
Diethyl ether (Et_2O)	dest.	Hanke + Seidel
N,N-Dimethylformamide (DMF)	99.8% (dry)	Acros Organics
Dimethyl sulfoxide (DMSO)	99.5%	Grüssing
Ethanol (EtOH)	99.5%	Grüssing
Ethyl acetate (EtOAc)	dest.	Stockmeier
iso-Hexane (*iso*-Hex)	techn.	Stockmeier
n-Hexane	techn.	Stockmeier
Hexafluoroisopropanol (HFIP)	99.5%+	Acros Organics
Methanol (MeOH)	99.5%	Grüssing
Phosphate-buffered saline (PBS)	/	Alfa Aesar
Tetrahydrofuran (THF)	99.5%	Grüssing
Tetrahydrofuran (THF)	99.8% (dry)	Acros Organics

Table 3-2: List of the chemicals used for synthesis and analysis.

Chemical	Purity	Manufacturer
Adipoyl chloride (ADP)	98%	Alfa Aesar
AD-Mix α	/	Sigma Aldrich
Benzyl chloroformate	95%	Alfa Aesar
Bis(2-hydroxyethyl)disulfide (BHED)	95%	Acros Organics
Borane tetrahydrofuran complex solution (BH_3-THF)	/	Acros Organics

2-Bromoethanol	97%	Alfa Aesar
1,4-Butanediol (BD)	99%+	Acros Organics
Dibutyltin dilaurate (DBTDL)	95%	Sigma Aldrich
4-(Dimethylamino)pyridine (DMAP)	99%+	Fluka
2,5-Dimethylanisole	99%	Sigma Aldrich
Diphenylcarbonate (DPC)	99%	Alfa Aesar
Dithiothreitol (DTT)	99%+	Sigma Aldrich
Hexamethylene diisocyanate (HDI)	99%+	Acros Organics
5-Hydroxy-2-nitrobenzaldehyde	98%	Acros Organics
Isophorone diisocyanate (IPDI)	98%	Acros Organics
Lithium acetylacetonate	99.5%	Alfa Aesar
L-Lysine ethyl ester diisocyanate (LDI)	97%	Alfa Aesar
Methyl bromoacetate	97%	Sigma Aldrich
Methyl triphenyl phosphonium bromide	98%	Sigma Aldrich
Nile red	/	abcr
2-Nitrobenzyl alcohol	97%	Sigma Aldrich
6-Nitropiperonal	97%+	TCI
2-Nitroterephthalic acid	99%+	Acros Organics
Polyethylene glycol 1000 Da (PEG1000)	/	Sigma Aldrich
Polyethylene glycol 400 Da (PEG400)	/	Merck
Polyethylene glycol monomethylether 5 kDa (mPEG5000)	/	Sigma Aldrich
Polyvinylalcohol (PVA) Mowiol 8-88	/	Sigma Aldrich
Potassium permanganate	99%	Alfa Aesar
Potassium *tert*-butoxide (KOtBu)	97%+	Grüssing
Pyridine	99.5% (dry)	Acros Organics
Sodium nitrite	99.6%	Fisher Sci
para-Toluenesulfonic acid monohydrate (pTSA)	98.5%+	Sigma Aldrich
1,1,1-Tris(hydroxymethyl)ethane	97%	Alfa Aesar

3.1.2. Measurements

Nuclear Magnetic Resonance (NMR) Spectroscopy

The ^{1}H NMR spectra were recorded at 500 MHz and the ^{13}C NMR spectra at 125 MHz using a Bruker AV500 spectrometer. $CDCl_3$ (99.8 D%) and DMSO-d_6 (99.8 D%) were used as the solvents for the measurements. MestReNova was used to process the data. The chemical shifts (δ) are listed in ppm and coupling constants (J) are listed in Hz, respectively.

Size Exclusion Chromatography (SEC)

An SEC system with THF as the eluent equipped with two consecutive columns (PSS-SDV, 10^5 Å and 10^3 Å) and operating at 1 mL/min was used for most of the measurements. A Merck L4200 UV detector at 260 nm and a Knauer RI detector were employed to obtain the molar masses as well as dispersities Đ (= M_w/M_n) using polystyrene standards for calibration.
In addition, a system with HFIP as the eluent equipped with two consecutive columns (PSS-PFG, 10^3 Å and 10^2 Å) and operating at 1 mL/min was used for measurements of less soluble samples. A Shodex RI 101 detector was employed to obtain the molar masses and Đ using poly methyl methacrylate standards for calibration.

Electrospray Ionization Mass Spectrometry (ESI-MS)

A Waters SYNAPT G2 HDMS™ was used for the electrospray ionization time-of-flight (ESI-ToF) measurements. Polymerix was used to process the data except for the degradation experiments of model compound **20** which were processed using ACD Spectrus Processor.

Differential Scanning Calorimetry (DSC)

For analysis of the glass transition temperatures (T_g) of the polymer samples a Netzsch DSC 204 F1 Phönix was employed at a heating rate of 10 K/min under nitrogen atmosphere.

UV/Vis

UV/Vis spectra were recorded on an Analytik Jena Specord 50 PLUS UV/Vis spectrophotometer using Aspect UV software.

Surface Plasmon Resonance (SPR) Spectroscopy

The SPR data were recorded using a ResTec RT2005 spectrometer with a LASFN9 prism that was connected to the sensor chip employing an immersion oil (Cargille Lab., USA) with a matching refractive index. The results were processed and fitted using the software Winspall.

Profilometry

A Bruker DekTakXT profilometer was used for the measurements.

Dynamic Light Scattering (DLS)

Count rate as well as particle size and particle size distribution (PDI) were obtained by DLS measurements at 20 °C and a backscattering angle of 173° using a Malvern Zetasizer Nano-ZS.

UV Light Source

Unless stated otherwise, a Lumen Dynamics Omnicure S1500 curing system with an intensity of 297 mW/cm^2 and a wavelength of 320-480 nm was used for the irradiation experiments.

Light Source for Two Photon Absorption

A Fianium WhiteLase WL-SC400-2 high power supercontinuum fiber laser was used for the two photon absorption experiments. The wavelength was set to 515-525 nm and an intensity of 20 mW.

Scanning Electron Microscopy (SEM)

A Zeiss Neon 40 Scanning Electron Microscope was used to obtain the SEM images.

3.2. Synthesis of Low Molecular Weight Compounds

3.2.1. Synthesis of (2-nitro-1,4-phenylene)dimethanol (2)

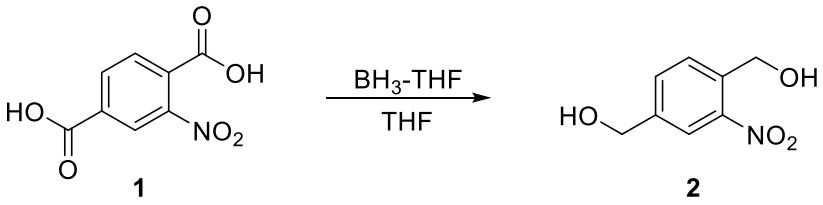

1 **2**

In a typical procedure 2-nitroterephthalic acid **1** (2.111 g; 10 mmol) was dissolved in anhydrous THF (10 mL) under nitrogen atmosphere. After cooling down in an ice bath, BH_3-THF (50 mL; 50 mmol) solution was added dropwise under stirring. The ice bath was removed after complete addition of the BH_3-THF solution and the mixture was stirred at room temperature for 1 h. Subsequently the reaction mixture was heated to 50 °C and stirred overnight. The solution was cooled in an ice bath and quenched by careful addition of HCl (2 M; 15 mL). H_2O (100 mL) was added and THF was removed using a rotary evaporator. The obtained aqueous phase was extracted four times with Et_2O (60 mL) and the combined organic layers were washed with aqueous Na_2CO_3 solution (sat.; 60 mL). After drying by addition of $MgSO_4$, Et_2O was removed and a yellow powder was received as the crude product. Recrystallization from $CHCl_3$ yielded 71% of the pure product **2** as light-yellow needles (literature[94]: 91%).

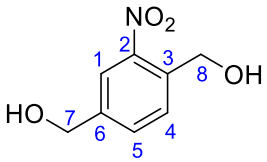

^{1}H NMR (DMSO-d_6): δ [ppm] = 4.59 (d, $^3J_{HH}$ = 5.7 Hz, $^8CH_2$), 4.80 (d, $^3J_{HH}$ = 5.5 Hz, $^7CH_2$), 5.44 (t, $^3J_{HH}$ = 5.6 Hz, ^8OH), 5.48 (t, $^3J_{HH}$ = 5.6 Hz, ^7OH), 7.68 (d, $^3J_{HH}$ = 7.8 Hz, ^5CH), 7.77 (d, $^3J_{HH}$ = 8 Hz, ^6CH), 7.97 (s, ^3CH)

3.2.2. Synthesis of (2-methoxy-5-nitro-1,4-phenylene)dimethanol (6)

*Synthesis of 4-nitro-2,5-dimethylanisol (**4**)*

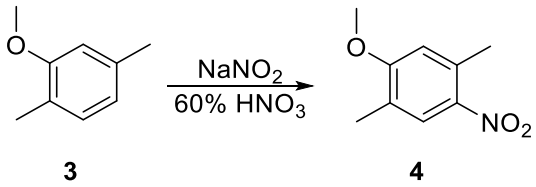

3 **4**

Compound **4** was synthesized according to a modified version of the procedure published by Jin *et al.*[119] $NaNO_2$ (54.00 g; 0.78 mol) was added to a three-neck round bottom flask and cooled in an ice bath. HNO_3 (600 mL) was added slowly and the solution was stirred for 15 min. Subsequently, 2,5-dimethylanisol (36.11 g; 0.27 mol) was added dropwise and the solution was stirred for 5 h while being cooled in an ice bath. The raw product was obtained as a brown solid by precipitation in H_2O. After recrystallization from MeOH and drying *in vacuo* 48% (literature[119]: 73%) of light-brown needles were yielded as the pure product.

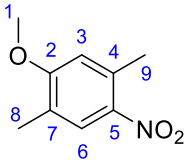

^{1}H NMR ($CDCl_3$): δ [ppm] = 2.21 (s, $^9CH_3$), 2.63 (s, $^8CH_3$), 3.90 (s, $^1CH_3$), 6.66 (s, ^3CH), 7.91 (s, ^6CH)

*Synthesis of 2-methoxy-5-nitroterephthalic acid **(5)***

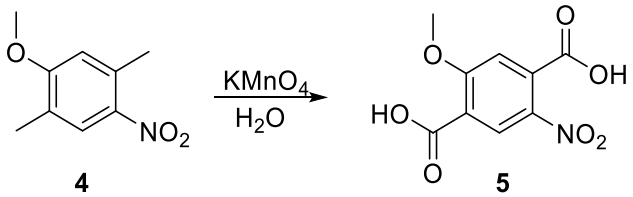

4 **5**

Synthesis of compound **5** was also performed according to a modified version of the procedure published by Jin *et al.*[119] In a two-neck round bottom flask **4** (23.00 g; 0.13 mol) and $KMnO_4$ (173.00 g; 1.1 mol) were dissolved in H_2O (1.2 L) and stirred under reflux for 5 h. After cooling to room temperature, the formed black precipitate was removed by filtration and the obtained filtrate was concentrated *in vacuo*. Upon

treatment of the resulting green residue with HCl (600 mL) product **5** was obtained as a white precipitate. After isolation and drying *in vacuo* 34% of the product were yielded as a white powder (literature[119]: 62%).

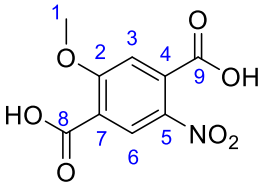

^{1}H NMR (DMSO-*d*$_6$): δ [ppm] = 3.99 (s, ^{1}CH$_3$), 7.42 (s, ^{3}CH), 8.32 (s, ^{6}CH), 13.0-14.30 (br, ^{8}COOH, ^{9}COOH)

Synthesis of (2-methoxy-5-nitro-1,4-phenylene)dimethanol ***(6)***

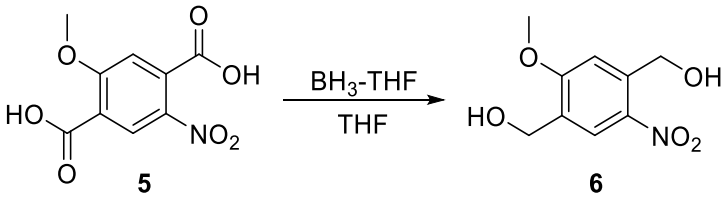

In a dried two-neck round bottom flask **5** (960 mg; 4.0 mmol) was dissolved in anhydrous THF (10 mL) under nitrogen atmosphere. BH_3-THF solution (20 mL; 20 mmol) was added dropwise under cooling in an ice bath and the reaction mixture was then stirred for 1 h at room temperature. Subsequently, the solution was heated to 55 °C and stirred overnight. The reaction was quenched by careful addition of H_2O (10 mL) under cooling and the THF was removed *in vacuo*. The raw product was precipitated by adding a $NaHCO_3$ solution (50 mL) and isolated. Recrystallization from THF yielded 78% of the pure product **6** as a light-yellow powder.

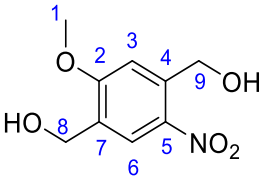

^{1}H NMR (DMSO-*d*$_6$): δ [ppm] = 3.92 (s, ^{1}CH$_3$), 4.52 (d, $^{3}J_{HH}$ = 5.6 Hz, ^{8}CH$_2$), 4.88 (d, $^{3}J_{HH}$ = 5.4 Hz, 2H, ^{9}CH$_2$), 5.34 (t, $^{3}J_{HH}$ = 5.7 Hz, ^{8}OH), 5,59 (t, $^{3}J_{HH}$ = 5.4 Hz, ^{9}OH), 7.40 (s, ^{3}CH), 8.16 (s, ^{6}CH)

^{13}C NMR (DMSO-*d*$_6$): δ [ppm] = 56.1 (^{1}C), 57.0 (^{8}C), 60.4 (^{9}C), 108.7 (^{3}C), 123.6 (^{6}C), 129.9 (^{7}C), 138.9 (^{5}C), 140.9 (^{4}C), 160.2 (^{2}C)

λ_{max}: 317 nm (in MeCN)

HRMS (ESI)**:** m/z: calcd. for $C_9H_{11}NO_5Na^+$ 236.0535; obsd. 236.0546 $[M+Na]^+$

IR (ATR): $\tilde{\nu}$ (cm^{-1}) = 3271 (m; O-H_{Alk}), 3182 (m; O-H_{Alk}), 3018 (w; C-H_{Ar}), 2988 (w; C-H_{Alk}), 2936 (w; C-H_{Alk}), 2853 (w; C-H_{Alk}), 1620 (m; C=C_{Ar}), 1574 (m; C=C_{Ar}), 1510 (s; N=O), 1466 (m; C-H_{Alk}), 1452 (m; C-H_{Alk}), 1425 (m; C-H_{Alk}), 1375 (s; N=O), 1356 (w; O-H), 1325 (s; O-H), 1263 (s; O-H), 1072 (w; C-O_{Alk}), 1042 (s; C-O_{Alk}), 986 (m; C-N), 901 (w; C-H_{Ar}), 872 (w; CH_{Ar}), 862 (w; C-H_{Ar}), 806 (w; C-H_{Ar})

T_m: 199.5 °C

3.2.3. Synthesis of (S)-1-(6-nitrobenzo[d][1,3]dioxol-5-yl)ethane-1,2-diol (9)

*Synthesis of 5-nitro-6-vinylbenzo[d][1,3]dioxole (**8**)*

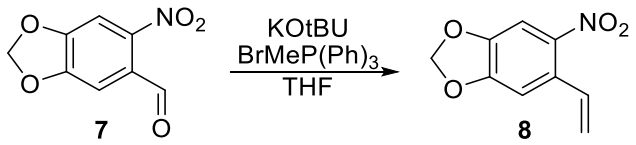

In a first step methyl triphenyl phosphonium bromide (1.858 g; 5.2 mmol) was added to a dry two-neck round bottom flask under nitrogen atmosphere and suspended in THF (12 mL). KOtBu (612 mg; 5.5 mmol) was added and the mixture was stirred for 1 h at room temperature. After 1 h the reaction mixture turned bright yellow, indicating formation of the ylide/ylene. Upon addition of 6-nitropiperonal (**7**; 778.3 mg; 4.0 mmol) dissolved in THF (3 mL) under stirring, the reaction mixture turned from bright yellow to a brownish red color. The mixture was stirred overnight and subsequently the solvent was removed by rotary evaporation. Brine was added and the mixture was extracted three times with EtOAc. The combined organic phases were washed with water and concentrated using a rotary evaporator. Purification by column chromatography (EtOAc/iso-hexane; 20/1; v/v; R_f = 0.25) over silica yielded a yellow powder (60%) as pure product **8**.

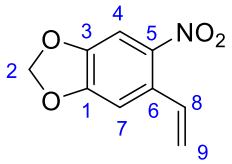

^{1}H NMR (DMSO-*d*$_6$): δ [ppm] = 5.43 (dd, $^{2}J_{HH}$ = 0.9 Hz, $^{3}J_{HH}$ = 11.0 Hz, ^{9}CH, cis), 5.84 (dd, $^{2}J_{HH}$ = 0.9 Hz, $^{3}J_{HH}$ = 17.2 Hz, ^{9}CH, trans), 6.23 (s, ^{2}CH$_2$), 6.99 (dd, $^{3}J_{HH}$ = 11.0 Hz, $^{3}J_{HH}$ = 17.5 Hz, ^{8}CH), 7.33 (s, ^{7}CH), 7.58 (s, ^{4}CH)

*Synthesis of (S)-1-(6-nitrobenzo[d][1,3]dioxol-5-yl)ethane-1,2-diol (**9**)*

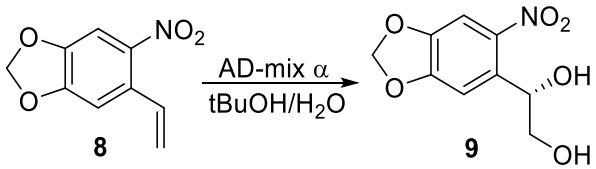

In a round bottom flask AD-mix α (5.46 g) was suspended in *tert*-butanol (16 mL) and water (16 mL) under heavy stirring. After cooling the mixture by employing an ice bath, **8** (754 mg; 3.9 mmol) was added and the reaction mixture was stirred overnight at room temperature. The reaction was stopped by addition of Na_2SO_3 and the mixture was extracted three times with EtOAc. After removal of the solvent, the crude product was purified employing column chromatography (EtOAc/iso-hexane; 1/1; v/v; R_f = 0.3) over silica. A yellow powder (75%) was obtained as pure product **9**.

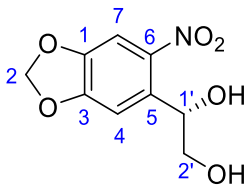

^{1}H NMR (DMSO-*d*$_6$): δ [ppm] = 3.39-3.47 (m, $^{2'}$CH$_2$), 4.85 (t, $^{3}J_{HH}$ = 5.9 Hz, $^{2'}$OH), 5.10 (dt, $^{3}J_{HH}$ = 4.5 Hz, $^{3}J_{HH}$ = 6.5 Hz, $^{1'}$CH), 5.59 (d, $^{3}J_{HH}$ = 4.7 Hz, $^{1'}$OH), 6.20 (dd, $^{2}J_{HH}$ = 18.6 Hz, $^{5}J_{HH}$ = 0.9 Hz, ^{2}CH$_2$), 7.22 (s, ^{4}CH), 7.52 (s, ^{7}CH)

^{13}C NMR (DMSO-*d*$_6$): δ [ppm] = 66.3 ($^{2'}$C), 69.1 ($^{1'}$C), 103.1 (^{2}C), 104.4 (^{7}C), 107.2 (^{4}C), 135.6 (^{5}C), 141.6 (^{6}C), 146.5 (^{1}C), 151.4 (^{3}C)

λ_{max} = 348 nm

HRMS (ESI): m/z calcd. for $C_9H_9NO_6Na^+$ 250.0322, obsd. 250.0339 $[M+Na]^+$

T_m = 101°C

3.2.4. Synthesis of 2-((3-hydroxymethyl)-4-nitrophenoxy)ethan-1-ol (13)

*Synthesis of methyl 2-(3-formyl-4-nitrophenoxy)acetate (**12**)*

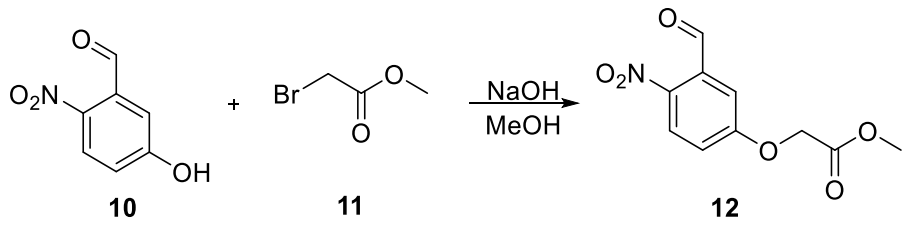

Compound **12** was synthesized according to a modified procedure published by Reinhard *et al.*[120] In a two-neck round bottom flask 5-hydroxy-2-nitrobenzaldehyde (**10**) (1.71 g; 10 mmol) was dissolved in a NaOH/MeOH solution (c = 20 mg/mL) and stirred for 1 h at room temperature. The solution turned from yellow to red, indicating the deprotonation of the phenol group. Methyl acetylbromide (**11**) (1.1 mL; 11.6 mmol) was added dropwise and subsequently the solution was stirred at 100 °C overnight. MeOH was removed and the resulting residue was suspended in DCM (25 mL) and H_2O (50 mL). Na_2CO_3 was added until clearance of the two phases was obtained and the organic phase was isolated. The aqueous phase was extracted three more times with DCM (25 mL) and the combined organic phases were washed with H_2O (10 mL). Removal of the DCM yielded an orange powder as the raw product. The pure product **12** (67%; literature[120]: 71%) was obtained as light orange needles by recrystallization from $Et_2O/CHCl_3$.

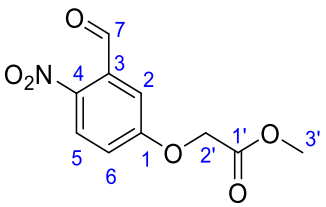

^{1}H NMR (DMSO-d_6): δ [ppm] = 3.72 (s, $^{3'}CH_3$), 5.07 (s, $^{2'}CH_2$), 7.29 (d, $^4J_{HH}$ = 2.9 Hz, ^{2}CH), 7.39 (dd, $^3J_{HH}$ = 9.1 Hz, $^4J_{HH}$ = 2.9 Hz, ^{6}CH), 8.18 (d, $^3J_{HH}$ = 9.1 Hz, ^{5}CH), 10.28 (s, ^{7}CH)

*Synthesis of 2-((3-hydroxymethyl)-4-nitrophenoxy)ethan-1-ol (**13**)*

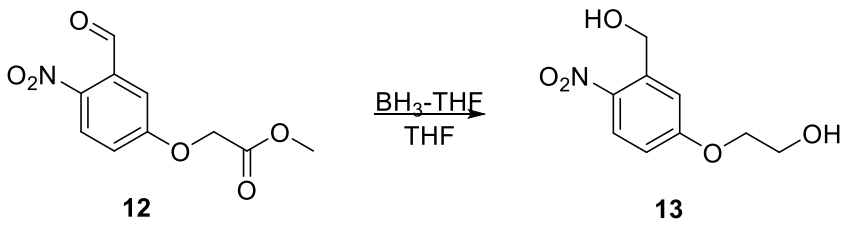

12 (2.132 g; 10 mmol) was dissolved in anhydrous THF (10 mL) under nitrogen atmosphere. After cooling in an ice bath, BH_3-THF (50 mL; 50 mmol) solution was added dropwise under stirring. The ice bath was removed after complete addition of the BH_3-THF solution and the mixture was stirred at room temperature for 1 h. Subsequently, the reaction mixture was heated to 50 °C and stirred overnight. The solution was cooled in an ice bath and quenched by careful addition of HCl (2 M; 15 mL). H_2O (100 mL) was added and THF was removed using a rotary evaporator. The obtained aqueous phase was extracted four times with Et_2O (60 mL) and the combined organic layers were washed with aqueous Na_2CO_3 solution (sat.; 60 mL). After drying by addition of $MgSO_4$, Et_2O was removed and a yellow powder was received as the crude product. Recrystallization from $CHCl_3$ yielded 50% of the pure product as light-yellow needles.

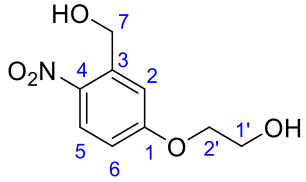

^{1}H NMR (DMSO-*d*$_6$): δ [ppm] = 3.75 (dd, $^3J_{HH}$ = 9.9 Hz, $^3J_{HH}$ = 5.3 Hz, $^{1'}CH_2$), 4.13 (dd, $^3J_{HH}$ = 6.1 Hz, $^3J_{HH}$ = 3.6 Hz, $^{2'}CH_2$), 4.85 (d, $^3J_{HH}$ = 5.4 Hz, $^7CH_2$), 4.92 (t, $^3J_{HH}$ = 5.5 Hz, $^{1'}OH$), 5.55 (t, $^3J_{HH}$ = 5.5 Hz, ^7OH), 7.03 (dd, $^3J_{HH}$ = 9.1 Hz, $^4J_{HH}$ = 2.9 Hz, ^6CH), 7.35 (d, $^4J_{HH}$ = 2.9 Hz, ^2CH), 8.12 (d, $^3J_{HH}$ = 9.1 Hz, ^5CH)

^{13}C NMR (DMSO-*d*$_6$): δ [ppm] = 59.3 ($^{1'}C$), 60.4 (^7C), 70.5 ($^{2'}C$), 112.8 (^6C), 113.3 (^2C), 127.5 (^5C), 139.3 (^3C), 142.5 (^4C), 163.2 (^1C)

λ_{max} = 310 nm (in DCM)

HRMS (ESI): m/z calcd. for $C_9H_{11}NO_5Na^+$ 236.0529, obsd. 236.0549 $[M+Na]^+$

T_m = 116 °C

3.2.5. Synthesis of 2-(3-(5-(hydroxymethyl)-5-methyl-1,3-dioxan-2-yl)-4-nitrophenoxy)ethan-1-ol (17)

*Synthesis of 5-(2-hydroxyethoxy)-2-nitrobenzaldehyde (**15**)*

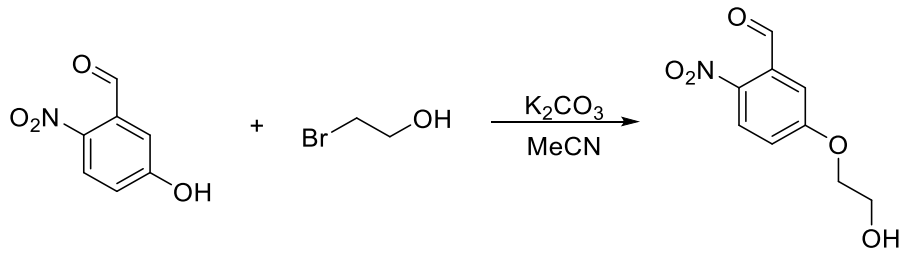

10 **14** **15**

10 (1.67 g; 10 mmol) and K_2CO_3 (1.66 g; 12 mmol) were dissolved in MeCN (25 mL) and stirred at room temperature for 1 h. After addition of bromoethanol (**14**) (0.78 mL; 11 mmol), the solution was heated to reflux and stirred overnight. The precipitated residues were removed by filtration, washed with DCM and the obtained organic phase was washed with HCl (0.1 M), brine and water. After drying over Na_2SO_4, the solvent was removed *in vacuo* and the crude product was purified via column chromatography (EtOAc/ iso-hexane; 6/3; R_f = 0.44) over silica yielding a beige powder as pure product **15** (67%).

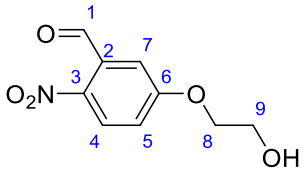

^{1}H NMR (DMSO-d_6): δ [ppm] = 3.75-3.78 (m, $^9CH_2$), 4.20-4.23 (m, $^8CH_2$), 4.96 (t, $^3J_{HH}$ = 5.5 Hz, ^{9}OH), 7.27 (d, $^4J_{HH}$ = 2.9 Hz, ^{7}CH), 7.37 (dd, $^3J_{HH}$ = 9.1 Hz, $^4J_{HH}$ = 2.9 Hz, ^{5}CH), 8.19 (d, $^3J_{HH}$ = 9.1 Hz, ^{4}CH), 10.29-10.31 (m, ^{1}CH)

*Synthesis of 2-(3-(5-(hydroxymethyl)-5-methyl-1,3-dioxan-2-yl)-4-nitrophenoxy)ethan-1-ol (**17**)*

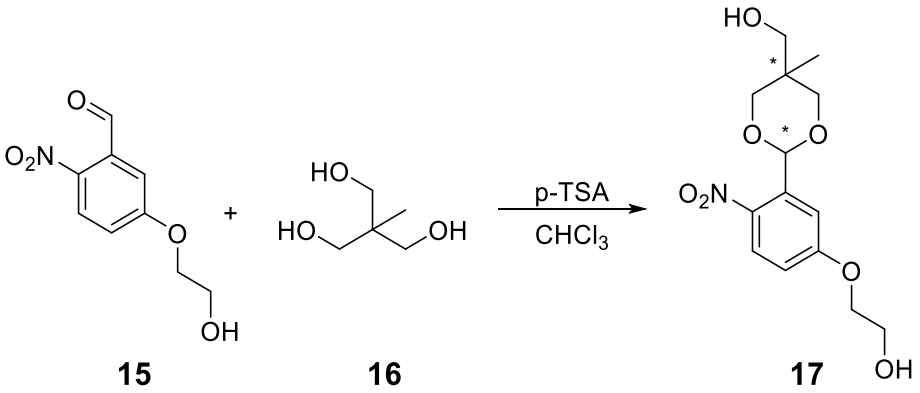

15 **16** **17**

15 (212 mg; 1 mmol), 1,1,1-tris(hydroxymethyl)ethane (**16**) (145 mg; 1.2 mmol) and pTSA (9 mg; 0.05 mmol) were dissolved in $CHCl_3$ (10 mL) under stirring. The solution was heated to reflux and a dean-stark-trap was attached to remove water from the reaction mixture. After stirring overnight, $CHCl_3$ was added and the organic phase was washed with aqueous Na_2CO_3 solution and water. The organic phase was dried over Na_2SO_4 and the solvent was removed *in vacuo* yielding a viscous orange liquid as the pure product **17** (68%).

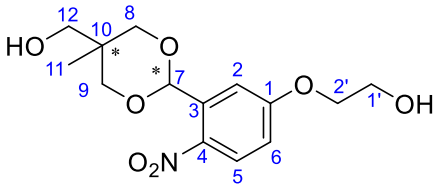

^{1}H NMR (DMSO-*d*$_6$): δ [ppm] = 0.70 (s, $^{11}CH_3$, trans), 1.12 (s, $^{11}CH_3$, cis), 3.18 (d, $^{3}J_{HH}$ = 5.4 Hz, $^{12}CH_2$, cis), 3.55 (d, $^{3}J_{HH}$ = 5.4 Hz, $^{12}CH_2$, trans), 3.65-3.77 (m, $^{8}CH_2$), 3.73–3.78 (m, $^{1'}CH_2$), 3.82-3.94 (m, $^{9}CH_2$), 4.11–4.16 (m, $^{2'}CH_2$), 4.66–4.71 (m, ^{12}OH), 4.92 (t, $^{3}J_{HH}$ = 5.7 Hz, $^{1'}OH$), 5.95 (s, ^{7}CH, cis), 6.00 (s, ^{7}CH, trans), 7.13–7.17 (m, ^{6}CH), 7.26 (d, $^{4}J_{HH}$ = 2.8 Hz, ^{2}CH, trans), 7.30 (d, $^{4}J_{HH}$ = 2.8 Hz, ^{2}CH, cis), 7.97–8.01 (m, ^{5}CH)

^{13}C NMR (DMSO-*d*$_6$): δ [ppm] = 16.7 ($^{11}C_{trans}$), 18.8 ($^{11}C_{cis}$), 34.6 ($^{10}C_{trans}$), 35.0 ($^{10}C_{cis}$) 59.3 ($^{1'}C$), 63.0 ($^{12}C_{trans}$), 64.7 ($^{12}C_{cis}$), 70.5 ($^{2'}C$), 72.5 (^{8}C), 73.9 (^{9}C), 96.1 ($^{7}C_{trans}$), 96.3 ($^{7}C_{cis}$), 113.3 (^{2}C), 114.4 (^{6}C), 127.2 (^{5}C), 134.7 ($^{3}C_{trans}$), 134.7 ($^{3}C_{cis}$), 140.7 (^{4}C), 162.1 ($^{1}C_{trans}$), 162.1 ($^{1}C_{cis}$)

HRMS (ESI): m/z calcd. for $C_{14}H_{19}NO_7Na^+$ 336.1059; obsd. 336.1042 $[M+Na]^+$

IR (ATR): ν [cm^{-1}] = 3460 (w; O-H_{Alc}), 3340 (w; O-H_{Alc}), 2962 (w; C-H_{Alk}), 2930 (w; C-H_{Alk}), 2874 (w; C-H_{Alk}), 1707 (vw; C=C_{Ar}), 1581 (m; C=C_{Ar}), 1519 (m; N=O), 1504 (s; C=C_{Ar}), 1388 (m; O-H), 1336 (m; N=O), 1205 (m; C-O-C), 1178 (m; C-O-C), 1149 (w; C-O-C), 1099 (s; C-O), 1072 (vs; C-O)

λ_{max} = 351 nm (in DCM)

T_m = 96.4 °C

3.2.6. Synthesis of benzyl (2-nitrobenzyl) carbonate (20)

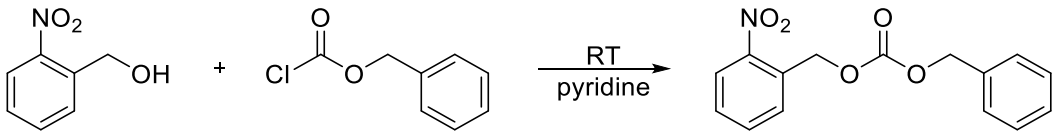

18 **19** **20**

2-Nitrobenzyl alcohol (1.53 g; 10 mmol) was dissolved in pyridine (5 mL) and the solution was cooled in an ice bath under stirring. Benzylchloroformate (1.4 mL; 10 mmol) was added dropwise and the ice bath was removed subsequently. After stirring overnight at room temperature, 1 M HCl (5 mL) was added upon which the crude product precipitated as a white solid. H_2O (5 mL) was added and the precipitate was isolated by filtration. Purification by column chromatography over silica (EtOAc/n-hexane; 1/1; R_f = 0.87) yielded 40% of pure product **20** as a white waxy solid.

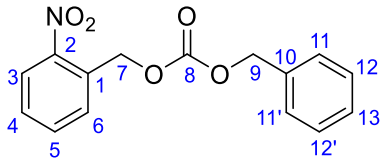

^{1}H NMR ($CDCl_3$): δ [ppm] = 5.22 (s, $^9CH_2$), 5.61 (s, $^7CH_2$), 7.31-7.43 (m, ^{11}CH, $^{11'}$CH, ^{12}CH, $^{12'}$CH, ^{13}CH), 7.45-7.52 (m, ^{4}CH), 7.61-7.68 (m, ^{5}CH, ^{6}CH), 8.31 (d, $^3J_{HH}$ = 8.1 Hz, ^{3}CH)

^{13}C NMR ($CDCl_3$): δ [ppm] = 66.30 (^{7}C), 70.25 (^{9}C), 125.29 (^{3}C), 128.57 (^{11}C, $^{11'}$C, ^{12}C, $^{12'}$C), 128.66 (^{6}C), 128.85 (^{13}C), 128.99 (^{4}C), 132.05 (^{1}C), 134.14 (^{5}C), 135.12 (^{10}C), 147.30 (^{2}C), 154.86 (^{8}C)

HRMS (ESI)**:** m/z: calcd. for $C_{15}H_{13}NO_5Na^+$ 310.0686; obsd. 310.069 $[M+Na]^+$

λ_{max}: 260 nm (in DCM)

T_m = 51.7 °C

3.3. Synthesis of Polycarbonates

General Procedure of Polycondensation in the Melt using DPC

In a typical procedure, diol monomers, DPC (1.05-1.3 mmol) and LiAcac (0.3 mg; 0.5 w%) were filled into a flask equipped with a stirring bar and a septum. The mixture was flushed with nitrogen for 15 min and subsequently heated until melting followed by stirring for 2 h. In a second step, the flask was equipped with a distillation apparatus and evacuated slowly while the temperature was increased. The mixture was then heated for another 2 h and the reaction was stopped by cooling and flushing with nitrogen. The pure product was obtained by precipitation from a suitable solvent and drying *in vacuo*.

3.3.1. Polycarbonates Based on Monomer 2

*Polycarbonate **21***

After polymerization employing the parameters given in *Table 3-3*, the obtained clear dark red residue was dissolved in THF and precipitated from MeOH yielding a beige powder as the pure product after drying *in vacuo*.

*Table 3-3: Parameters for the synthesis of polymer **21.***

Sample	T_1 [°C]	T_2 [°C]	Ratio [2]/[DPC]	Yield [%]
a	130	150	1/1.05	49
b	130	165	1/1.05	82
c	130	180	1/1.05	/[a]

[a]an insoluble brown residue has emerged

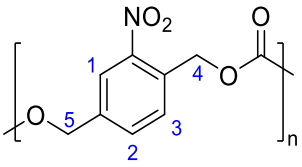

^{1}H-NMR (DMSO-d$_6$): δ [ppm] = 5.22-5.40 (m, ^{5}CH$_2$), 5.43-5.64 (m, ^{4}CH$_2$), 7.63-7.74 (m, ^{3}CH), 7.77-7.88 (m, ^{2}CH), 8.10-8.24 (m, ^{1}CH)

*Co-Polycarbonate **22** Based on Monomer **2** and BD*

1,4-Butanediol (BD) was used as a comonomer and the parameters given in *Table 3-4* were used. After polymerization, the obtained clear dark red residue was dissolved in THF and precipitated from MeOH yielding a beige powder as the pure product after drying *in vacuo*.

*Table 3-4: Parameters for the synthesis of copolymer **22.***

Sample	T_1 [°C]	T_2 [°C]	Ratio [2]/[BD]/[DPC]	Yield [%]
a	130	165	0.5/0.5/1.05	23
b	130	165	0.5/0.5/1.2	61
c	130	165	0.5/0.5/1.3	minor
d	130	165	0.75/0.25/1.2	57
e	130	165	0.25/0.75/1.2	60

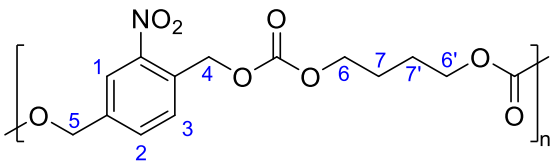

^{1}H-NMR (DMSO-d$_6$): δ [ppm] = 1.54-1.81 (m, $^{7'}$CH$_2$, ^{7}CH$_2$), 3.97-4.29 (m, $^{6'}$CH$_2$, ^{6}CH$_2$), 5.16-5.35 (m, ^{5}CH$_2$), 5.41-5.57 (m, ^{4}CH$_2$), 7.61-7.94 (m, ^{2}CH$_2$, ^{3}CH$_2$), 8.09-8.26 (m, ^{1}CH$_2$)

*Co-Polycarbonate **23** Based on Monomer **2** and PEG1000*

For the synthesis, the same parameters were used as for copolymer **22b** (*Table 3-4*) only using PEG1000 as a comonomer**.** After polymerization, the obtained clear dark red residue was dissolved in THF and precipitated from Et_2O. The isolated solid was dissolved in DCM and washed three times with brine. Subsequently, the pure product was precipitated from EtOH as a yellow solid and dried *in vacuo* (41%).

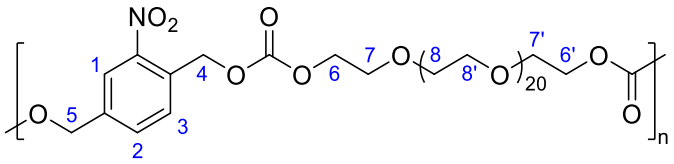

^{1}H-NMR (DMSO-d$_6$): δ [ppm] = 3.41-3.70 (m, $^{7'}CH_2$, $^{7}CH_2$, $^{8'}CH_2$, $^{8}CH_2$), 4.12-4.29 (m, $^{6'}CH_2$, $^{6}CH_2$), 5.19-5.35 (m, $^{5}CH_2$), 5.43-5.58 (m, $^{4}CH_2$), 7.59-7.90 (m, $^{2}CH_2$, $^{3}CH_2$), 8.03-8.22 (m, $^{1}CH_2$)

3.3.2. Polycarbonate 24 Based on Monomer 6

Due to the high T_m of monomer **6**, the amount of DPC was increased to completely dissolve **6** in molten DPC during the first step. After cooling, the reaction mixture was dissolved in DMSO and added to MeOH. None of the listed parameters (*Table 3-5*) led to the formation of polymer **24**.

*Table 3-5: Parameters for the synthesis of polymer **24.***

Sample	T_1 [°C]	T_2 [°C]	Ratio [6]/[DPC]	Yield [%]
a	130	180	1/1.05	/[a]
b	120	165	1/1.4	minor
c	120	120	1/1.4	minor

[a]an insoluble brown residue has emerged

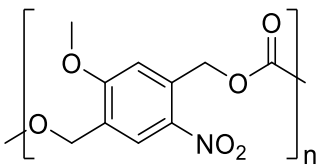

3.3.3. Polycarbonate 25 Based on BHED

After cooling, the residue was dissolved in THF and added to MeOH without causing precipitation. None of the listed parameters (*Table 3-6*) led to the formation of product **25**.

*Table 3-6: Parameters for the synthesis of polymer **25.***

Sample	T_1 [°C]	T_2 [°C]	Ratio [BHED]/[DPC]	Yield [%]
a	120	150	1/1.05	/
b	90	120	1/1.05	/
c	80[a]	100	1/1.05	/
d	80[a]	80	1/1.05	/

[a]was stirred overnight in a first step

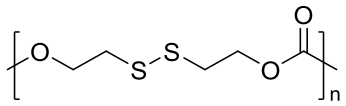

3.4. Synthesis of Polyurethanes

General Procedure of Polyaddition in Solution Employing DBTDL

In a two-neck round bottom flask, monomers (1 mmol in total) were dissolved in DMF under nitrogen atmosphere. The solution was heated under stirring and diisocyanate (DI; 1-1.1 mmol) was added dropwise. Subsequently, DBTDL (1 mol%) was added and the mixture was stirred for a certain amount of time. The reaction was stopped by addition of either MeOH or mPEG and the products were isolated by precipitation from a suitable solvent or dialysis as well as drying *in vacuo*.

3.4.1. LDI-Based Polyurethanes

*LDI-Based Polyurethane **26** from BHED*

After synthesis employing the parameters given in *Table 3-7*, the pure product was obtained as a transparent melt by precipitation from MeOH and drying *in vacuo*.

*Table 3-7: Parameters for the synthesis of polymer **26.***

Sample	T [°C]	Time [h]	$V_{Solvent}$ [mL]	Ratio [BHED]/[LDI]	Yield [%]
a	40	3	2	1/1.05	62
b	40	3	2[a]	1/1.05	55
c	50	overnight	1	1/1.05	95

[a]THF was used as solvent

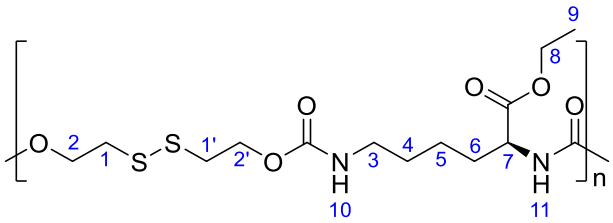

^{1}H-NMR (DMSO-d$_6$): δ [ppm] = 1.12-1.20 (m, $^9CH_3$), 1.21-1.45 (m, $^4CH_2$, $^5CH_2$), 1.46-1.71 (m, $^6CH_2$), 2.87-3.09 (m, $^3CH_2$, $^2CH_2$, $^{2'}CH_2$), 3.89-4.37 (m, ^7CH, $^8CH_2$, $^1CH_2$, $^{1'}CH_2$), 7.06-7.21 (m, ^{10}NH), 7.55-7.71 (m, ^{11}NH)

*LDI-Based Polyurethane **27** from Monomer **2***

In order to stop the polymerization employing the parameters given in *Table 3-8* MeOH was added and the pure polymer was obtained by precipitation from MeOH. After drying *in vacuo,* a yellow powder was obtained.

*Table 3-8: Parameters for the synthesis of polymer **27.***

Sample	T [°C]	Time [h]	$V_{Solvent}$ [mL]	Ratio [2]/[LDI]	Yield [%]
a	40	3.5	2	1/1.05	minor
b	40	overnight	2	1/1.05	57
c	50	overnight	1	1/1.05	98

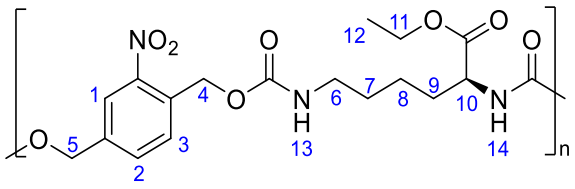

^{1}H-NMR (DMSO-d$_6$): δ [ppm] = 1.06-1.20 (m, $^{12}CH_3$), 1.21-1.47 (m, $^7CH_2$, $^8CH_2$), 1.49-1.73 (m, $^9CH_2$), 2.91-3.04 (m, $^6CH_2$), 3.89-4.15 (m, ^{10}CH, $^{11}CH_2$), 5.03-5.22 (m,

$^{5}CH_2$), 5.27-5.44 (m, $^{4}CH_2$), 7.28-7.42 (m, ^{13}NH), 7.58-7.90 (m, ^{2}CH, ^{3}CH, ^{14}NH), 8.00-8.14 (m, ^{1}CH)

*LDI-Based Co-Polyurethane **28** from Monomer **2** and BHED*

In order to stop the polymerization, which was performed employing the parameters given in *Table 3-9*, MeOH was added and the pure polymer was obtained by precipitation from MeOH. After drying *in vacuo,* a yellow sticky solid was obtained.

*Table 3-9: Parameters for the synthesis of polymer **28.***

Sample	T [°C]	Time [h]	$V_{Solvent}$ [mL]	Ratio [2]/[BHED]/[LDI]	Yield [%]
a	50	overnight	1	0.75/0.25/1.05	75
b	50	overnight	1	0.5/0.5/1.05	73
c	50	overnight	1	0.25/0.75/1.05	69

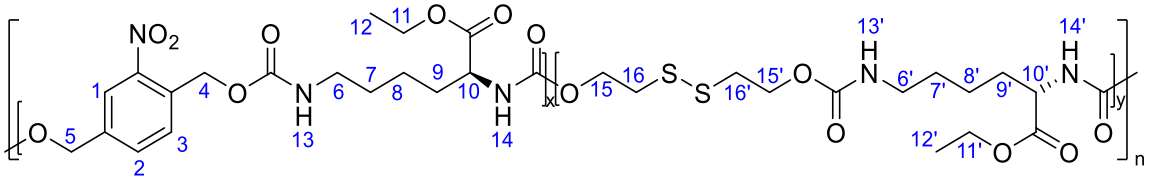

^{1}H-NMR (DMSO-d$_6$): δ [ppm] = 1.12-1.20 (m, $^{12}CH_3$, $^{12'}CH_3$), 1.21-1.45 (m, $^{7}CH_2$, $^{8}CH_2$, $^{7'}CH_2$, $^{8'}CH_2$), 1.46-1.71 (m, $^{9}CH_2$, $^{9'}CH_2$), 2.85-3.03 (m, $^{6}CH_2$, $^{6'}CH_2$, $^{15}CH_2$, $^{15'}CH_2$), 3.87-4.25 (m, ^{10}CH, $^{11}CH_2$, $^{10'}CH$, $^{11'}CH_2$, $^{16}CH_2$, $^{16'}CH_2$), 5.03-5.25 (m, $^{5}CH_2$), 5.27-5.44 (m, $^{4}CH_2$), 7.10-7.19 (m, $^{13'}NH$), 7.28-7.41 (m, ^{13}NH), 7.54-7.89 (m, ^{2}CH, ^{3}CH, ^{14}NH, $^{14'}NH$), 8.04-8.12 (m, ^{1}CH)

*LDI-Based Co-Polyurethane **29** from Monomer **2** and PEG400*

In order to stop the polymerization, which was performed employing the parameters given in *Table 3-10*, MeOH was added and the pure polymer was obtained by precipitation from MeOH except for sample **29c** which was precipitated from Et_2O. After drying *in vacuo,* a yellow sticky solid was obtained.

*Table 3-10: Parameters for the synthesis of polymer **29.***

Sample	T [°C]	Time [h]	$V_{Solvent}$ [mL]	Ratio [2]/[BHED]/[LDI]	Yield [%]
a	50	overnight	1	0.75/0.25/1.05	86
b	50	overnight	1	0.5/0.5/1.05	63
c	50	overnight	1	0.25/0.75/1.05	62

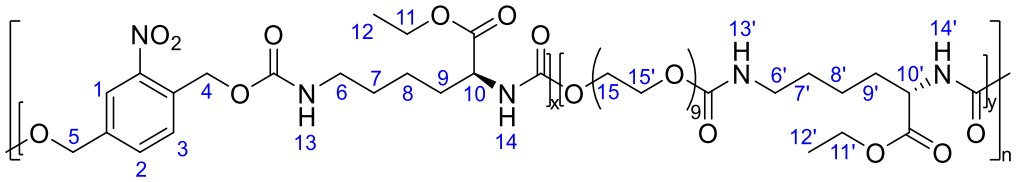

^{1}H-NMR (DMSO-d$_6$): δ [ppm] = 1.05-1.20 (m, $^{12}CH_3$, $^{12'}CH_3$), 1.21-1.46 (m, $^{7}CH_2$, $^{8}CH_2$, $^{7'}CH_2$, $^{8'}CH_2$), 1.47-1.73 (m, $^{9}CH_2$, $^{9'}CH_2$), 2.90-3.04 (m, $^{6}CH_2$, $^{6'}CH_2$), 3.45-3.59 (m, $^{15}CH_2$, $^{15'}CH_2$), 3.85-4.17 (m, ^{10}CH, $^{11}CH_2$, $^{10'}CH$, $^{11'}CH_2$), 5.04-5.23 (m, $^{5}CH_2$), 5.25-5.44 (m, $^{4}CH_2$), 7.09-7.20 (m, $^{13'}NH$), 7.28-7.46 (m, ^{13}NH), 7.54-7.91 (m, ^{2}CH, ^{3}CH, ^{14}NH, $^{14'}NH$), 8.02-8.13 (m, ^{1}CH)

*LDI-Based Polyurethane **30** from Monomer **6***

The same parameters as for sample **27c** (*Table 3-8*) were used for the polymerization. After the reaction was stopped by addition of MeOH, the pure polymer was obtained as a light-yellow powder by precipitation from MeOH and drying *in vacuo* (55%).

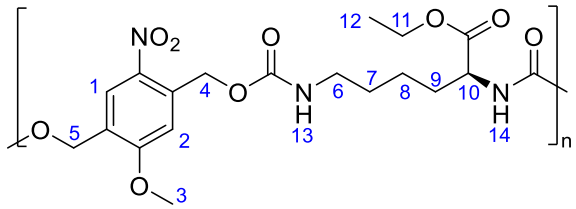

^{1}H-NMR (DMSO-d$_6$): δ [ppm] = 1.07-1.20 (m, $^{12}CH_3$), 1.21-1.48 (m, $^{7}CH_2$, $^{8}CH_2$), 1.49-1.74 (m, $^{9}CH_2$), 2.91-3.05 (m, $^{6}CH_2$), 3.88-4.15 (m, $^{3}CH_3$, ^{10}CH, $^{11}CH_2$), 5.33-5.52 (m, $^{5}CH_2$), 5.67-5.79 (m, $^{4}CH_2$), 7.19-7.29 (m, ^{2}CH), 7.31-7.54 (m, ^{13}NH), 7.79-8.03 (m, ^{14}NH), 8.09-8.20 (m, ^{1}CH)

*LDI-Based Polyurethane **31** from Monomer **13***

The same parameters as for sample **27c** (*Table 3-8*) were used for the polymerization of samples **31a** and **31b**. In case of sample **31a** the reaction was stopped by addition

of MeOH, and the pure product was obtained as a light-yellow powder by precipitation from MeOH and drying *in vacuo* (82%). In case of **31b** the reaction was stopped by addition of mPEG5000 in DMF and the pure product was obtained as a light-yellow powder after dialysis as well as drying *in vacuo* (80%).

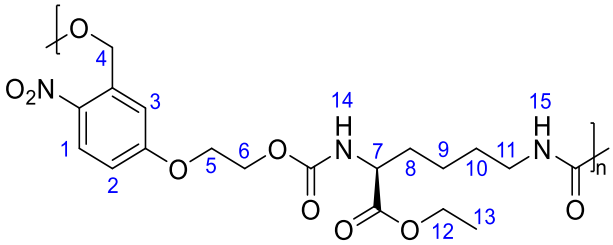

^{1}H-NMR (DMSO-d$_6$): δ [ppm] = 1.11-1.20 (m, $^{13}CH_3$), 1.21-1.47 (m, $^{9}CH_2$, $^{10}CH_2$), 1.48-1.73 (m, $^{8}CH_2$), 2.83-3.07 (m, $^{11}CH_2$), 3.90-4.15 (m, ^{7}CH, $^{12}CH_2$), 4.20-4.41 (m, $^{5}CH_2$, $^{6}CH_2$), 5.29-5.52 (m, $^{4}CH_2$), 7.04-7.20 (m, ^{1}CH, ^{2}CH), 7.21-7.53 (m, ^{15}NH), 7.67-7.98 (m, ^{14}NH), 8.11-8.23 (m, ^{3}CH)

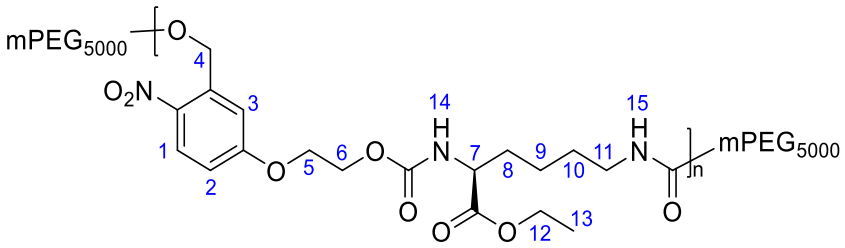

^{1}H-NMR (DMSO-d$_6$): δ [ppm] = 1.11-1.20 (m, $^{13}CH_3$), 1.21-1.47 (m, $^{9}CH_2$, $^{10}CH_2$), 1.48-1.73 (m, $^{8}CH_2$), 2.83-3.07 (m, $^{11}CH_2$), 3.47-3.56 (m, mPEG5000), 3.90-4.15 (m, ^{7}CH, $^{12}CH_2$), 4.20-4.41 (m, $^{5}CH_2$, $^{6}CH_2$), 5.29-5.52 (m, $^{4}CH_2$), 7.04-7.20 (m, ^{2}CH, ^{3}CH), 7.21-7.53 (m, ^{15}NH), 7.67-7.98 (m, ^{14}NH), 8.11-8.23 (m, ^{3}CH)

*LDI-Based Polyurethane **32** from Monomer **17***

The same parameters as for sample **27c** (*Table 3-8*) were used for the polymerization of samples **32a** and **32b**. In case of sample **32a** the reaction was stopped by addition of MeOH, and the pure product was obtained as a light-yellow powder by precipitation and drying *in vacuo* (72%). In case of **32b** the reaction was stopped by addition of mPEG5000, and the crude product was obtained by precipitation from Et_2O. The crude product was dissolved in DCM, washed twice with brine and added to Et_2O yielding the pure product as a light-yellow powder after drying *in vacuo* (59%).

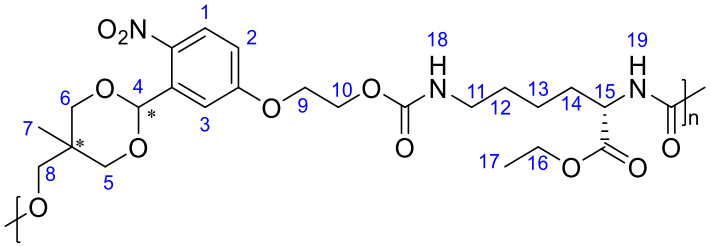

^{1}H-NMR (DMSO-d$_6$): δ [ppm] = 0.66-0.78 (m, $^{7}CH_3$), 1.10-1.21 (m, $^{17}CH_3$), 1.21-1.46 (m, $^{13}CH_2$, $^{12}CH_2$), 1.47-1.71 (m, $^{14}CH_2$), 2.95 (br, $^{11}CH_2$), 3.65-3.98 (m, $^{15}CH_2$, $^{5}CH_2$, $^{6}CH_2$), 4.00-4.19 (m, ^{16}CH, $^{9}CH_2$), 4.24-4.36 (br, $^{10}CH_2$, $^{8}CH_2$), 5.92-6.04 (m, ^{4}CH), 7.03-7.28 (m, ^{19}NH, ^{2}CH, ^{3}CH), 7.48-7.71 (m, ^{18}NH), 7.94-8.02 (m, ^{1}CH)

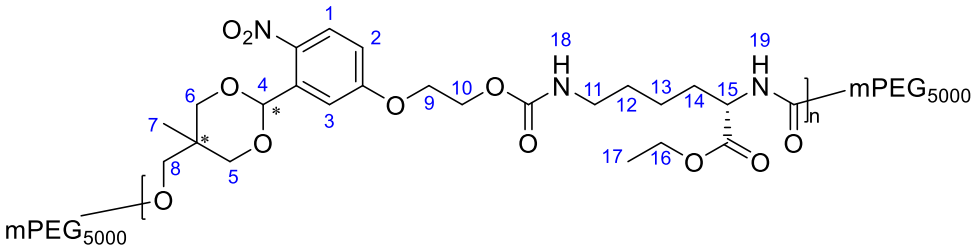

^{1}H-NMR (DMSO-d$_6$): δ [ppm] = 0.66-0.78 (m, $^{7}CH_3$), 1.10-1.21 (m, $^{17}CH_3$), 1.21-1.46 (m, $^{13}CH_2$, $^{12}CH_2$), 1.47-1.71 (m, $^{14}CH_2$), 2.95 (br, $^{11}CH_2$), 3.51 (s, mPEG5000), 3.65-3.98 (m, $^{15}CH_2$, $^{5}CH_2$, $^{6}CH_2$), 4.00-4.19 (m, ^{16}CH, $^{9}CH_2$), 4.24-4.36 (br, $^{10}CH_2$, $^{8}CH_2$), 5.92-6.04 (m, ^{4}CH), 7.03-7.28 (m, ^{19}NH, ^{2}CH, ^{3}CH), 7.48-7.71 (m, ^{18}NH), 7.94-8.02 (m, ^{1}CH)

*LDI-Based Polyurethane **33** from Monomer **9***

The polymerization employing the parameters given in *Table 3-11* was stopped by addition of MeOH, and the pure product was obtained as a light-yellow powder by precipitation from MeOH as well as drying *in vacuo*.

*Table 3-11: Parameters for the synthesis of polymer **33**.*

Sample	T [°C]	Time [h]	$V_{Solvent}$ [mL]	Ratio [9]/[LDI]	Yield [%]
a	50	overnight	1	1/1.05	/[a]
b	40	48	1	1/1.05	4
c	40	overnight	1[b]	1/1.05	18
d	45	overnight	1	1/1.05	24

[a]an insoluble residue has emerged; [b]THF was used as solvent

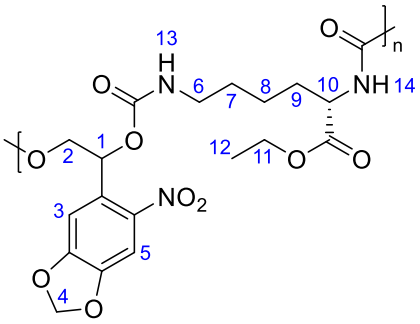

^{1}H-NMR (DMSO-d$_6$): δ [ppm] = 1.10-1.40 (m, $^{7}CH_2$, $^{8}CH_2$, $^{12}CH_3$), 1.45--1.70 (br, $^{9}CH_2$), 2.84-3.02 (br, $^{6}CH_2$), 3.80-4.13 (br, ^{10}CH, $^{11}CH_2$), 4.29-4.40 (br, $^{2}CH_2$), 6.03-6.33 (br, ^{1}CH, $^{4}CH_2$), 6.99-7.99 (m, ^{3}CH, ^{5}CH, ^{13}NH, ^{14}NH)

3.4.2. IPDI-Based Polyurethanes

*IPDI-Based Polyurethane **34** from Monomer **2***

The polymerization of all samples (*Table 3-12*) was stopped by addition of isophorone diamine (0.5 mL; 2.7 mmol) dissolved in DMF (1 mL). The mixture was subsequently poured into MeOH, whereas the pure product precipitated as a white powder which was isolated and dried *in vacuo*.

*Table 3-12: Parameters for the synthesis of polymer **34**.*

Sample	T [°C]	Time [h]	$V_{Solvent}$ [mL]	Ratio [2]/[IPDI]	Yield [%]
a	50	70	1	1/1.05	9
b	70	70	1	1/1.05	58
c	90	48[a]	1	1/1.05	/

[a]an insoluble residue has emerged after 48 h

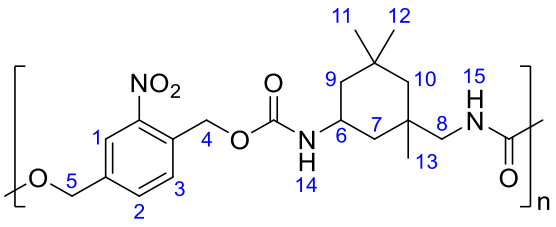

^{1}H-NMR (DMSO-d$_6$): δ [ppm] = 0.65-1.17 (m, $^{9}CH_2$, $^{10}CH_2$, $^{11}CH_3$, $^{12}CH_3$, $^{13}CH_3$), 1.27-1.69 (m, $^{7}CH_2$), 2.61-2.86 (m, $^{8}CH_2$), 3.64-3.72 (m, ^{6}CH), 5.00-5.19 (m, $^{5}CH_2$), 5.25-5.40 (m, $^{4}CH_2$), 7.16-7.50 (m, ^{3}CH, ^{15}NH), 7.57-7.80 (m, ^{2}CH, ^{14}NH), 8.00-8.14 (br, ^{1}CH)

*IPDI-Based Polyurethane **35** from Monomer **9***

The same parameters as for sample **34b** (*Table 3-12*) were used for the synthesis of polymer **35** and the reaction was stopped by addition of MeOH. Precipitation from MeOH yielded a light-yellow powder (68%).

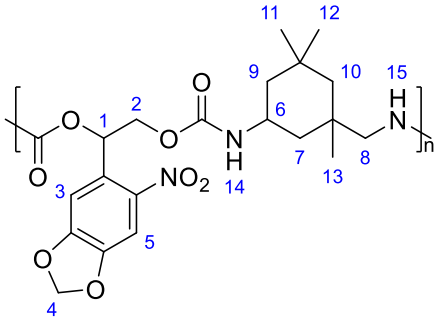

^{1}H NMR (DMSO-d6): δ [ppm] = 0.68-1.15 (m, $^{9}CH_2$, $^{10}CH_2$, $^{11}CH_3$, $^{12}CH_3$, $^{13}CH_3$), 1.27-1.69 (m, $^{7}CH_2$), 2.58-3.16 (m, $^{8}CH_2$), 3.42-3.77 (m, ^{6}CH), 4.06-4.56 (m, 2H, $^{2}CH_2$), 6.08-6.33 (m, ^{1}CH, $^{4}CH_2$), 7.01-7.50 (m, ^{3}CH, ^{14}NH, ^{15}NH), 7.64 (m, ^{5}CH)

3.4.3. HDI-Based Polyurethanes

*HDI-Based Polyurethane **36** from BHED*

The polymerizations were carried out employing the parameters given in *Table 3-13*. A white precipitate was formed after 10 min of reaction in case of **36a** and the polymerization was stopped by addition of MeOH after 1 h yielding an insoluble white precipitate as a product. In case of sample **36b**, the reaction mixture turned into an insoluble swollen gel after 10 min. Sample **36c** was stopped by addition of MeOH leading to the formation of an insoluble white precipitate.

*Table 3-13: Parameters for the synthesis of polymer **36.***

Sample	T [°C]	Time [h]	$V_{Solvent}$ [mL]	Ratio [BHED]/[HDI]	Yield [%]
a	40	1	2	1/1.05	/[a]
b	80	/	2	1/1.05	/[a]
c	RT	overnight	2	1/1.05	/[a]

[a]an insoluble residue has emerged

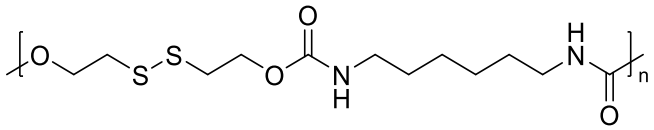

*HDI-Based Polyurethane **37** from Monomer **2***

The reaction mixture was stirred in an ice bath before HDI was added. Afterwards the ice bath was removed and the solution was stirred at room temperature overnight yielding a swollen gel. MeOH was added to stop the reaction.

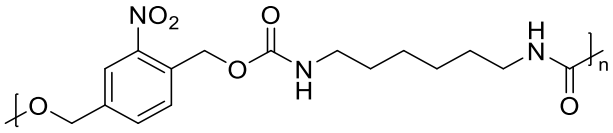

*HDI-Based Polyurethane **38** from Monomer **13***

A swollen gel was formed after 10 min synthesizing sample **38a**. In case of **38b** (*Table 3-14*) the reaction mixture was stirred in an ice bath before HDI was added. The reaction was stopped by addition of MeOH and a white powder was obtained by precipitation from MeOH.

*Table 3-14: Parameters for the synthesis of polymer **38.***

Sample	T [°C]	Time [h]	$V_{Solvent}$ [mL]	Ratio [13]/[HDI]	Yield [%]
a	50	/[a]	1	1/1.05	/
b	RT	overnight	1	1/1.05	minor

[a]an insoluble residue has emerged after 10 min

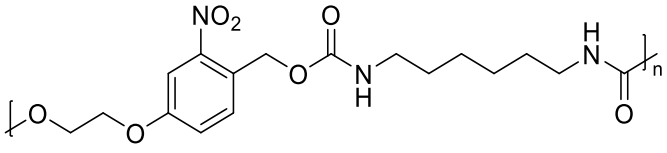

3.5. Synthesis of Polyesters

General Procedure of Polycondensation using Adipoylchloride

In a typical procedure, diol monomer (1 mmol) and pyridine (1 mL; 12.5 mmol) were dissolved in DMF (3 mL) under nitrogen atmosphere. ADP (0.16 mL; 1.1 mmol) dissolved in DCM (2 mL) was added dropwise and the solution was stirred overnight at room temperature. MeOH was added to stop the polymerization and the reaction mixture was poured into MeOH.

3.5.1. Polyester 39 from Monomer 2

No product was obtained.

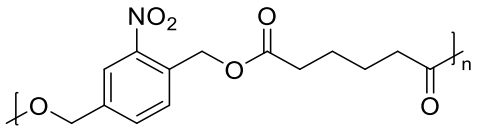

3.5.2. Polyester 40 from Monomer 13

No product was obtained.

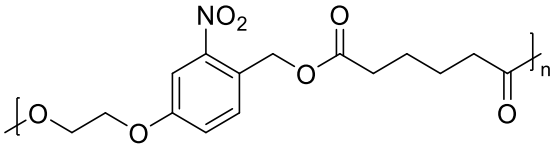

3.5.3. Polyester 41 from Monomer 9

THF was used as a solvent instead of a DMF/DCM mixture. In case of samples **41b-41c** (*Table 3-15*) DMAP was used as a catalyst. None of the listed parameters led to the successful synthesis of polyester **41**.

*Table 3-15: Parameters for the synthesis of polymer **41.***

Sample	T [°C]	Time [h]	$V_{Solvent}$ [mL]	n_{DMAP} [µmol]	Yield [%]
a	RT	48	5	/	/
b	RT	overnight	5	3	/
c	RT	overnight	5	50	/
d	50	overnight	5	7.5	/

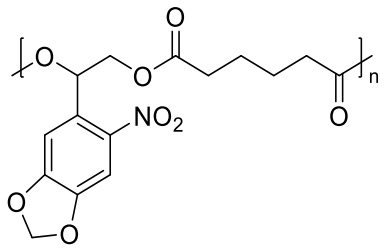

3.6. Analysis and Application

3.6.1. Investigation of Stimuli-Triggered Degradation

UV/Vis Analysis of Light-Triggered Degradation in Solution

Light-responsive material was dissolved in DCM (40 mg/L) and exposed to UV light in a quartz cuvette for certain periods of time. For sample **35** DMSO (0.2 vol%) was added due to a lower solubility in DCM. The absorbance change of the polymer solution was monitored by a UV/Vis spectrophotometer.

SEC Analysis of Light-Triggered Degradation

Stock solutions of light-responsive polymer in DCM (1.6 mg/mL) were prepared and aliquots of these solutions were irradiated with UV light in a quartz cuvette for 30 s, 90 s, 150 s and 240 s. For sample **35** DMSO (4 vol%) was added due to a lower solubility in DCM. After irradiation, the samples were dried *in vacuo* and subsequently measured via SEC in THF.

*MS Analysis of Light-Triggered Degradation of Compound **20***

Analogously to the SEC investigations, light-responsive model compound **20** was dissolved in DCM (1.5 mg/mL) and irradiated with UV light in a quartz cuvette for 150 s.

The sample was dried *in vacuo* after irradiation and measured via ESI-ToF MS.

*SEC Analysis of Redox-Triggered Degradation of Samples **28a-28c***

The redox-responsive copolymers were dissolved in THF (6 mg/mL) and 1 mL of each solution was precipitated dropwise under stirring into aqueous dithiothreitol (DTT) solution (10 mL; 10 mM) under nitrogen atmosphere. The mixtures were stirred overnight, subsequently centrifuged and the isolated solid residues were analyzed by SEC in THF.

3.6.2. Formation of Micelles, Nano- and Microparticles

Formation of Blank Nanoparticles

Nanoparticles from polymers **21**, **26** and **27** were prepared by a nanoprecipitation method using different solvents. While THF was used for polymer **21**, DMSO was used for polymers **26** and **27**. In general, the polymer (10 mg) was dissolved in the organic solvent (1 mL) and added dropwise to a vigorously stirred aqueous PVA solution (2 %). After the mixture was stirred overnight, the nanoparticles were purified by repeated centrifugation and redispersion in water (10 mL). The aqueous nanoparticle dispersions were analyzed regarding size and size distribution employing a Zetasizer Nano-ZS.

Formation of Nile Red Loaded Nanoparticles

Nile red loaded nanoparticles were prepared in the same fashion as the blank particles only differing in the addition of nile red (0.2 mg) to the polymer solution.

Formation of Blank Microparticles

In a typical method, polymer (10 mg) was dissolved in DCM (1 mL) and added to either a 2.5%, 5% or 7.5% aqueous PVA solution (10 mL). After emulsification for 30 s using an Ultra-Turrax®, a magnetic stirring bar was added, and the emulsion was stirred vigorously overnight to evaporate the organic solvent. The particles were purified by centrifugation and redispersed in water.

Formation of Nile Red Loaded Microparticles

The model compound loaded particles were formed in the same fashion as the blank microparticles only differing in the addition of nile red (0.2 mg) to the polymer DCM solution. Based on the findings of blank microparticle formation, a concentration of 2.5% PVA was used for the nile red loaded microparticles.

Formation of Blank Micelles

PBS (pH 7.4; 1 mL) was added to a solution of polymer in THF (0.1 mL; 10 mg/mL) and the mixture was kept in the dark without stirring until the organic solvent was evaporated.

Formation of Nile Red Loaded Micelles

Analogously to the blank micelles, polymer (1 mg) was dissolved in a solution of nile red in THF (0.1 mL; 2 mg/mL) and, subsequently, pH 7.4 PBS (1 mL) was added. The obtained mixture was filtrated to remove the precipitated excess nile red, yielding a clear purple solution, which was stored in the dark. For the analysis, one aliquot of this solution was added to pH 7.4 PBS (1 mL) and let sit for 15 min prior to the measurement.

3.6.3. Characterization of Triggered Micelle, Nano- and Microparticle Degradation

DLS Analysis of Light-Induced Nanoparticle and Micelle Degradation

One aliquot of the initial suspension was diluted to a concentration of 0.1 mg/mL with the solvent used for preparation and filled into a quartz cuvette. The sample was measured via DLS, irradiated with UV light and, subsequently, measured again.

DLS Analysis of Redox-Induced Nanoparticle Degradation

One aliquot of the particle suspension was diluted with water to a concentration of 0.1 mg/mL and filled into a cuvette. The sample was measured via DLS, treated with

DTT until a concentration of 10 mmol/L was reached and, subsequently, measured again.

DLS Analysis of pH-Induced Micelle Degradation

One aliquot of the micelle suspension was added to buffered solutions at pH 7.4, 5 and 3 (0.1 mg/mL) and DLS measurements of the obtained samples were carried out.

Fluorescence Measurements of Light-Induced Nile Red Release

In a typical procedure, one aliquot of the initial suspension was diluted to a concentration of 0.1 mg/mL with the solvent used for preparation and filled into a quartz cuvette. Fluorescence spectroscopy was measured and afterwards the sample was exposed to UV light for different periods of time, while a fluorescence measurement was carried out after each irradiation step.

4. Results

4.1. Synthesis of Low Molecular Weight Compounds

4.1.1. (2-Nitro-1,4-phenylene)dimethanol (Monomer 2)

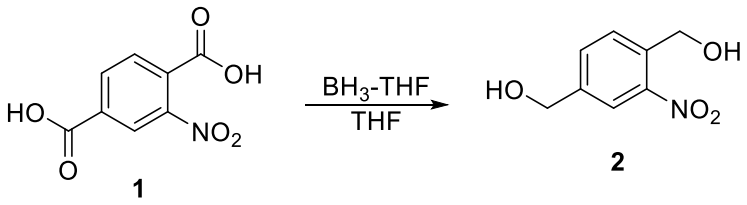

*Scheme 4-1: Synthesis of monomer **2**.*

As a first light-responsive monomer, **2** was synthesized by a modified procedure published by Klinger *et al.* (*Scheme 4-1*) to gain access to backbone-degradable polymers.[94] In short, BH_3-THF complex solution was used to reduce 2-nitroterephthalic acid to **2** at 50 °C. In contrast to the published procedure, a modified aqueous workup was necessary to separate the raw product from side products like boric acid. After recrystallization from $CHCl_3$ 71% of light-yellow to white needles were obtained as the pure product, which was proven by NMR. Though the procedure was performed several times, in no case the reported yield of 91 %[94] could be reached. In addition, UV/Vis analysis of compound **2** in DCM solution revealed an absorbance maximum (λ_{max}) at 267 nm, which is in the typical wavelength range of similar oNB structures.[85] Diol **2** consists of a light-responsive *ortho*-nitrobenzylic hydroxyl function and a non-light-responsive benzylic hydroxyl group. On the one hand, these benzylic functions should have a similar reactivity towards addition or condensation reactions compared to alkylic alcohols, which is advantageous for copolymerization. On the other hand, the difference in light-responsiveness of both hydroxyl functions offers the possibility of polymer degradation product modification by copolymerization.

4.1.2. (2-Methoxy-5-nitro-1,4-phenylene)dimethanol (Monomer 6)

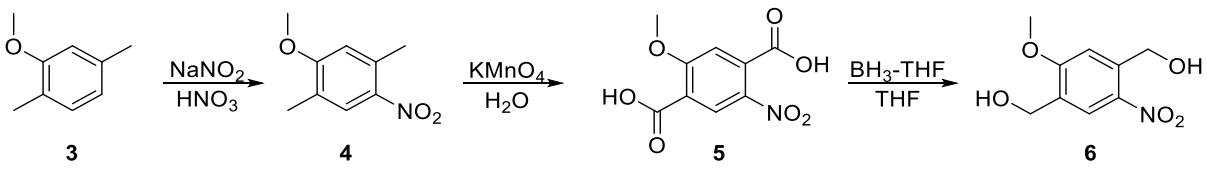

*Scheme 4-2: Synthesis of monomer **6**.*

Due to the UV absorption of human tissue, light of higher wavelength is typically desired for medical applications. In order to enable polymer degradation at higher wavelength, light-responsive monomers with red-shifted λ_{max} should be synthesized. The synthesis of novel monomer **6** was carried out in three steps (*Scheme 4-2*) using modified procedures reported in the literature.[119] Starting from 2,5-dimethylanisol (**3**), pure **4** was obtained in a yield of 48% by nitration in HNO_3 and recrystallization from MeOH. Using MeOH for recrystallization was found to improve the yield compared to the EtOH/H_2O mixture suggested in the literature. Nevertheless, the reported yield of 73% could not be achieved repeatedly. In a second step, **4** was oxidized employing $KMnO_4$ in water, yielding 32% of **5**. Upon heating the mixture to reflux, as reported in the literature, significant amounts of **4** crystallized from the cooler possibly leading to decreased yields. Thus, the reaction temperature was lowered to 80 °C which reduced the loss of **4** but did not lead to higher yield. Analogously to monomer **2**, final diol **6** was obtained by recrystallization from THF in a yield of 78% after reduction using BH_3-THF. Due to a lower solubility of **6**, the crude product precipitated from the aqueous phase simplifying separation from the side products. Though all syntheses were performed several times, the acquired yields of all steps were significantly lower compared to the findings provided by the literature. The successful synthesis of the products was confirmed by ^{1}H NMR spectroscopy after each step. Additionally, **6** was characterized by ^{13}C NMR, ATR-FTIR as well as MS measurements. UV/Vis analysis of **6** revealed a λ_{max} value of 317 nm in MeCN solution which is in line with similar structures reported in the literature.[85] UV/Vis analysis using DCM as a solvent was not possible due to low solubility of **6**. The increase in λ_{max} compared to monomer **2** is due to the electron donating methoxy group which is known to induce bathochromic shifts on such compounds. Determination of the melting point showed a T_m of 199.5 °C.

4.1.3. (S)-1-(6-Nitrobenzo[d][1,3]dioxol-5-yl)ethane-1,2-diol (Monomer 9)

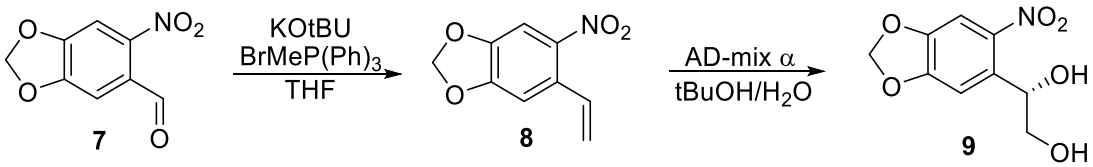

*Scheme 4-3: Synthesis of monomer **9**.*

Nitropiperonal (**7**) based diol **9** contains a light-responsive secondary hydroxyl group

instead of a primary, which is known to enhance the quantum yield of the photoreaction. In addition, the *ortho*-nitrosobenzoketone derivatives formed as a product of the light-triggered degradation are known to be less toxic than the analogous aldehydes.[85] Starting from 6-nitropiperonal (**7**), monomer **9** was synthesized in two steps (*Scheme 4-3*). In a first step, a Wittig reaction was performed employing $MePh_3P^+Br^-$ and KOtBu in THF. Purification by column chromatography yielded 60% of styrene derivative **8** as determined by NMR. In a second step, compound **8** was dihydroxylated via Sharpless dihydroxylation yielding 75% of diol **9** after purification by column chromatography. In a first attempt, $KMnO_4$ was used for the dihydroxylation of **8** but no product was obtained, thus Sharpless dihydroxylation was employed as a convenient method for the preparation of **9**. The successful synthesis of the monomer was determined by NMR spectroscopy as well as MS, while the T_m was determined to be 101.0 °C. UV/Vis analysis in DCM solution revealed absorbance maxima at 298 nm and 348 nm. Compared to monomer **6**, λ_{max} is even further increased due to the second electron donating group of **9**. In contrast to the quantum yield, λ_{max} is only slightly affected by the secondary hydroxyl group.[85]

4.1.4. 2-((3-Hydroxymethyl)-4-nitrophenoxy)ethan-1-ol (Monomer 13)

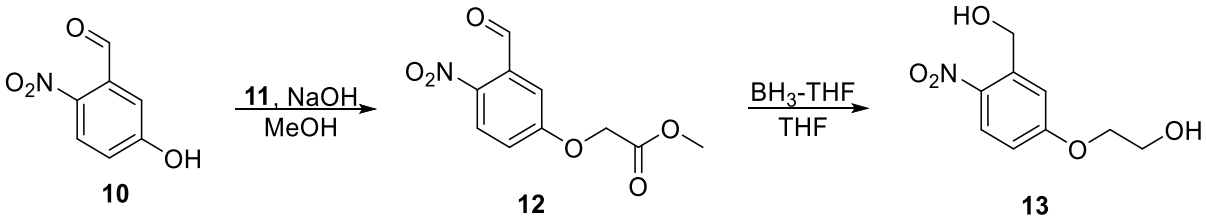

*Scheme 4-4: Synthesis of monomer **13**.*

Monomer **13** was developed as an alternative to monomer **6** offering less steric hinderance with very similar λ_{max} values by introduction of the hydroxy ethoxy group to the aromatic core instead of the methoxy and hydroxymethyl functions of **6**. Furthermore, the route (*Scheme 4-4*) used to prepare **13** exhibits greater versatility, potentially enabling further functionalization of the monomer, e.g., by variation of the electrophile for the etherification reaction. Based on modified literature procedures, novel monomer **13** was synthesized in two steps starting from 5-hydroxy-2-nitrobenzaldehyde (**10**).[94],[120] At first, **12** was obtained by etherification of **10** with methyl acetylbromide (**11**) employing NaOH in MeOH. NMR analysis proved

the successful synthesis and the obtained yield of 67% aligns with the results provided in the literature (71%). Analogously to **2**, monomer **13** was synthesized successfully in a yield of 50% by reduction of **12** using BH_3-THF and recrystallization from $CHCl_3$ as confirmed by NMR and MS analysis. The UV/Vis analysis of the product revealed a λ_{max} of 310 nm in DCM, which is similar to **6** proving the structural similarity and equal bathochromic shifts. In contrast, the determined T_m of 116.0 °C is significantly lower than the T_m of **6**. Overall, the synthesis of **13** proved to be advantageous due to greater experimental convenience as well as a higher combined yield compared to monomer **6**.

4.1.5. 2-(3-(5-(Hydroxymethyl)-5-methyl-1,3-dioxan-2-yl)-4-nitrophenoxy)ethan-1-ol (Monomer 17)

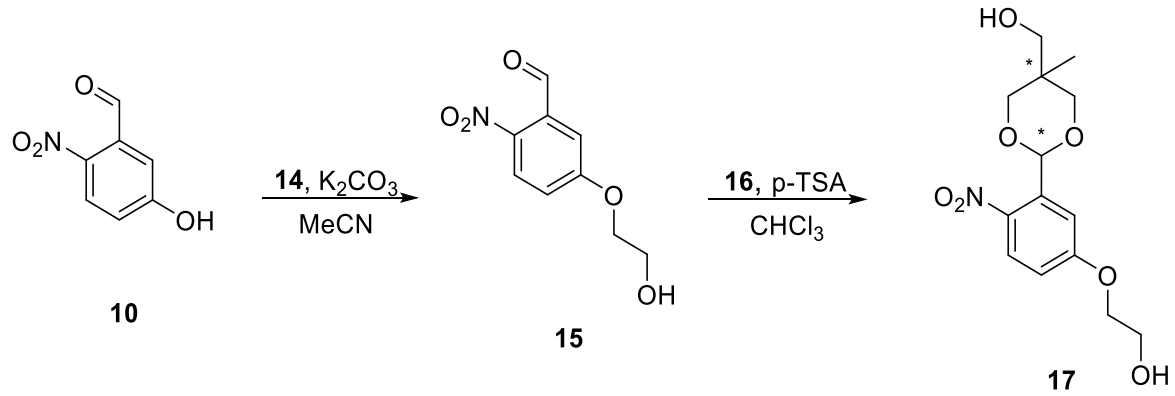

*Scheme 4-5: Synthesis of monomer **17**.*

As a first modification of **13**, pH- and light-responsive monomer **17** was synthesized in two steps (*Scheme 4-5*). Considering the metabolism driven acidification of the tumor microenvironment, lowered pH appeared to be a suitable second trigger to improve the DDS targeting ability.[98] Starting from **10**, 2-bromoethanol (**14**) was used for etherification in MeCN with K_2CO_3 as a base yielding 67% of **15** in a first step. Although column chromatography was used to obtain the pure product, further investigation revealed the crude product after aqueous work up to be sufficiently pure for the second step. In a second step, a typical pTSA catalyzed acetalization in $CHCl_3$ was carried out using a dean-stark trap to obtain monomer **17** from **15** and 1,1,1-tris(hydroxymethyl)ethane (**16**). Without further purification 68% of the pure product was yielded as confirmed by NMR, IR and MS measurements. In line with similar acetal compounds reported in the literature,[121] the NMR measurements

revealed distinguishable peaks for the *cis* and *trans* isomer of **17**. A separation of these isomers was not possible. However, since no difference in hydroxyl group reactivity was expected, a separation was not necessary for the following polymerization. In addition, a T_m of 96.4 °C was determined.

4.1.6. Benzyl (2-nitrobenzyl) carbonate (Model Compound 20)

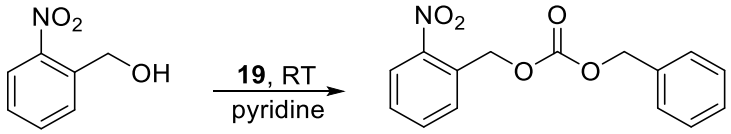

18 **20**

*Scheme 4-6: Synthesis of model compound **20**.*

In order to gain a better insight into the light-triggered polymer degradation a low molecular weight model compound which resembles the backbone of polycarbonate **21** should be synthesized. Thus, **20** was prepared by condensation of 2-nitrobenzylalcohol with benzylchloroformate in pyridine at room temperature (*Scheme 4-6*). The crude product was purified employing column chromatography yielding 40% of a white waxy solid as the pure product as confirmed by NMR as well as MS analysis. UV/Vis analysis revealed a λ_{max} of 260 nm in DCM solution, which is in line with the results of polycarbonate **21**. Furthermore, a T_m of 51.7 °C was determined.

4.2. Synthesis of Polycarbonates

For the polycarbonate synthesis a phosgene-free polycondensation in the melt using LiAcac as a catalyst and DPC was applied, which typically consisted of two steps. In a first step the reaction mixture was heated until melting under a nitrogen atmosphere and stirred until equilibrium between hydroxyl-terminated oligomers and phenyl carbonate-terminated oligomers was reached. In a second step vacuum was applied and the temperature was increased further to remove phenol and shift the equilibrium to the product side. The use of DPC instead of phosgene is considered less toxic, safer to use as well as less harmful to the environment from a green chemistry perspective.[52] However, this of course presumes a phosgene-free preparation of

DPC, e.g., from DMC.[53] Since higher reaction temperatures are necessary to melt the reaction mixture, temperature-sensitive compounds can be degraded during the process.

4.2.1. Polycarbonates from Monomer 2

*Homopolymer **21***

For the preparation of homopolymer **21** (*Scheme 4-7*), **2** and DPC were added in a ratio of 1/1.05.

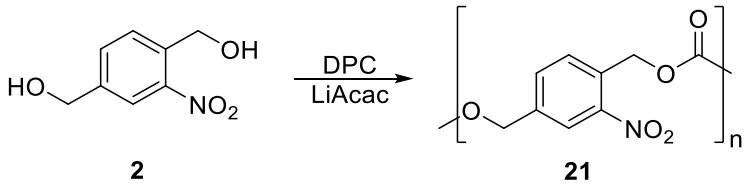

2 **21**

*Scheme 4-7: Synthesis of homopolymer **21**.*

In a first step a reaction temperature of 130 °C was sufficient to melt both, DPC and **2**, enabling formation of oligomeric carbonates. Three different temperatures were tested as a second step in order to achieve maximum conversion and M_n (*Table 4-1*). The crude product resulting from the synthesis was purified by precipitation in MeOH.

*Table 4-1: Results of the synthesis of homo-polycarbonate **21**.*

Sample	T_2 [°C]	M_n[b] [g/mol]	Đ[b]	Yield [%]
a	150	3500	1.7	49
b	165	9300	2.1	82
c	180	3900	1.8	/[a]

[a]an insoluble brown residue has emerged

[b]determined via SEC in THF (PS-calibration)

Sample **21b** showed the best results of the tested parameters, while sample **21a** in comparison exhibited significantly reduced yield and only low M_n as observed by SEC in THF. Possible reasons for this are an increased reaction rate as well as increased removal of the phenol side product due to the higher temperature in case of **21b**. Further increase of T_2 led to the formation of an insoluble brown residue during synthesis of sample **21c**, indicating the temperature-induced degradation of the

monomer. The SEC results shown for sample **21c** were acquired by stirring the residue in THF overnight and isolating the supernatant for measurement. Sample **21b** showed good solubility in typical organic solvents like THF, DCM, DMSO and DMF. Measurements of the thermal properties of **21b** were performed by DSC revealing a T_g of 50.1 °C.

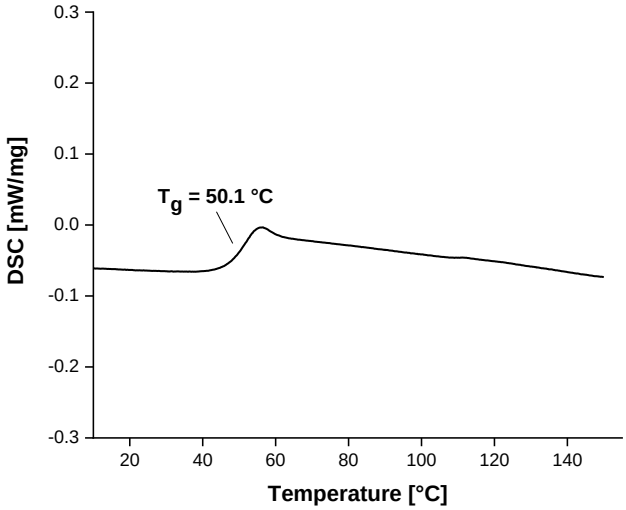

*Figure 4-1: DSC result of homopolymer **21**.*

In addition, UV/Vis measurements of **21b** in DCM solution showed a λ_{max} value of 260 nm, which is in line with the monomer and model compound **20**.

*Copolymer **22** using BD*

As the properties of a polymer directly correlate with the nature of their built-in compounds, copolymerization is regarded a powerful tool for tailoring the functionality and applicability of a polymer.[122] Based on the results of the homopolymerization, the synthesis of copolymers should be tested using BD as a cheap and well-known hydrophobic comonomer (*Scheme 4-8*).[6]

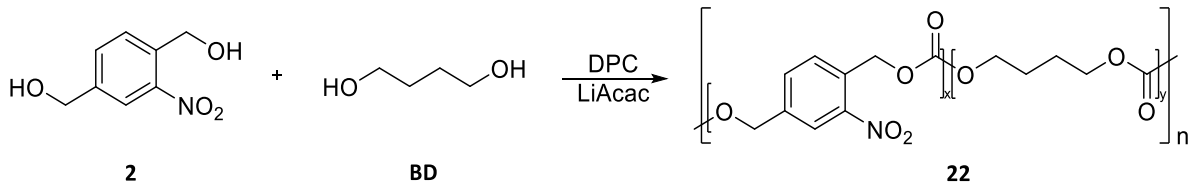

*Scheme 4-8: Synthesis of copolymer **22**.*

Since no thermal degradation was expected from BD, the ideal values for T_1 and T_2 of the homopolymer synthesis were used for synthesis of the copolymers. Variation of the monomer/DPC ratio was investigated (*Table 4-2*) to optimize the copolymerization.

*Table 4-2: Results of the synthesis of co-polycarbonate **22**.*

Sample	Ratio [2]/[BD]/[DPC][a]	Ratio [2]/[BD][b]	M_n[c] [g/mol]	Đ[c]	Yield [%]
a	0.5/0.5/1.05	/	6300	2.4	23
b	0.5/0.5/1.2	1/1.3	8500	2.6	61
c	0.5/0.5/1.3	/	3000	1.8	minor
d	0.75/0.25/1.2	2.9/1	5000	2.3	57
e	0.25/0.75/1.2	1/6.6	5600	1.6	60

[a]feed ratio; [b]determined via NMR in DMSO-d_6; [c]determined via SEC in THF (PS-calibration)

Even though sample **22a** showed a higher M_n using the ideal feed ratio of homopolymer **21**, as observed by SEC in THF, only a small yield was obtained. Thus, higher amounts of DPC in the reaction mixture were evaluated. While **22c** showed only minor yield and low M_n, **22b** revealed satisfying yield and high M_n, proving a monomer/DPC ratio of 1/1.2 as being ideal. In addition to the 1/1 samples **22a-c**, the comonomer ratio was varied to test the capability of the copolymerization. Both, sample **22d** and **22e**, showed higher M_n and similar yields compared to sample **22b**. In contrast, only the comonomer ratio of sample **22d** is in good accordance with the feed as observed by NMR measurements. Sample **22b** exhibited only a small excess of BD but sample **22e** showed a significantly increased amount of BD compared to the initial feed. This lack of experimental reproducibility limited the applicability of the procedure for copolymerization with BD.

*Copolymer **23** using PEG1000*

In addition to BD, PEG1000 was tested as a common hydrophilic comonomer employing the synthesis parameters of sample **22b** (*Scheme 4-9*).[7] Besides the altered solubility of the polymer and its degradation products, the incorporation of PEG into a polymeric matrix for drug delivery applications, either by using copolymers or polymer blends, is known to enhance the circulation lifetimes by formation of a PEG hydrating layer on the particle surface.[35]

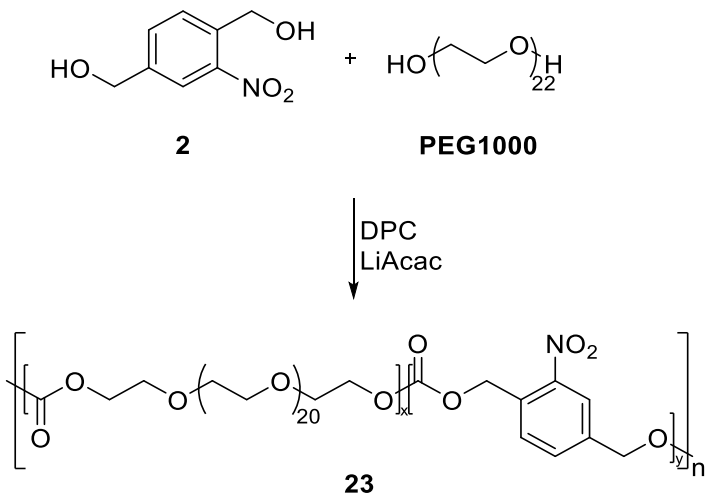

*Scheme 4-9: Synthesis of copolymer **23**.*

Due to the enhanced solubility of sample **23** in MeOH induced by the PEG comonomer, the crude product was purified by precipitation from Et_2O. Characterization of the obtained product by SEC in THF revealed a significant shoulder at higher elution volumes indicating unreacted PEG. Thus, the sample was further purified by thorough washing with brine and subsequent precipitation in EtOH yielding 80% of a yellow solid as pure product. SEC analysis confirmed a unimodal distribution and a high M_n of 13000 g/mol. The small Đ value of 1.4 obtained for sample **23**, is probably due to partial removal of low M_n fractions during the purification process. Again, NMR analysis revealed a difference between the obtained comonomer ratio (1/2; **[2]/[PEG1000]**) and the feed ratio (1/1), proving the results of samples **22a-e**. In addition to the mismatched comonomer ratios, several attempts of copolymer synthesis led to the formation of an insoluble brown residue similar to sample **21c**, which further highlighted the lack of reproducibility of the method for copolymerization.

4.2.2. Polycarbonate 24 from Monomer 6

In order to synthesize light-degradable polycarbonates with a higher λ_{max}, polymer **24** should be synthesized from monomer **6**. Because of the high T_m of **6**, sample **24a** was synthesized using the same parameters as for sample **21c** (*Table 4-3*).

*Table 4-3: Results of the synthesis of homo-polycarbonate **24**.*

Sample	T_1 [°C]	T_2 [°C]	Ratio [6]/[DPC]	M_n[a] [g/mol]	Đ[a]	Yield [%]
a	130	180	1/1.05	/	/	/[b]
b	120	165	1/1.4	1400	1.7	minor
c	120	120	1/1.4	1500	1.6	minor

[a]determined via SEC in HFIP (PMMA-calibration); [b]an insoluble brown residue has emerged

Though complete dissolution of monomer **6** was not achieved, further increase of T_2 above 180 °C was not possible in the used setup. However, similar to the results of polycondensation of monomer **2**, the formation of an insoluble brown residue was observed. Thus, instead of increased reaction temperature, the feed ratio of monomer/DPC was varied from 1/1.05 to 1/1.4 in order to completely dissolve **6** in the molten DPC. To prevent thermal degradation, the reaction temperature in both steps was reduced leading to the successful formation of DMSO soluble yellow solids as samples **24b** and **24c**. Besides DMSO, HFIP was the only other solvent found to dissolve the samples. Thus, SEC measurements of both samples were carried out using HFIP as the eluent. The results of both samples showed only formation of oligomeric compounds (*Table 4-3*), indicating that **6** is not a suitable monomer for polycarbonate formation by polycondensation in the melt.

4.2.3. Polycarbonate 25 Based on BHED

In addition to the light-responsive polymers, the synthesis of redox-responsive backbone-degradable polycarbonates based on BHED was investigated (*Scheme 4-10*).

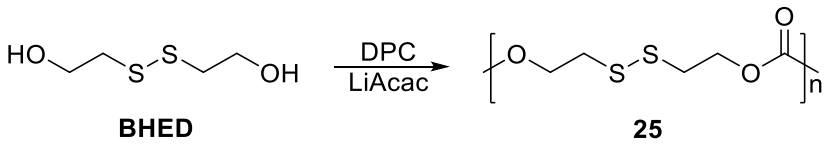

BHED **25**

*Scheme 4-10: Synthesis of homopolymer **25**.*

Successful preparation of homopolymer **25** could yield suitable parameters for the synthesis of dual-responsive backbone-degradable copolymers using BHED and **2**. Disulfide moieties are generally considered suitable redox-responsive functions for DDS applications, since reductive cleavage of cysteine disulfide bonds is a common

process in the human body. Compared to sample **21** slightly lower reaction temperatures were employed for sample **25a** (*Table 4-4*) due to the boiling point of BHED (163 °C). The residue obtained after synthesis was dissolved in THF and added to MeOH upon which no precipitate was formed.

*Table 4-4: Results of the synthesis of homo-polycarbonate **25**.*

Sample	T_1 [°C]	T_2 [°C]	Ratio [BHED]/[DPC]	M_n [g/mol]	Đ	Yield [%]
a	120	150	1/1.05	/	/	/
b	90	120	1/1.05	/	/	/
c	80[a]	100	1/1.05	/	/	/
d	80[a]	80	1/1.05	/	/	/

[a]was stirred overnight in a first step

Analysis of the precipitate after the removal of MeOH showed that the polymerization was unsuccessful. To rule out a temperature induced degradation, synthesis of sample **25b** was carried out at lower reaction temperatures in both steps. Again, no polymer was obtained, which led to further reductions of the reaction temperature for samples **25c** and **25d**. Furthermore, to compensate the lower temperatures, the reaction time of the first step was increased. The analysis of the samples showed no polymer was formed indicating BHED is not a suitable monomer for polycondensation in the melt.

4.3. Synthesis of Polyurethanes

For the synthesis of stimuli-responsive backbone-degradable polyurethanes a polyaddition in DMF using DBTDL as a catalyst was employed. It is known that DBTDL forms complexes of hydroxyl as well as isocyanate functions and is therefore catalyzing the polyaddition while preventing biuret and allophanate formation.[64],[65] Three different diisocyanates were investigated for the polymerization, of which LDI was the most promising for application as DDS. Lysine is an essential amino acid used in the human body, therefore LDI-based polyurethanes are supposed to be more biocompatible compared to other diisocyanates, especially regarding the degradation products. Besides LDI, the well-known diisocyanates HDI and IPDI were also investigated for polymerization. Due to the typically lower reaction temperatures of these reactions this approach is milder than polycondensation in the melt, potentially enabling polymerization of less stable monomers.

4.3.1. Polyurethanes from BHED

*LDI-Based Homo-Polyurethane **26***

For the preparation of homopolymers based on BHED and LDI a ratio of 1/1.05 (**[BHED]**/**[LDI]**) was chosen based on previous findings (*Scheme 4-11*).[7]

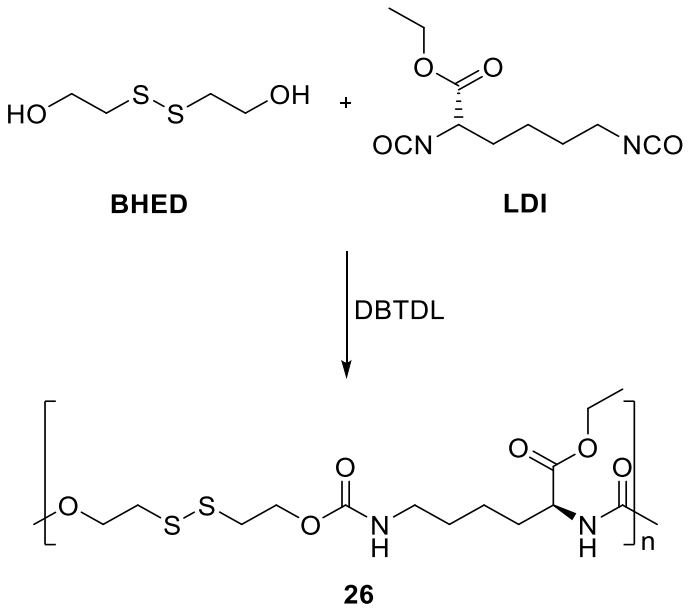

*Scheme 4-11: Synthesis of homopolymer **26**.*

As is pointed out in the literature, a ratio of 1/1 yields the highest M_n for such reactions. However, a slight excess of DI enables uniform endgroups as well as functionalization by termination with alcohols or amines. In a typical procedure, BHED was reacted with LDI for 3 h at 40 °C in 2 mL DMF. Precipitation from MeOH and drying yielded 62% of pure sample **26a** as a transparent melt. Analogously to **26a**, sample **26b** was synthesized using THF as a solvent instead of DMF. A transparent melt in a slightly lower yield of 55% was obtained after precipitation from MeOH and drying. SEC measurements in THF revealed very similar M_n values but a significantly lower Đ value of **26a** (*Table 4-5*).

*Table 4-5: Results of the synthesis of homo-polyurethane **26**.*

Sample	T [°C]	Time [h]	$V_{Solvent}$ [mL]	M_n[a] [g/mol]	Đ[a]	Yield [%]
a	40	3	2	11930	1.3	62
b	40	3	2[b]	13130	2.0	55
c	50	overnight	1	22690	2.3	95

[a]determined via SEC in THF (PS-calibration); [b]THF was used as a solvent

Though both solvents showed suitability for the polymerization, DMF was more promising due to the higher yield and lower Đ. To enhance the yield, sample **26c** was synthesized at a slightly increased reaction temperature and a decreased amount of solvent (*Table 4-5*). After stirring overnight and precipitating from MeOH a transparent melt was obtained as the pure product in a high yield of 95%. NMR analysis confirmed the successful synthesis and SEC measurements in THF showed high M_n and a typical Đ value for polyurethanes prepared by polyaddition.[49] The polymer was soluble in typical organic solvents like THF, DMF, DMSO and DCM. Due to the successful preparation of a BHED homo-polyurethane, the synthesis of multi-responsive copolymers appeared to be possible.

*HDI-Based Homo-Polyurethane **36***

In order to test the versatility of BHED as a monomer, HDI, which is a widely applied DI for the synthesis of linear polyurethanes,[7] was used for the synthesis of polymer **36** (*Scheme 4-12*).

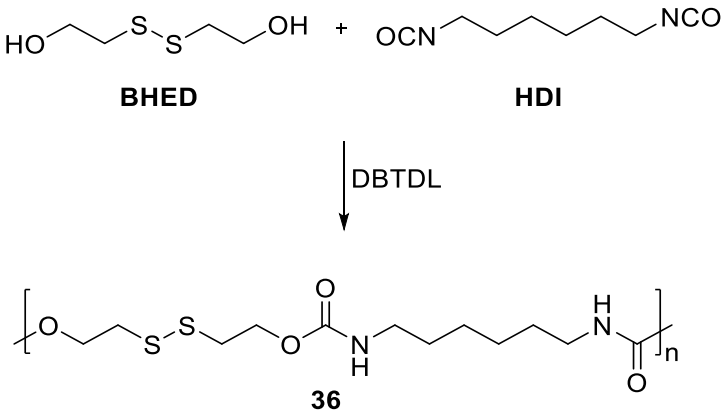

*Scheme 4-12: Synthesis of homopolymer **36**.*

Based on the results of sample **26a**, **36a** was synthesized at a reaction temperature of 40 °C employing a **[BHED]**/**[HDI]** ratio of 1/1.05 and DMF as a solvent (*Table 4-6*).

*Table 4-6: Results of the synthesis of homo-polyurethane **36**.*

Sample	T [°C]	Time [h]	M_n [g/mol]	Đ	Yield [%]
a	40	1	/[a]	/	/
b	80	/	/[a]	/	/
c	RT	overnight	/[a]	/	/

[a]an insoluble gel has emerged

A white precipitate was formed after 10 min and the reaction was stopped by addition of MeOH after 1 h yielding an insoluble white precipitate as a product. In order to increase the solubility during synthesis, a higher reaction temperature was used for sample **36b**. The reaction mixture turned to an insoluble swollen gel after 10 min of reaction, which implied crosslinking of the sample. Thus, synthesis of sample **36c** was carried out at room temperature. Again, the reaction was stopped by addition of MeOH leading to the formation of an insoluble white precipitate, also indicating crosslinking of the product. None of the investigated parameters led to the successful formation of polymer **36**.

4.3.2. Polyurethanes from Monomer 2

*LDI-Based Homo-Polyurethane **27***

For the preparation of a light-responsive backbone-degradable homo-polyurethane from monomer **2**, LDI was tested first. DMF was used as a solvent and a **[2]**/**[LDI]** ratio of 1/1.05 was employed for synthesis of polymer **27** (*Scheme 4-13*).

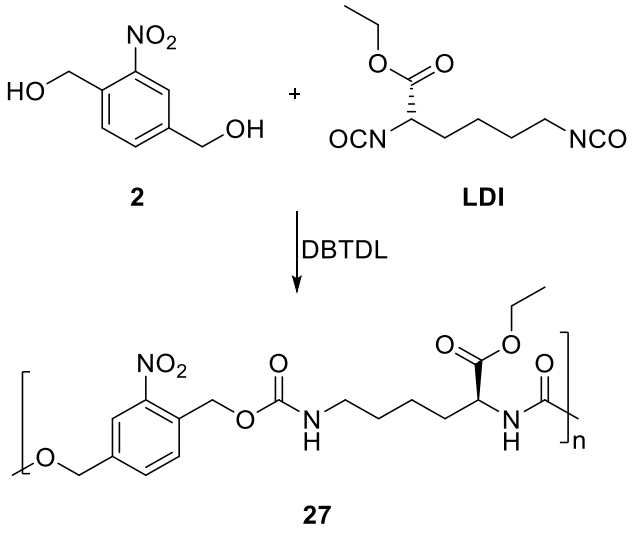

*Scheme 4-13: Synthesis of homopolymer **27**.*

Analogously to sample **26a**, synthesis of **27a** was carried out at 40 °C for 3.5 h using 2 mL of solvent. Though precipitation from MeOH yielded only minor amounts of a light-yellow powder, SEC measurements in THF revealed decent M_n and low Đ (*Table 4-7*).

*Table 4-7: Results of the synthesis of homo-polyurethane **27**.*

Sample	T [°C]	Time [h]	$V_{Solvent}$ [mL]	M_n[a] [g/mol]	Đ[a]	Yield [%]
a	40	3.5	2	5080	1.3	minor
b	40	overnight	2	5910	1.3	57
c	50	overnight	1	7800	1.7	98

[a]determined via SEC in THF (PS-calibration)

In a second attempt, **27b** was prepared at the same parameters as **27a**, but with an elongated reaction time. The pure product was obtained as a yellow powder in significantly increased yield by precipitation from MeOH. In contrast, the SEC results showed equal Đ values and only minor increase in M_n compared to **27a**. Thus, sample **27c** was synthesized at slightly higher reaction temperatures and a reduced amount of solvent (*Table 4-7*). Again, the pure product was obtained as a yellow powder by precipitation from MeOH revealing a highly increased yield of 98%. The successful synthesis was confirmed by NMR analysis and SEC measurements revealed increased M_n and Đ compared to previous samples **27a** and **27b**. UV/Vis measurements of **27c** in DCM solution showed a similar absorbance pattern as polycarbonate **21** and the same λ_{max} value of 260 nm, indicating λ_{max} to be independent

from the used polymerization technique. Furthermore, sample **27c** was soluble in typical organic solvents like DMF, DMSO, THF as well as DCM. DSC measurements exhibited a T_g of 23 °C, which is significantly lower than T_g of similar polycarbonate **21**, because of the more flexible LDI moieties (*Figure 4-2*).

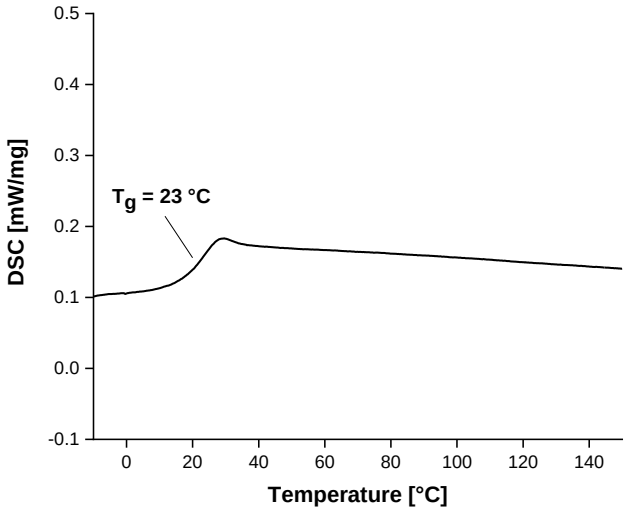

*Figure 4-2: DSC result of homopolymer **27**.*

*LDI-Based BHED Co-Polyurethane **28***

The combination of different stimuli-degradable moieties in one copolymer is regarded useful for, e.g., adjustment of the DDS release profile based on the different degradation rates and mechanisms of the addressed stimuli. Thus, BHED was selected as a functional comonomer to prepare light- and redox-responsive copolymer **28** (*Scheme 4-14*).

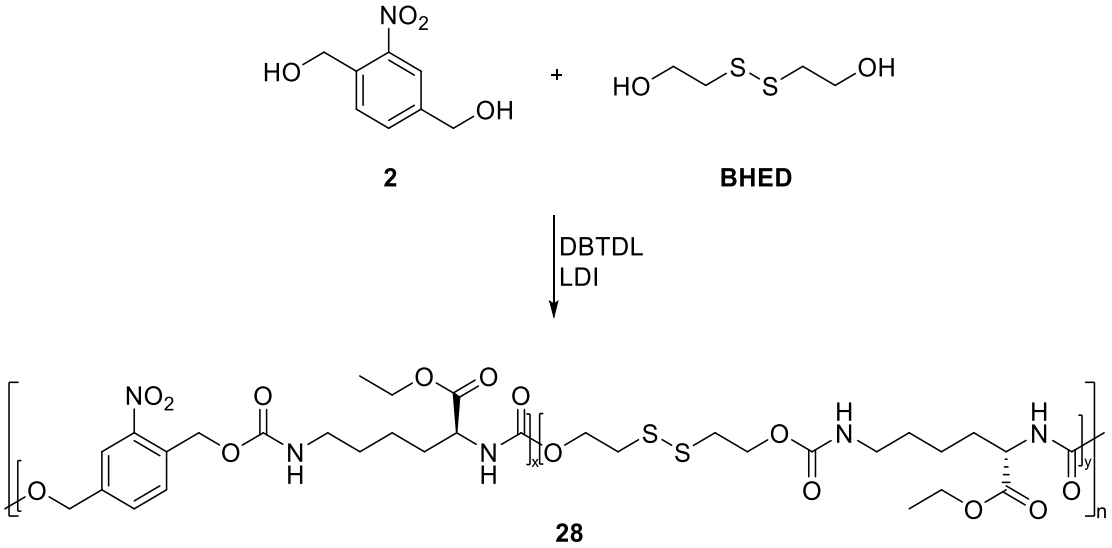

*Scheme 4-14: Synthesis of copolymer **28**.*

The comonomers were used in ratios of 3/1, 1/1 and 1/3, analogously to co-polycarbonate **22**, and all syntheses were carried out using the same parameters as for homo-polyurethane sample **27c** (*Table 4-8*).

*Table 4-8: Results of the synthesis of co-polyurethane **28**.*

Sample	Ratio [2]/[BHED][a]	M_n[b] [g/mol]	Đ[b]	Yield [%]
a	3/1	7150	1.4	75
b	1/1	6440	1.5	73
c	1/3	10410	1.5	69

[a]determined via ^{1}H-NMR; [b]determined via SEC in THF (PS-calibration)

Precipitation from MeOH led to the formation of a sticky yellow solid in good yields for all samples. NMR analysis confirmed the successful synthesis and showed good accordance between feed and obtained comonomer ratio. Furthermore, the results of SEC measurements in THF were in line with the results of homopolymer preparation, showing high M_n. UV/Vis measurements of each sample in DCM solution showed the same absorbance pattern and λ_{max} as homopolymer **27** confirming only minor contribution of BHED to the light absorbance. The thermal properties of all samples were measured by DSC revealing T_g values of 11.1 °C for sample **28a**, 7.1 °C for sample **28b** and -9.9 °C for sample **28c** (*Figure 4-3*).

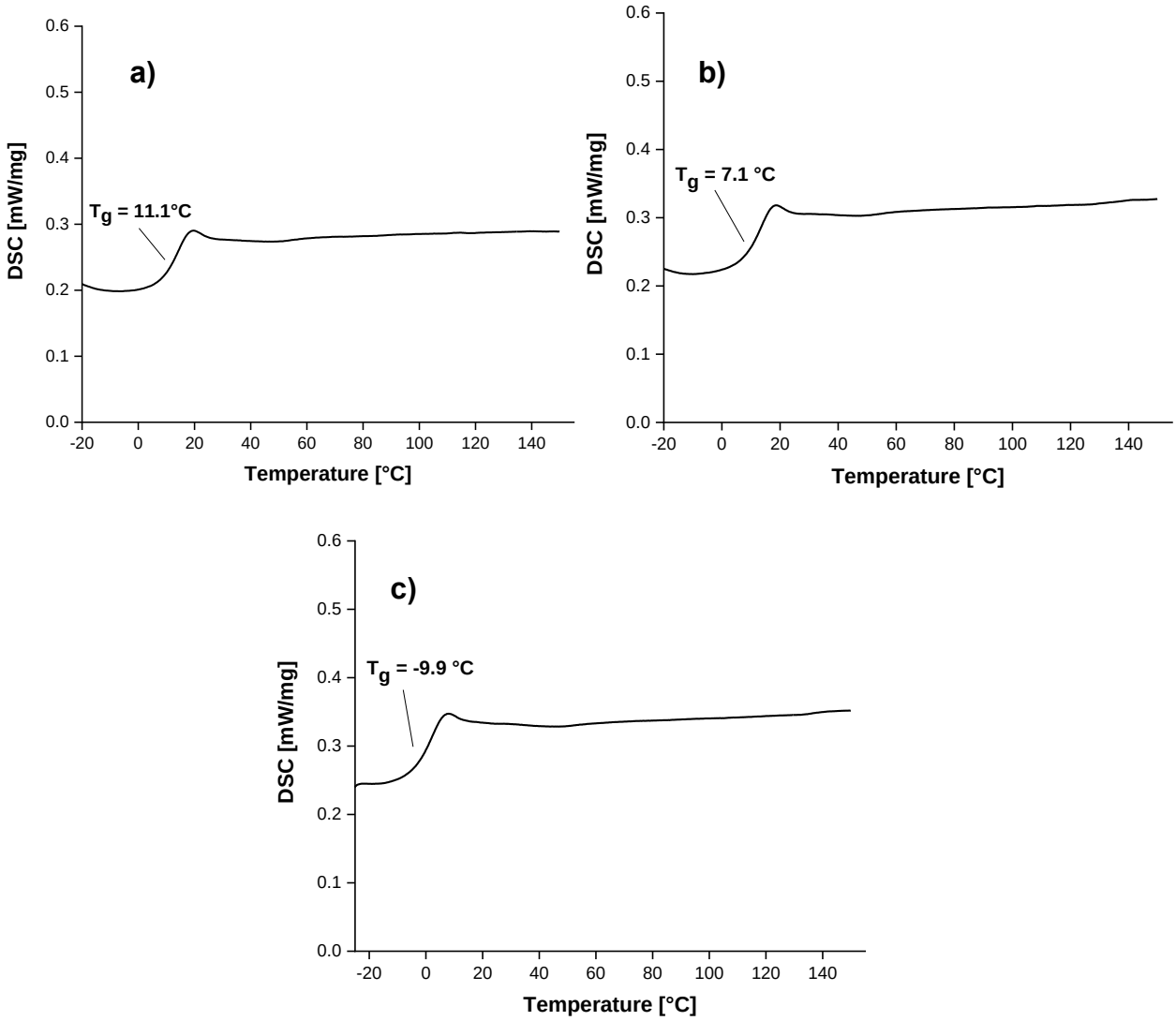

*Figure 4-3: DSC results of copolymers **28a** (a), **28b** (b) and **28c** (c).*

Due to the more flexible BHED moieties, the T_g is reduced with increasing amount of BHED. Higher chain flexibility induced by the comonomer is also the reason for the lower T_g compared to homopolymer **27**. To ensure equal distribution of light-responsive monomer **2**, the composition of samples **28a**-**28c** was analyzed by determining the weight fraction *w* of each comonomer for each slice of the SEC elugram. Composition analysis can be performed using an SEC system equipped with a UV detector and an RI detector.[123] In a typical procedure, LDI-based homo-polyurethanes of each comonomer were used to determine their detector specific response factors *f*. Therefore, a dilution series of the homo-polyurethanes in THF was prepared and measured by SEC. The peak areas of the resulting detector signals were determined for both detectors. Plotting of these peak areas against the used sample concentration yielded a calibration line with *f* as the slope for each series. Based on the obtained

response factors, the weight fraction *w* of each comonomer can be calculated from the detector signals *x* of the copolymer SEC measurement by equation (4-1).[123]

$$\frac{1}{w_a} = 1 - \frac{(\frac{x_{UV}}{x_{RI}} \cdot f_{RI,a} - f_{UV,a})}{(\frac{x_{UV}}{x_{RI}} \cdot f_{RI,b} - f_{UV,b})} \qquad (4\text{-}1)$$

The obtained course of weight fraction w_2 of light-responsive monomer **2** over the elution volume for copolymers **28a**-**28c** is shown in *Figure 4-4*.

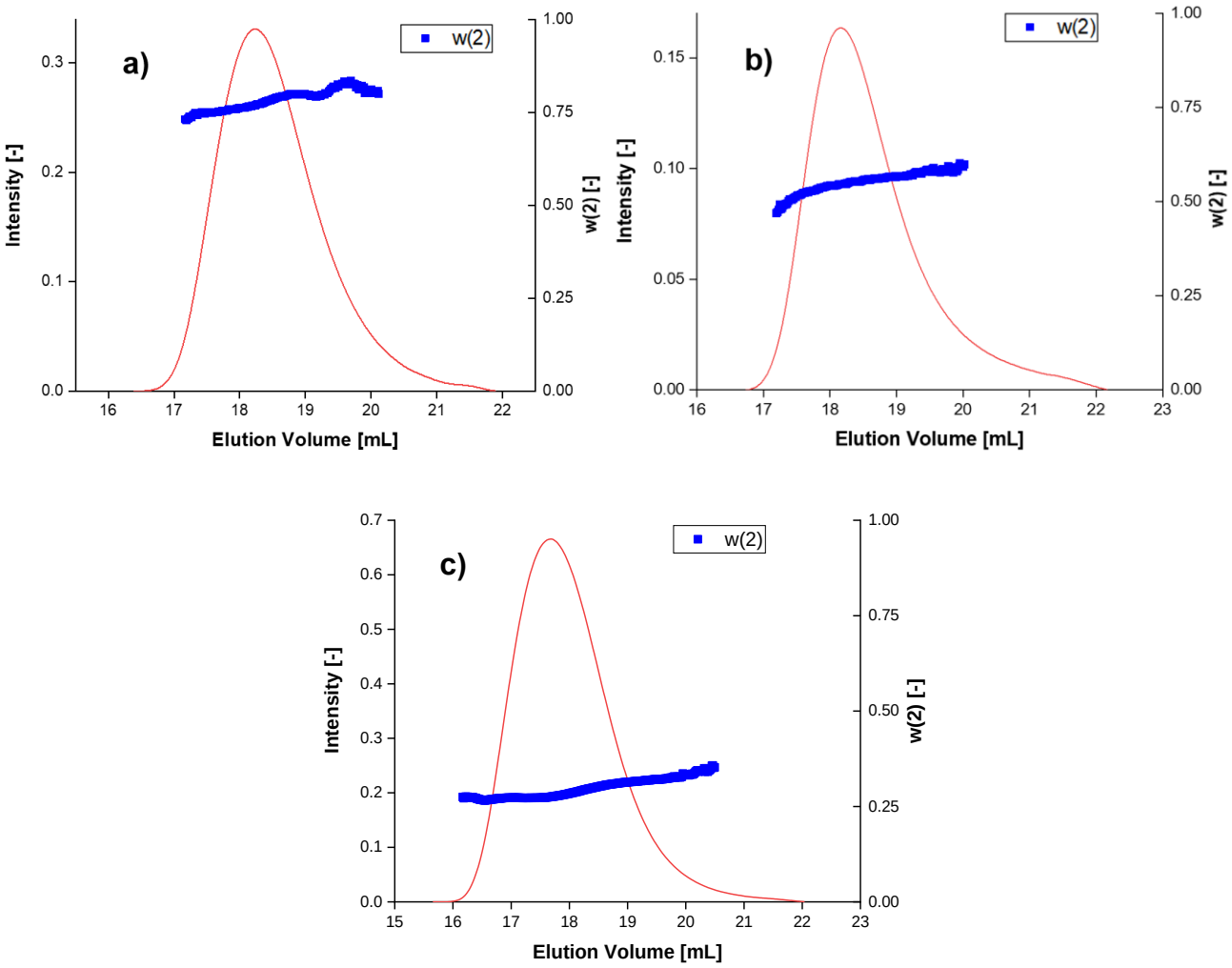

*Figure 4-4: Composition analysis of BHED copolymer **28a** (a), **28b** (b) and **28c** (c).*

The results proved the successful incorporation of both monomers for all three samples. Generally good agreement with the feed ratio was confirmed with only a slight excess of **2**. Interestingly, w_2 corresponded to the feed ratio at low elution volumes but showed a drift from lower to higher elution volumes, indicating a higher reactivity of

monomer **2** compared to comonomer BHED. Furthermore, the slope increased with higher amounts of **2** in the copolymer sample, which also implies a higher reactivity of the light-responsive monomer.

*LDI-Based PEG400 Co-Polyurethane **29***

In analogy to co-polycarbonate **23**, PEG400 was used as a functional comonomer to incorporate hydrophilic moieties into polymer **29** (*Scheme 4-15*). PEG400 was used instead of PEG1000 to enhance the degradation product hydrophilicity while maintaining hydrophobicity of the polymer for nanoparticle preparation.

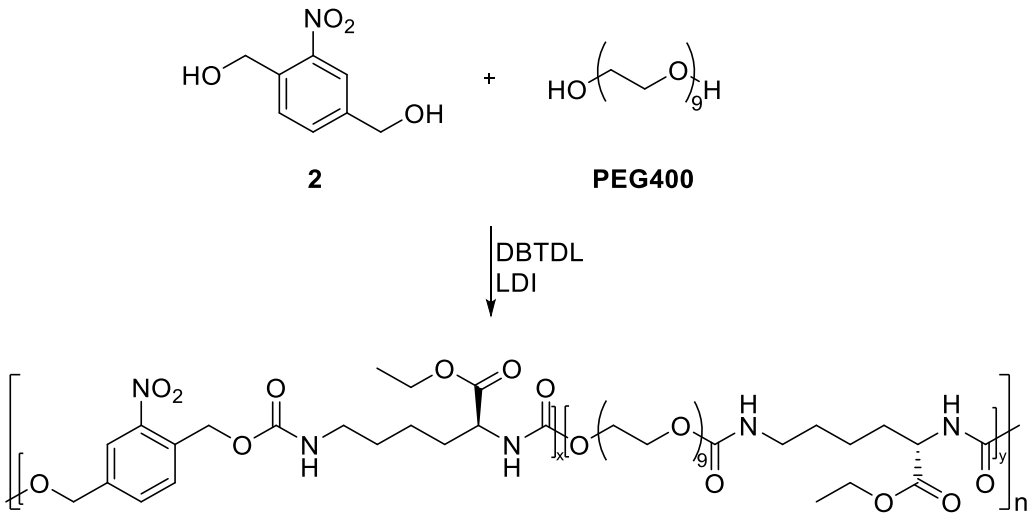

*Scheme 4-15: Synthesis of copolymer **29**.*

All samples were synthesized using the same parameters as for homopolymer sample **27c** and the same comonomer ratios as for copolymer samples **28a**-**28c** (*Table 4-9*).

*Table 4-9: Results of the synthesis of co-polyurethane **29**.*

Sample	Ratio [2]/[PEG400][a]	M_n[b] [g/mol]	Đ[b]	Yield [%]
a	3/1	11600	1.6	86
b	1/1	16990	2.1	63
c	1/3	35240	1.5	62

[a]determined via ^{1}H-NMR; [b]determined via SEC in THF (PS-calibration)

Sample **29a** and **29b** were purified by precipitation from MeOH resulting in sticky yellow

solids in good yields. Due to the increased amount of hydrophilic PEG400, sample **29c** was soluble in MeOH and was thus purified by precipitation from Et_2O. Similar to samples **29a** and **29b**, a sticky yellow solid was obtained in good yield. In line with the flexibility of the PEG moieties, the samples appeared to increase in stickiness with higher amounts of PEG400 in the feed ratio. These observations were underlined by the DSC results revealing a T_g of 13 °C for sample **29a**, a T_g of -0.7 °C for sample **29b** and a T_g of -20.6 °C for sample **29c** (*Figure 4-5*).

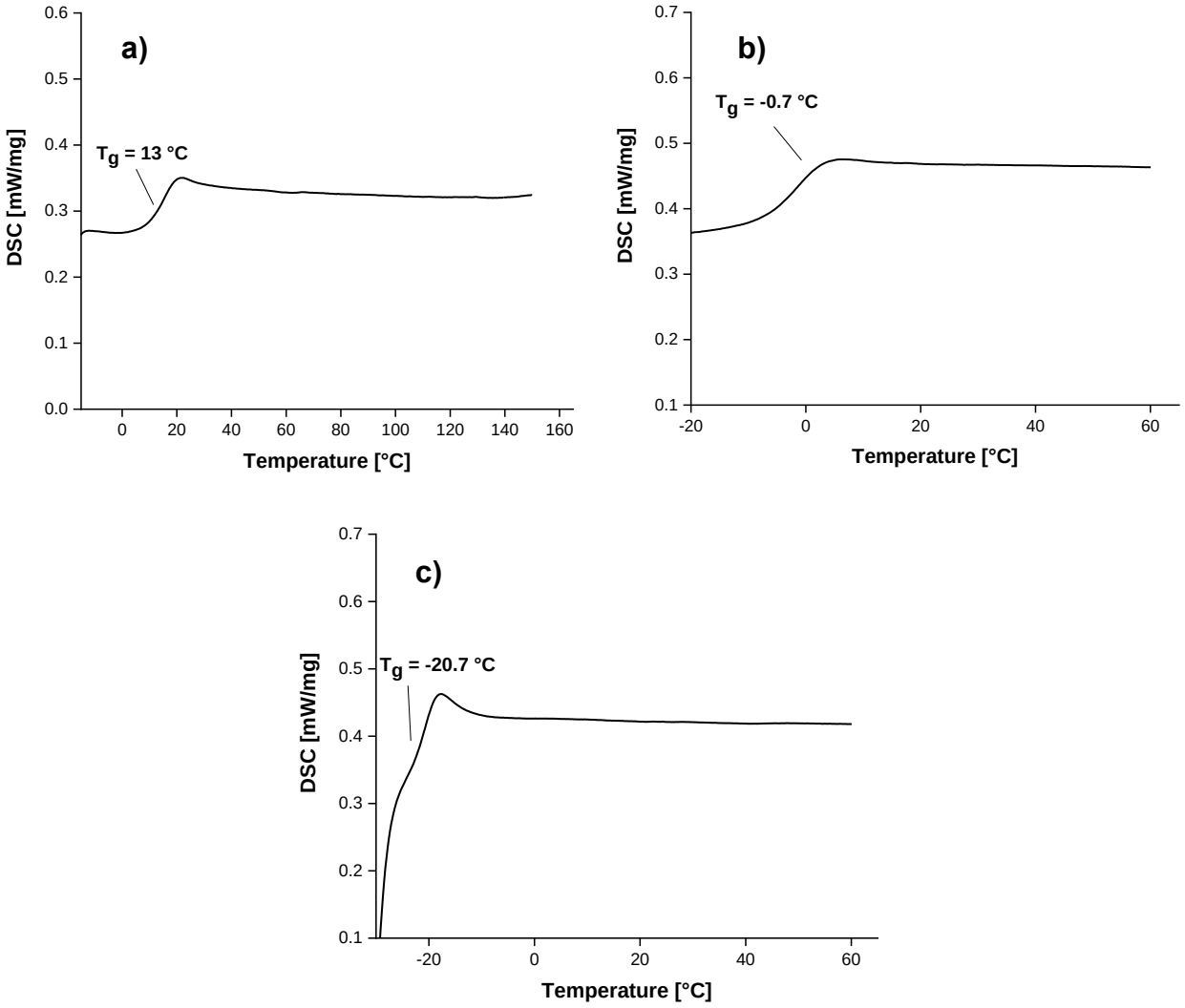

*Figure 4-5: DSC results of copolymers **29a** (a), **29b** (b) and **29c** (c).*

The observed thermal properties also align with the DSC results of copolymers **28a**-**28c**, although the decrease is significantly stronger for PEG400 as a comonomer, which is due to the longer chain length. NMR measurements confirmed the successful synthesis and showed good accordance of initial feed and obtained comonomer ratio

for all samples. In addition, SEC analysis in THF revealed high M_n values and UV/Vis measurements showed the same absorbance pattern and λ_{max} as homopolymer **27**, proving no contribution from PEG400 to the UV absorbance. Analogously to samples **28a**-**28c** composition of the comonomers was analyzed for polymers **29a**-**29c** (*Figure 4-6*).

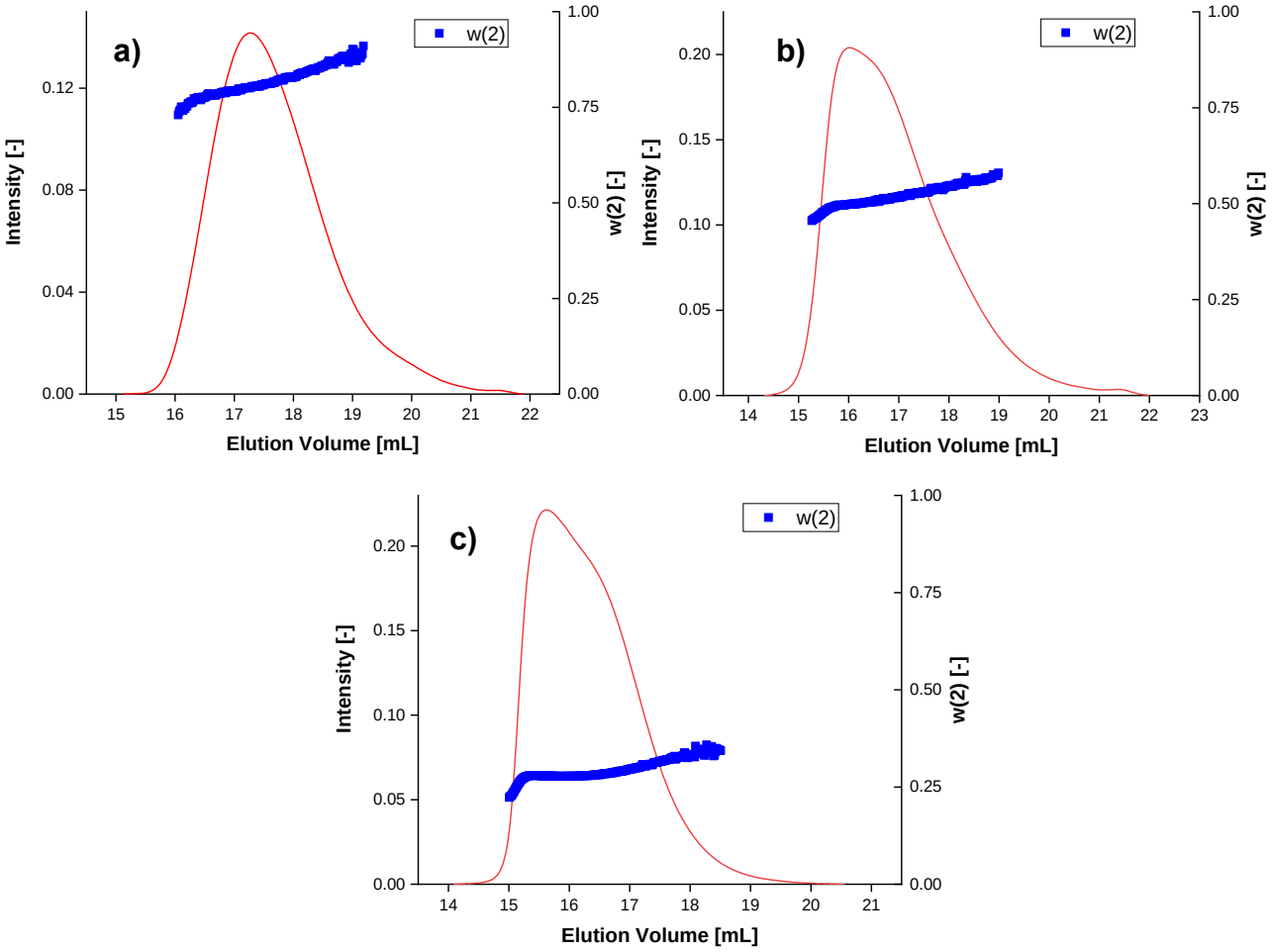

*Figure 4-6: Composition analysis of PEG400 copolymer **29a** (a), **29b** (b) and **29c** (c).*

The results are in line with samples **28a**-**28c** proving the successful incorporation of both monomers for all three samples. The same drift from lower to higher elution volumes was revealed, which underlines the higher reactivity of monomer **2** compared to comonomers PEG400 and BHED. Comparison of the composition analysis results of samples **28a**-**28c** and **29a**-**29c** showed a higher slope for the PEG400 samples than for the BHED samples, indicating a higher reactivity difference of PEG400 as a comonomer. While for PEG400 copolymer **29a** a drift of 18% could be observed, BHED copolymer **28a** showed a variation of 12%. However, all investigated copolymer

samples showed incorporation of the light-responsive moiety over all chains enabling the photo-triggered degradation of the polymeric material.

*IPDI-Based Homo-Polyurethane **34***

As a second DI, IPDI was investigated for the preparation of light-degradable polyurethane **34** (*Scheme 4-16*). After synthesis, functionalization with amine end groups should be tested by termination with isophorone diamine (IPDA). Amine terminated polymers can be used as, e.g., agents for post-polymerization crosslinking or for multi-step preparation of block copolymers.

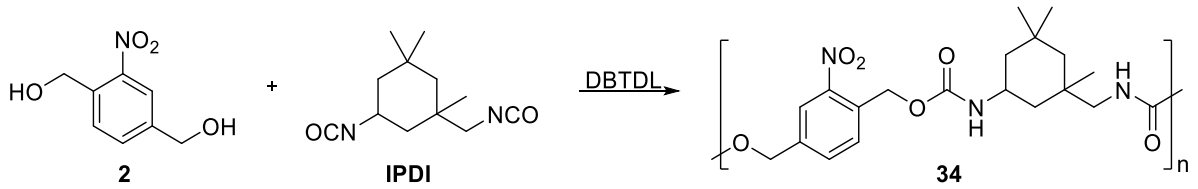

*Scheme 4-16: Synthesis of homopolymer **34**.*

In a first attempt, **34a** was synthesized using the same parameters as for LDI-based polyurethane **27c**. It was known that IPDI is less reactive than LDI, thus the reaction time was elongated to 70 h. After termination with IPDA and precipitation from MeOH a white powder was obtained in a small yield of 9%. Besides the small yield, SEC measurements in THF also showed a low M_n proving the synthesis was unsuccessful (*Table 4-10*).

*Table 4-10: Results of the synthesis of homo-polyurethane **34**.*

Sample	T [°C]	Time [h]	M_n[a] [g/mol]	Đ[a]	Yield [%]
a	50	70	3790	1.8	9
b	70	70	9800	1.5	58
c	90	48*	/[b]	/	/

[a]determined via SEC in THF (PS-calibration); [b]an insoluble residue has emerged

Therefore, the reaction temperature was increased to 70 °C synthesizing sample **34b**. After 70 h, IPDA was added and precipitation from MeOH yielded 58% of a white powder as the pure product as confirmed by NMR analysis. SEC measurements in THF showed an M_n of 9800 g/mol and a Đ value which is slightly smaller than the Đ

value polyurethanes prepared by polyaddition usually have. To further optimize the reaction, sample **34c** was prepared further increasing the reaction temperature to 90 °C. After 48 h an insoluble swollen gel was formed indicating crosslinking of the sample. Sample **34b** showed the best results of the investigated synthesis parameters.

*HDI-Based Homo-Polyurethane **37***

HDI was the last DI investigated for the synthesis of linear homo-polyurethanes from monomer **2** (*Scheme 4-17*).

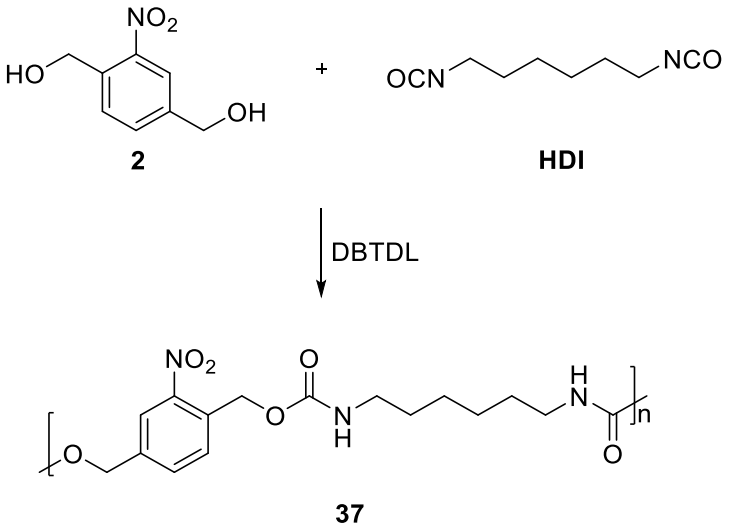

*Scheme 4-17: Synthesis of homopolymer **37**.*

A **[2]**/**[HDI]** ratio of 1/1.05 was used to prepare polymer **37** in DMF. Based on the results of BHED-based homo-polyurethane **36**, an ice-bath was employed to cool the reaction mixture prior to HDI addition and thus reduce crosslinking side-reactions. After stirring overnight, a swollen gel was obtained, and the reaction was stopped by adding MeOH. The gel could be dissolved in boiling DMSO and an aliquot was precipitated in MeOH for analysis. Besides boiling DMSO, only HFIP was found to be a suitable solvent for complete dissolution of the polymer indicating sample **37** was physically crosslinked. SEC measurements in HFIP using PMMA calibration revealed only low M_n of 2800 g/mol proving that the low solubility is not due to a high degree of polymerization. Overall, synthesis of a linear polymer was not successful, and the obtained gel was not processable.

4.3.3. Polyurethane 30 from Monomer 6

Similar to polyurethane **27** from monomer **2**, the preparation of polyurethanes from higher absorbing monomer **6** and LDI was investigated (*Scheme 4-18*).

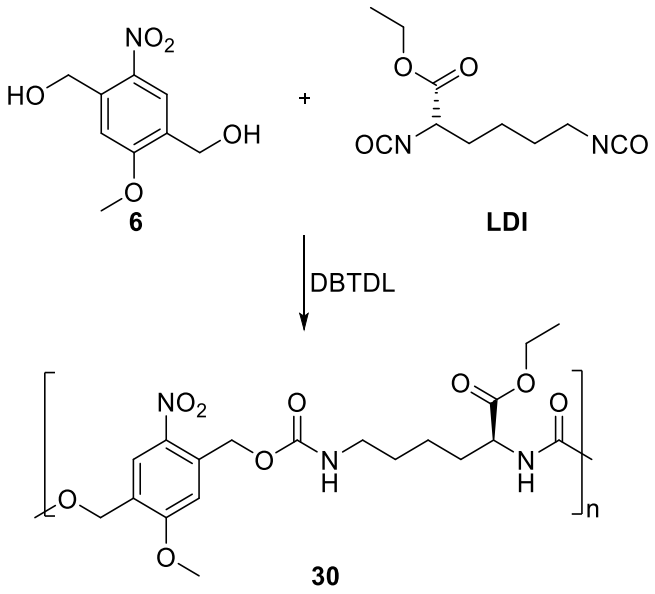

*Scheme 4-18: Synthesis of homopolymer **30**.*

The reaction was carried out at 50 °C using DMF as a solvent and applying a **[6]**/**[LDI]** ratio of 1/1.05. Precipitation from MeOH yielded 55% of pure polymer **30** as a light-yellow powder. The successful synthesis was confirmed by NMR measurement as well as analysis by SEC in THF showing an M_n of 7450 g/mol and a Đ of 1.3. As expected, a λ_{max} of 315 nm was observed by UV/Vis measurements in DCM solution, which is a significant increase compared to polymer **27** and in line with the results of monomer **6**. Characterization of the thermal properties of polymer **30** revealed a T_g of 41 °C (*Figure 4-7*).

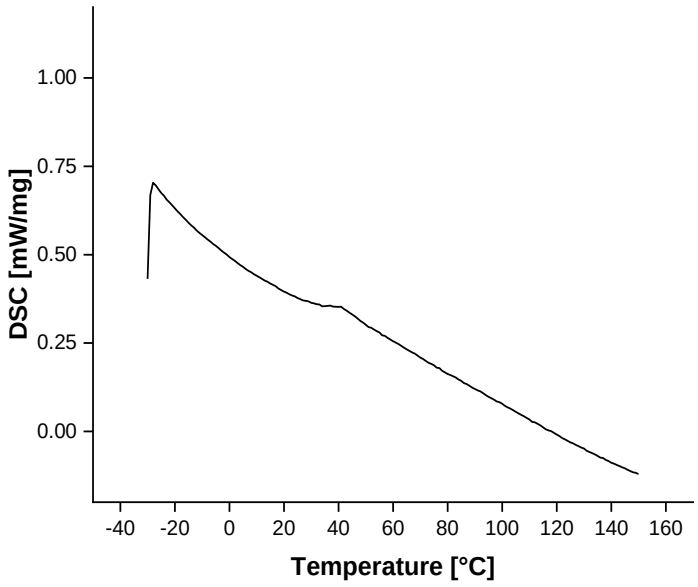

*Figure 4-7: DSC result of homopolymer **30**.*

The significant difference to the T_g of polymer **27** is probably due to the higher steric hinderance of monomer **6**.

4.3.4. Polyurethanes from Monomer 13

*LDI-Based Polyurethane **31***

In addition to monomer **6**, similar monomer **13** was investigated for the preparation of light-degradable polyurethanes. LDI-based polyurethane **31** was prepared with the same parameters as sample **30** using DMF as a solvent and a **[13]/[LDI]** ratio of 1/1.05 (*Scheme 4-19*).

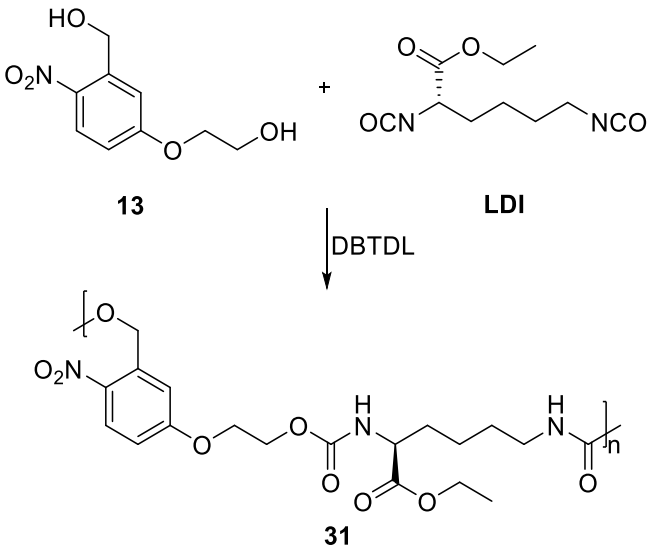

*Scheme 4-19: Synthesis of polymer **31**.*

Sample **31a** was obtained after precipitation from MeOH as a light-yellow powder in a yield of 82%. The successful synthesis was confirmed by NMR, and SEC measurements in THF showed an M_n of 7800 g/mol and a Đ of 1.4. While similar M_n values were obtained, the increased yield indicated a better polymerizability of monomer **13** compared to monomer **6**. UV/Vis measurements in DCM solution revealed a λ_{max} of 309 nm, which is only slightly lower than the value found for polymer **30** and thereby underlines the structural similarity of both light-responsive units. Analysis of the thermal properties of **31a** using DSC showed a T_g of 33.8 °C which is, as expected, slightly lower than for polymer **30** (*Figure 4-8*).

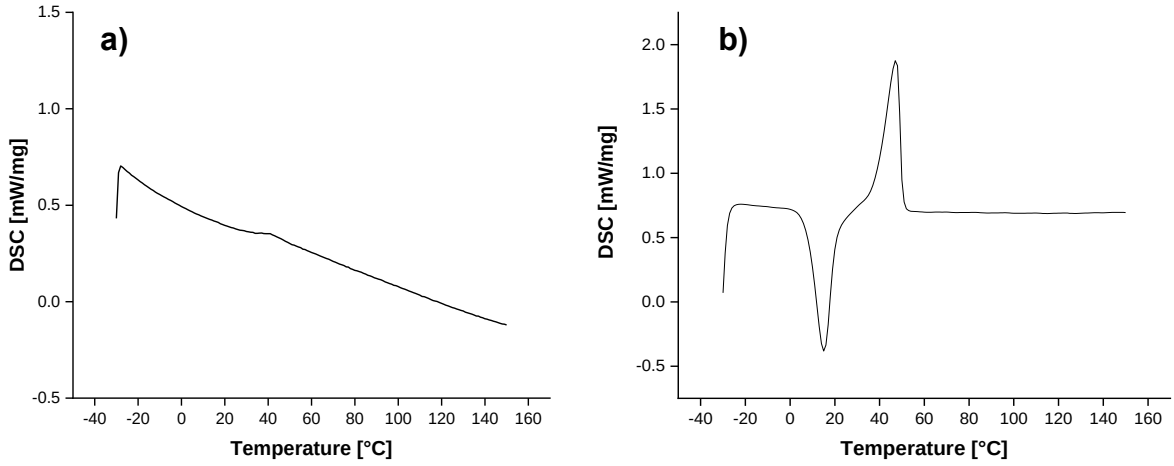

*Figure 4-8: DSC results of homopolymer **31a** (a) and copolymer **31b** (b).*

In order to synthesize an amphiphilic triblock copolymer, sample **31b** was prepared

employing the same method as for **31a**, but the reaction was stopped by adding mPEG5000, which led to end-capping with hydrophilic PEG blocks. Besides the already mentioned stealth properties by formation of a PEG hydrating layer, the synthesis of amphiphilic copolymers is advantageous. Due to the capability of micelle self-assembly by microphase separation, amphiphilic block copolymers enable the encapsulation of hydrophobic compounds inside the micelle core.[124],[125] After termination, polymer **31b** was purified by dialysis in water yielding 80% of a light-yellow powder, which is in good accordance with sample **31a**. Purification by precipitation from MeOH or H_2O was not possible, due to the enhanced solubility in polar protic solvents. The successful synthesis was confirmed by NMR, and SEC measurements in THF showed a higher M_n of 13860 g/mol as well as a similar Đ of 1.3 compared to homopolymer **31a**. As expected, UV/Vis measurements in DCM solution also revealed the same λ_{max} value of 309 nm. Analysis of the thermal properties of polymer **31b** exhibited a T_g of 19.3°C, which is significantly lower than the T_g of **31a** due to the mPEG5000 blocks (*Figure 4-8*).

*HDI-Based Homo-Polyurethane **38***

In analogy to the previous samples, HDI-based polyurethane **38** was synthesized from **13** and HDI in DMF (*Scheme 4-20*).

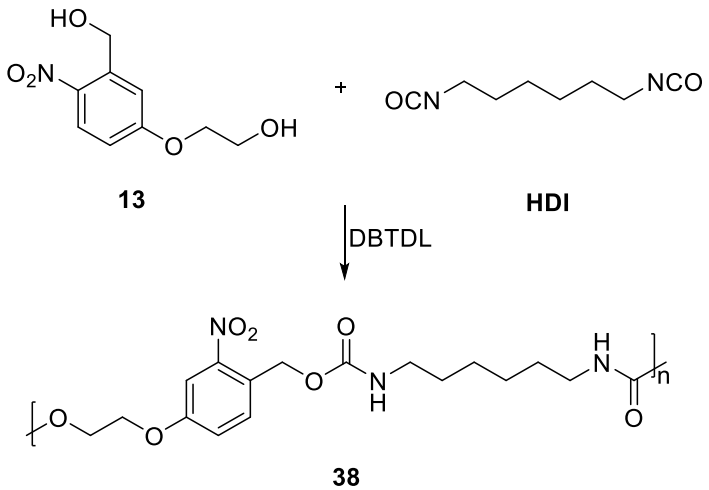

*Scheme 4-20: Synthesis of homopolymer **38**.*

In a first attempt, sample **38a** was prepared using the same parameters as for LDI-based polyurethane **31** (*Table 4-11*).

*Table 4-11: Results of the synthesis of homo-polyurethane **38**.*

Sample	T [°C]	Time [h]	M_n[a] [g/mol]	Đ[a]	Yield [%]
a	50	/[b]	/	/	/
b	RT	overnight	2300	1.6	minor

[a]determined via SEC in HFIP (PMMA-calibration)

[b]an insoluble residue has emerged after 10 min

After a reaction time of 10 min, an insoluble swollen gel was formed instead of the desired product. Thus, in a second approach, sample **38b** was prepared similar to **37** using an ice-bath to cool the reaction mixture before adding HDI. After precipitation from MeOH a white powder was obtained in a minor yield. The product was only soluble in DMF, DMSO and HFIP, therefore SEC measurements in HFIP were performed revealing only low M_n of 2300 g/mol. In line with the previous results, the synthesis of an HDI-based polyurethane was not possible.

4.3.5. Polyurethane 32 from Monomer 17

Monomer **17** was introduced as a first variation of monomer **13** combining both, pH- and light-cleavable moieties, in one compound. Thus, LDI-based polyurethane **32** was synthesized in the same fashion as **31** (*Scheme 4-21*).

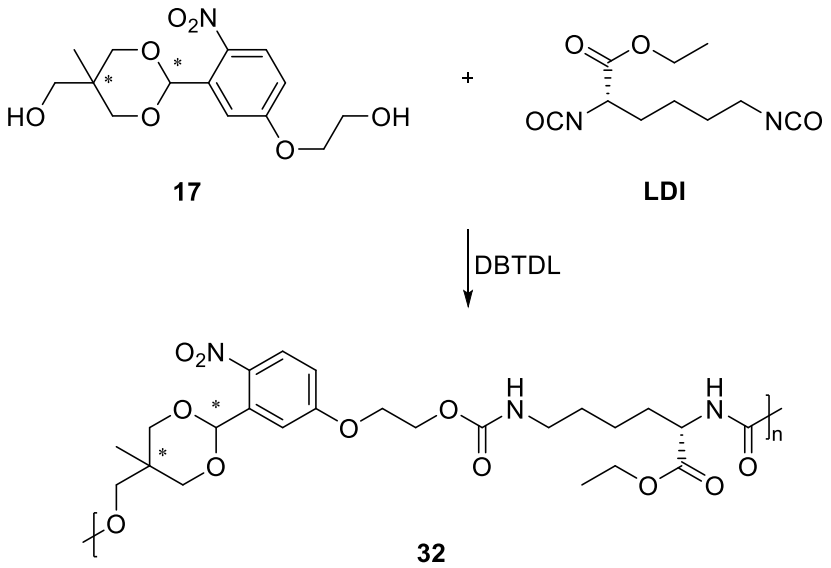

*Scheme 4-21: Synthesis of polymer **32**.*

Sample **32a** was stopped by adding MeOH and precipitation from MeOH yielded 72% of the pure product as a light-yellow powder. The successful synthesis was confirmed by NMR, and SEC measurements in THF showed an M_n of 9730 g/mol and a Đ of 1.9. Interestingly, due to incorporation of an acetal unit instead of a benzyl alcohol, λ_{max} was slightly decreased to a value of 303 nm as observed by UV/Vis analysis. For the preparation of triblock copolymer **32b**, the synthesis was stopped by addition of mPEG5000, and the crude product was precipitated from Et_2O. To remove remaining mPEG5000, the crude product was washed with brine and added to Et_2O to yield 59% of the pure product as a light-yellow powder. NMR analysis confirmed the successful synthesis and SEC measurements in THF revealed an M_n of 14770 g/mol and a Đ of 1.6.

4.3.6. Polyurethanes from Monomer 9

*LDI-Based Homo-Polyurethane **33***

In order to synthesize a light-responsive backbone-degradable polyurethane with high λ_{max} and enhanced quantum yield, polymer **33** should be synthesized from **9** and LDI (*Scheme 4-22*).

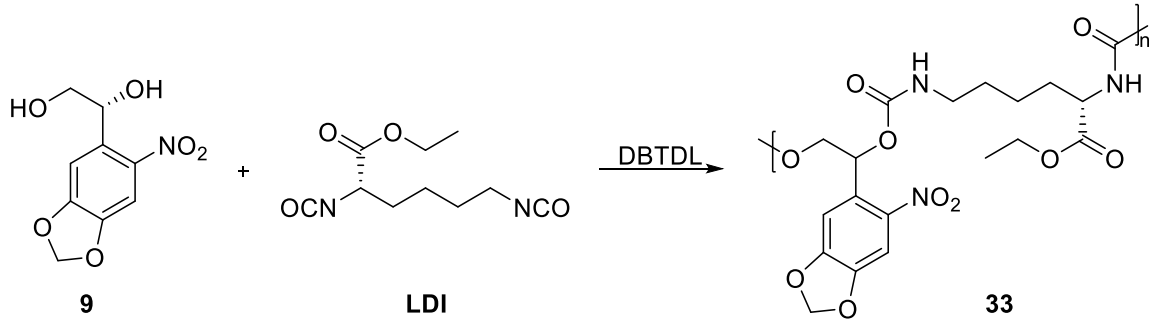

*Scheme 4-22: Synthesis of homopolymer **33**.*

Both, THF and DMF, were tested as solvents for the synthesis and a **[9]**/**[LDI]** ratio of 1/1.05 was used for all samples. In a first attempt, sample **33a** was synthesized at 50 °C overnight, leading to the formation of an insoluble swollen gel instead of the desired product (*Table 4-12*).

*Table 4-12: Results of the synthesis of homo-polyurethane **33**.*

Sample	T [°C]	Time [h]	M_n[a] [g/mol]	Đ[a]	Yield [%]
a	50	overnight	/	/	/[b]
b	40	48	6950	1.3	4
c[c]	40	overnight	4900	1.3	18
d	45	overnight	6000	1.3	24

[a]determined via SEC in THF (PS-calibration)

[b]an insoluble residue has emerged

[c]THF was used as solvent

Thus, sample **33b** was prepared at lower reaction temperatures to prevent crosslinking of the sample. After stirring overnight, an aliquot of the reaction mixture was collected and measured via SEC in THF. Since the results showed moderately increased M_n of 4900 g/mol, the reaction time was elongated to 48 h. Although SEC measurements in THF revealed a further increased M_n of 6900 g/mol, precipitation from MeOH yielded only 4% of the pure product as a light-yellow powder indicating only minor influence of the elongated reaction time. In order to obtain higher yield, THF was tested as a solvent for preparation of sample **33c**. The product was isolated by precipitation from MeOH in a yield of 18% after stirring overnight. Though a significantly higher yield was obtained compared to **33b**, the amount of product formed was still insufficient. In addition, the results of sample **33c** lacked reproducibility, which prevented further tests of the use of THF as a solvent. Thus, as a last approach, synthesis of sample **33d** was carried out in DMF at a slightly increased reaction temperature of 45 °C. Again, only a small yield was obtained after precipitation from MeOH, indicating low compatibility of monomer **9** and LDI. Nevertheless, the structures of all samples were confirmed by NMR analysis.

*IPDI-Based Homo-Polyurethane **35***

Besides LDI, IPDI was tested for the preparation of light-degradable polyurethane from monomer **9** (*Scheme 4-23*).

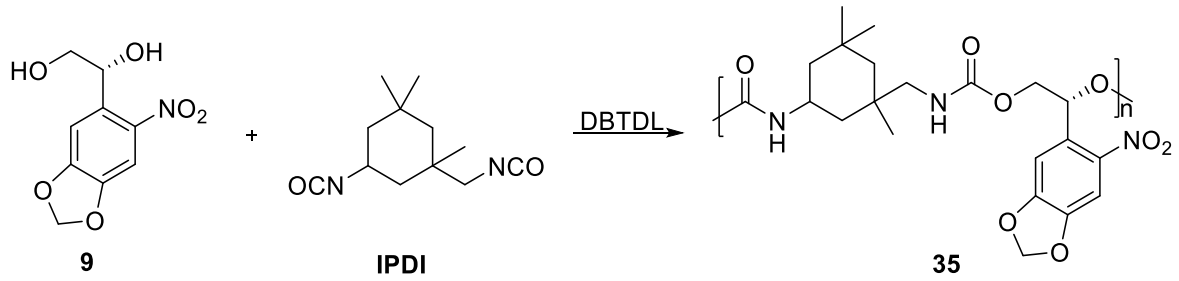

*Scheme 4-23: Synthesis of homopolymer **35**.*

Based on the results of **34**, sample **35** was synthesized at 70 °C using DMF as a solvent. After stirring for 70 h, the pure product was obtained in a yield of 68% as a light-yellow powder by precipitation from MeOH. The successful synthesis was confirmed by NMR, and SEC measurements in THF revealed high M_n of 15800 g/mol as well as a Đ of 1.7. Due to a reduced solubility in DCM compared to the previously synthesized samples, UV/Vis measurements were performed in DCM containing 0.2 vol% DMSO. The results revealed a λ_{max} of 350 nm, which is the highest value of all synthesized samples. In line with the bulky structure of polymer **35**, DSC analysis also showed the highest T_g of all synthesized samples with a value of 97 °C.

4.4. Synthesis of Polyesters

In order to investigate the scope of polymerizability of the synthesized monomers, polyesters should be prepared as a third category of polymers. The preparation of stimuli-responsive backbone-degradable polyesters from the synthesized monomers was carried out based on a well-known method.[6] Therefore, pyridine was used as a base and a **[monomer]/[ADP]** ratio of 1/1.1 was applied for all samples.

4.4.1. Polyester 39 from Monomer 2

Sample **39** was synthesized from ADP and monomer **2** in a DMF/DCM mixture at room temperature (*Scheme 4-24*).

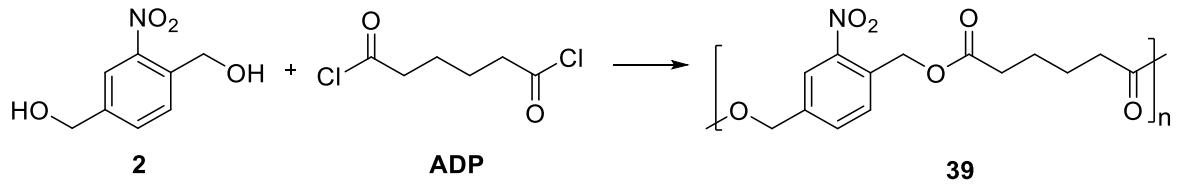

2 ADP 39

*Scheme 4-24: Synthesis of homopolymer **39**.*

Precipitation in MeOH yielded no product and the analysis of the residue after removal of the MeOH proved that the polymerization was unsuccessful.

4.4.2. Polyester 40 from Monomer 13

Sample **40** was synthesized from ADP and monomer **2** in a DMF/DCM mixture at room temperature (*Scheme 4-25*).

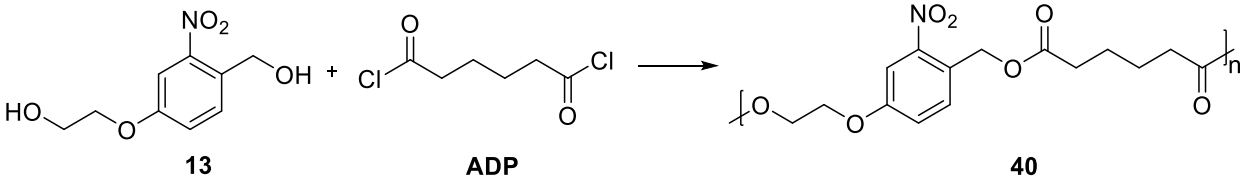

13 ADP 40

*Scheme 4-25: Synthesis of homopolymer **40**.*

Precipitation in MeOH yielded no product and the analysis of the residue after removal of the MeOH confirmed that the polymerization was unsuccessful.

4.4.3. Polyester 41 from Monomer 9

Instead of a DMF/DCM mixture, THF was used as a solvent for preparation of polyester **41** from monomer **9** and ADP (*Scheme 4-26*).

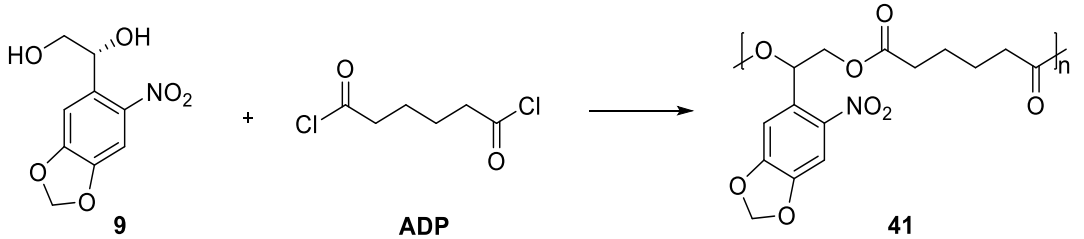

9 ADP 41

*Scheme 4-26: Synthesis of homopolymer **41**.*

In a first attempt, sample **41a** should be synthesized analogously to samples **39** and **40** only using THF as a solvent, but no product could be obtained (*Table 4-13*).

*Table 4-13: Results of the synthesis of homo-polyester **41**.*

Sample	T [°C]	Time [h]	n_{DMAP} [µmol]	M_n [g/mol]	Yield [%]
a	RT	48	/	/	/
b	RT	overnight	3	/	/
c	RT	overnight	50	/	/
d	50	overnight	7.5	/	/

In a second attempt, DMAP, which is a common organocatalyst for the preparation of esters,[126] was added for the synthesis of **41b**. Despite the addition of a catalyst, the polymerization was not successful as no polymer was obtained. Thus, sample **41c** was prepared with a vastly increased amount of added catalyst compared to **41b** which also did not lead to the successful formation of polymer **41**. As a last approach, sample **41d** should be synthesized at an elevated reaction temperature using moderately increased amounts of DMAP compared to **41b**. As in the previous experiments, no polymer formation could be observed indicating monomer **9** cannot be polymerized by ADP.

4.5. Degradation Analysis

The key property of the synthesized compounds, the stimuli-induced degradability, was tested as well as characterized by several different methods. Especially for the decomposition of the light-degradable polymers, an extensive investigation of various aspects of the degradation process could be covered. A better insight into this process ensures, on the one hand, functionality of the later formed stimuli-degradable DDS. On the other hand, it might enable optimization of the degradation rates and thus enable fine-tuning of the release rates.

4.5.1. UV/Vis Polymer Degradation Experiments

UV/Vis spectroscopy enables the investigation of light-induced electron transfers of an analyte by measuring the absorbance *A* at certain wavelengths. Basically, the initial

intensity I_0 of a light beam that passes a homogeneous, isotropic medium of certain length d is reduced to a value of I by both, reflectance as well as absorption of the analyte. In case of a diluted solution, which contains only the analyte as an absorbing compound, the intensity decrease is proportional to the concentration c and the molar attenuation coefficient ε, as given by the Beer-Lambert law (4-2).[127]

$$A = log\left(\frac{I_0}{I}\right) = \varepsilon \cdot d \cdot c \qquad (4\text{-}2)$$

Therefore, UV/Vis spectroscopy is a useful tool for, e.g., the investigation of reaction kinetics, if at least one of the compounds involved in the reaction absorbs light in the UV/Vis range. Due to their high transmittance even below 200 nm, saturated hydrocarbons as well as MeCN and water are typically considered as very suitable solvents for UV/Vis measurements. Furthermore, DCM can be used down to 220 nm, while THF can only be used above 280 nm most of the time.[127]

UV/Vis Analysis of Light-Induced Degradation in Solution

UV/Vis spectroscopy is a very sensitive method which is particularly useful for the investigation of the oNB photoreaction as both, educts and products, can be detected. Since no workup or collection of the sample is needed, any number of measurement points can be recorded, which enables monitoring of small conversions. However, while UV/Vis is very suitable for investigating the photoreaction, no conclusions can be drawn about the variation in M_n. In order to investigate the influence of the comonomers as well as the used polymerization technique on the photo-degradation, homo- and copolymers based on monomer **2** were analyzed. Thus, DCM solutions of homo-polycarbonate **21**, homo-polyurethane **27**, BHED co-polyurethanes **28a-c** and PEG400 co-polyurethanes **29a-c** were prepared. One aliquot of each solution was filled into a quartz cuvette and the initial spectrum of the non-irradiated sample was measured. As already stated, all spectra showed very similar absorbance patterns and λ_{max} values, confirming the photo-responsive moiety to be the only group absorbing in the investigated wavelength range. Afterwards, the samples were irradiated with UV light for certain periods of time up to 300 s and analyzed by UV/Vis spectroscopy after each step. The spectra of all investigated polymers exhibited responsive behavior upon irradiation with UV light, which can be seen for homopolymers **21** and **27** in *Figure 4-9.*

Due to the high similarity of the obtained graphs, the results of the other samples are listed in *Table 4-14*.

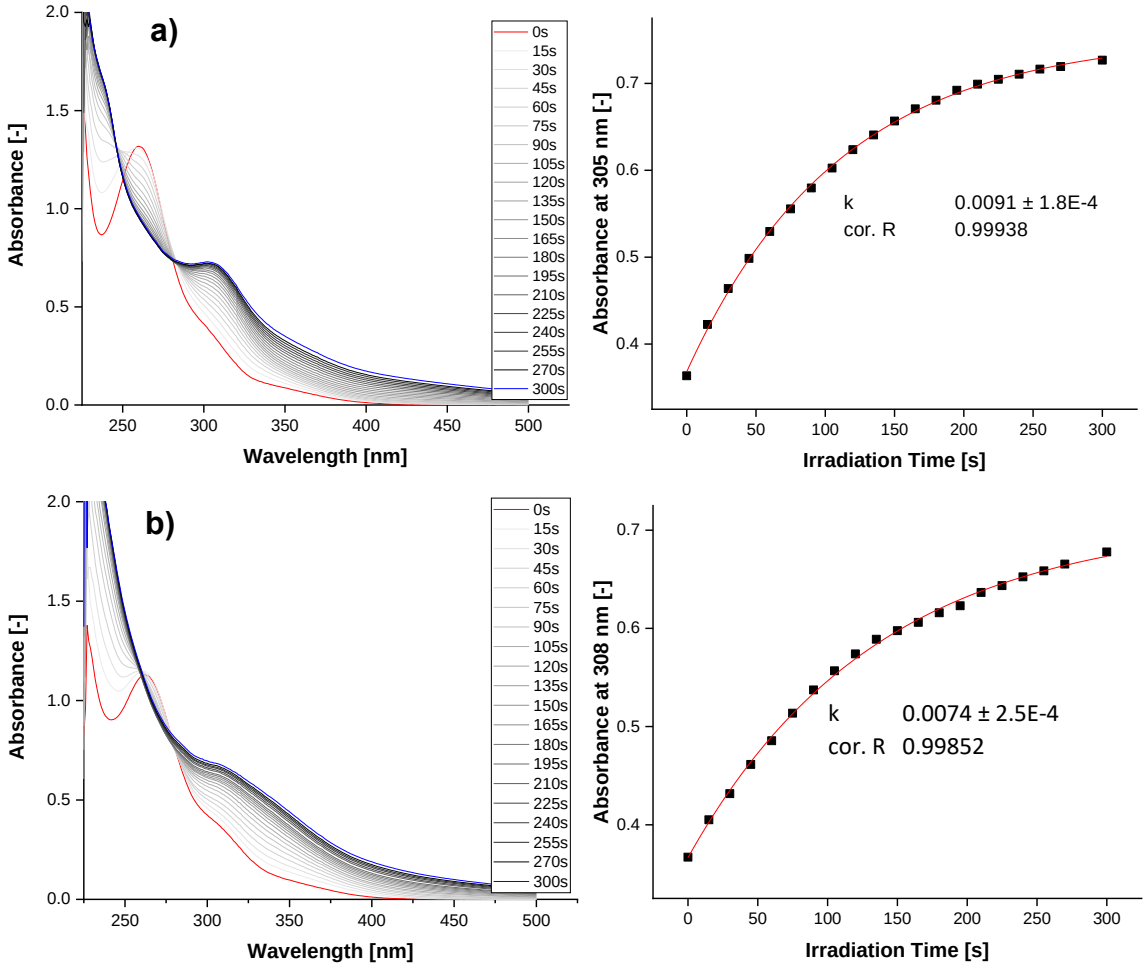

*Figure 4-9: Absorbance variation (left) and increase of the degradation product absorbance at λ_{max} (right) upon irradiation with UV light for polycarbonate **21** (a) and polyurethane **27** (b) in DCM solution.*

As shown, all samples exhibited a clear decrease of the initial absorbance maximum at 260 nm, which indicated the degradation of the photo-responsive moiety. Furthermore, the rise of a new absorbance maximum at approximately 305 nm was found, indicating the formation of the *o*-nitrosobenzaldehyde derivatives upon irradiation. Superposition of the initial maximum and the lower maximum of the degradation product was observed for the polycarbonate as well as for the polyurethanes after certain irradiation times. Therefore, the kinetics of the photoreaction was investigated regarding the formation of photodegradation products by plotting the absorbance at 305 nm relative to the irradiation time for all samples. The plotted data showed a course of first order kinetics for the light degradation process of all samples, which is in line with the degradation mechanism of oNB

compounds. A non-linear fit corresponding to the rate equation of first order kinetics was applied to the data with good accordance, as shown in *Figure 4-9*. The resulting apparent rate constants of the photodegradation $k_{app,UV/Vis}$ are very similar for all polymer samples ranging from 0.0064 ± 0.0002 s^{-1} to 0.0107 ± 0.0005 s^{-1} with a mean average of 0.0083 ± 0.0014 s^{-1}. Thus, it can be assumed that the rate of the photoreaction is not affected by the used comonomers or by the type of polymer.

*Table 4-14: Results of the UV/Vis degradation kinetics of polymers based on **2**.*

	21	**27**	**29a**	**29b**	**29c**	**28a**	**28b**	**28c**
$k_{app,UV/Vis}$ [s^{-1}]	0.00906	0.0074	0.00995	0.00639	0.00712	0.00639	0.00906	0.01073
σ_k [s^{-1}]	±0.000181	±0.000251	±0.000264	±0.000195	±0.000343	±0.000259	±0.000261	±0.000454
$R^2_{corr.}$	0.9993	0.9985	0.9988	0.9991	0.9972	0.9983	0.9986	0.9962

The analysis of model compound **20** was performed analogously to the polymer UV/Vis analysis revealing identical absorbance pattern and absorbance maxima of the degradation products (*Figure 4-10*).

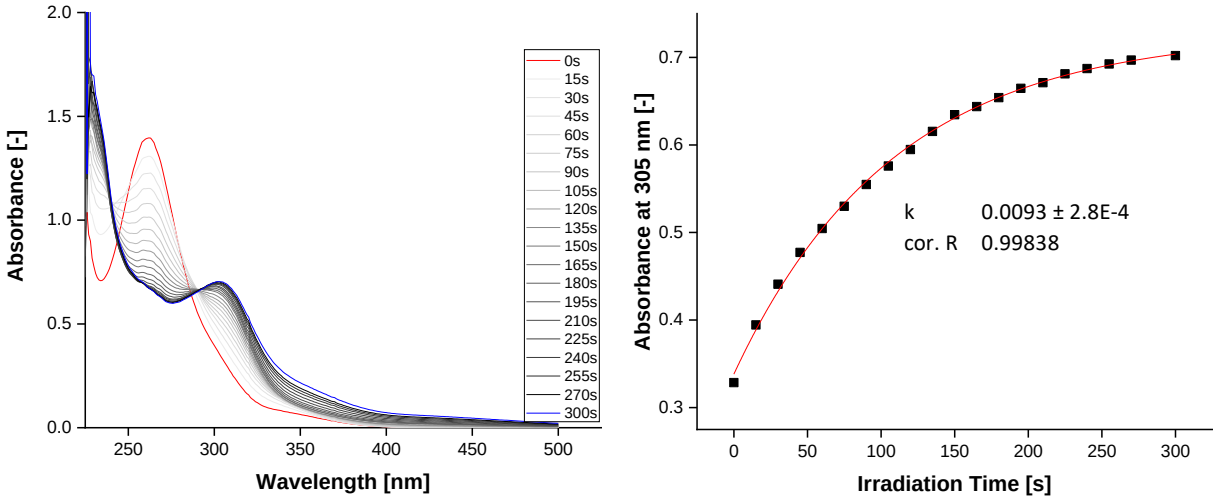

*Figure 4-10: Absorbance variation (left) and increase of the degradation product absorbance at λ_{max} (right) upon irradiation with UV light for model compound **20** in DCM solution.*

As expected, plotting of the absorbance maximum at 305 nm versus the irradiation time showed photoreaction kinetics that are similar to the polymers. The apparent rate constant $k_{app,UV/Vis}$ of 0.0093 ± 0.0003 s^{-1} resembles the results of the polymer analysis, underlining the successful photoisomerization.

Due to higher biological safety, light in the UV-A region (315-400 nm) is typically employed for UV irradiation in medical or therapeutic applications. Though polymers based on monomer **2** showed fast degradation, λ_{max} of these polymers is significantly below the UV-A range, limiting the reaction rate. Thus, it is desirable to employ polymers with higher λ_{max} so a higher portion of emitted light can be used for the reaction. Though the functionalization of the aromatic core is known to potentially reduce the quantum yield, the higher λ_{max} can outweigh the lower quantum yield using UV-A light sources.[128] Polymers based on monomers **6** and **13** showed higher λ_{max} values due to the substitution of the aromatic core of each monomer. Therefore, the photoreaction of polymers **30**, **31a** and **31b** was analyzed in the same fashion as the previous samples (*Figure 4-11*).

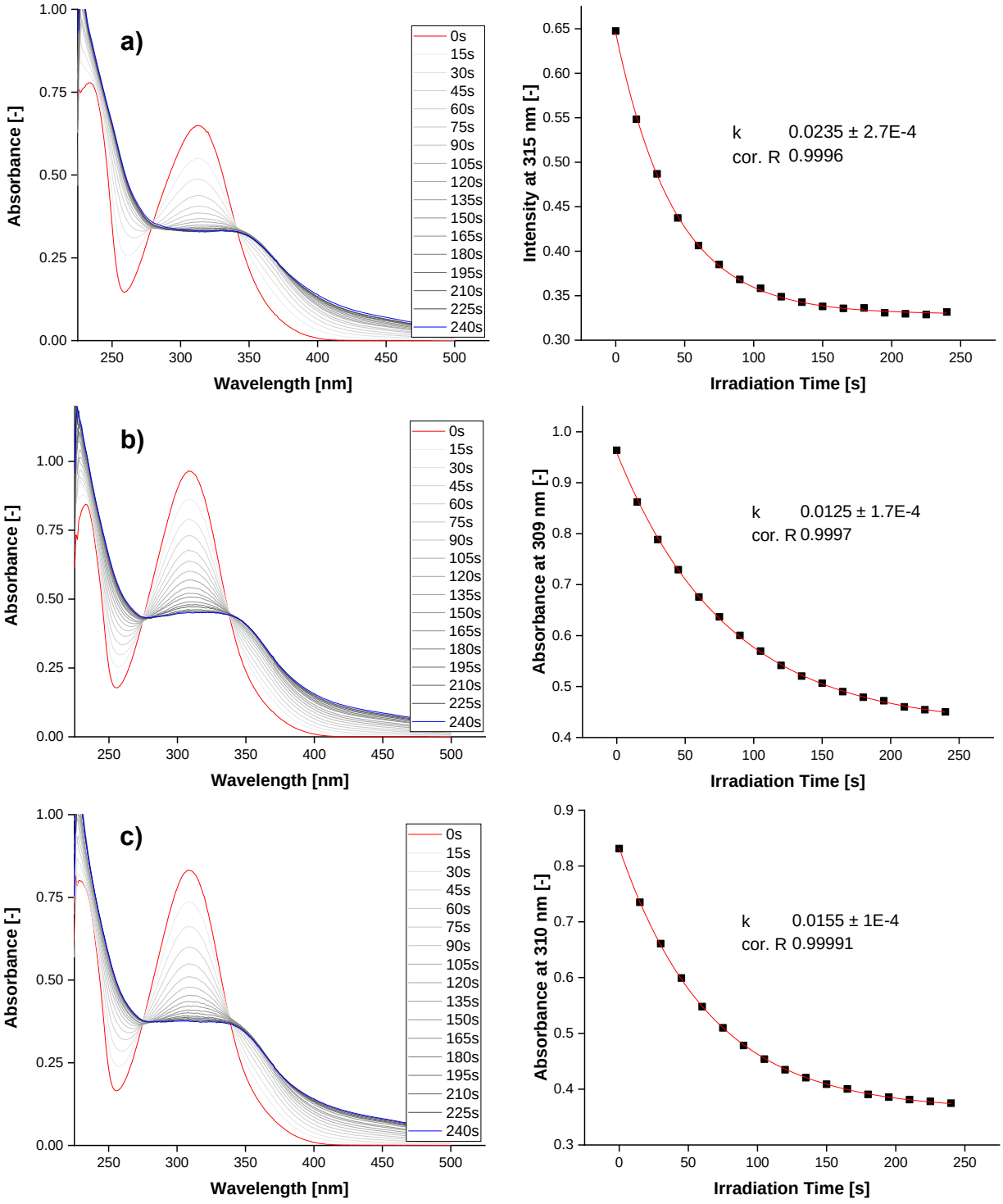

*Figure 4-11: Absorbance variation (left) and increase of the degradation product absorbance at λ_{max} (right) upon irradiation with UV light for polyurethane **30** (a), **31a** (b) and **31b** (c) in DCM solution.*

The resulting spectra revealed a very similar course of reaction for all three samples and, in contrast to the polymers based on **2**, only negligible superposition of the initial maximum and the lower degradation product maximum (<230 nm). Interestingly, the

bathochromic effect of the substituents appears to induce different λ_{max} shifts on the light-responsive moiety and the corresponding degradation product. Comparing polymers **27** and **30**, which are identical in structure except for the methoxy group attached to the light-responsive unit of **30**, λ_{max} before irradiation is increased by 55 nm (260 nm to 315 nm), while λ_{max} after irradiation is increased by only 30 nm (308 nm to 338 nm). The same behavior was observed for samples **31a** and **31b**, probably because of the structural similarity of these three samples. Due to this, only a moderate absorbance increase was visible for the degradation product signal, while the absorbance decrease of the initial maximum was clearly visible. Therefore, in contrast to the previous samples, the kinetic investigation was carried out using the decrease of the initial λ_{max} of the non-irradiated polymers (*Figure 4-11*). All three samples revealed enhanced $k_{app,UV/Vis}$ values compared to the samples based on **2**. However, while polymers **31a** and **31b** showed quite similar values of 0.0125 ± 0.0002 s^{-1} and 0.0155 ± 0.0001 s^{-1}, sample **30** exhibited a significantly higher $k_{app,UV/Vis}$ of 0.0235 ± 0.0003 s^{-1}. These results indicate a much faster photoreaction for polymer **30** than for samples **31a** and **31b**, which is in sharp contrast to the similar structure of the investigated polymers. Considering the λ_{max} values of these polymers, this indicates a higher quantum yield of monomer **6** compared to monomer **13**, that could be related to the hydroxymethyl substituent of **6**.

It is well known that λ_{max} can be increased even further by introducing a second bathochromic ether moiety.[85] Therefore, the photoreaction of monomer **9** based polymer **35** was also analyzed via UV/Vis. The same procedure was used for the measurements as for the previous samples, but 0.2 vol% DMSO had to be added to the DCM solution to completely dissolve the polymer. In addition, the samples were irradiated in 1 s intervals up to 10 s instead of 15 s intervals, because of the much faster reaction rate (*Figure 4-12*).

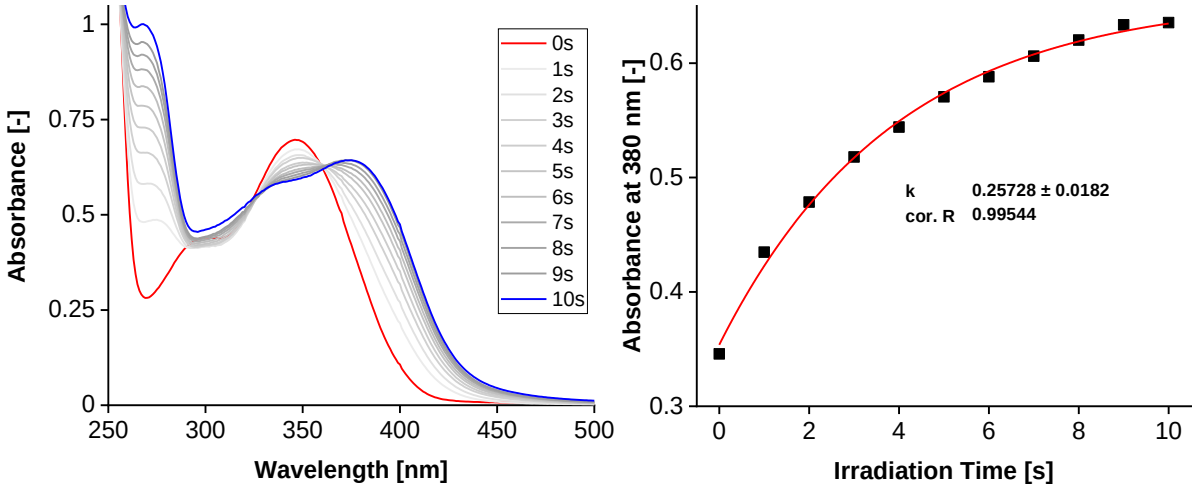

*Figure 4-12: Absorbance variation (left) and increase of the degradation product absorbance at λ_{max} (right) upon irradiation with UV light for polyurethane **35** in DCM/DMSO solution.*

The λ_{max} of approximately 350 nm showed a clear decrease in absorbance implying degradation of the photo-responsive unit. Furthermore, the appearance of two new absorbance maxima around 260 nm and 380 nm was observed, indicating formation of the expected *o*-nitrosobenzoketone derivatives as photodegradation products. In line with the previous samples, the course of the plotted data indicates first order kinetics for the light degradation process of **35** in solution. However, this 6-nitropiperonal-based polymer showed the highest rate constant of all investigated polymers with a $k_{app,UV/Vis}$ of approximately 0.26 s^{-1}. Besides the high λ_{max}, that is perfectly within the UV-A range, functionalization of the benzyl carbon in *ortho*-position to the nitro group is known to enhance the quantum yield, which also significantly increases the reaction rate. Though all polymers exhibited first order kinetics, only the spectra of polymer **35** showed a uniform photoreaction as observed by AD diagrams. AD diagrams are created by plotting the absorbance differences $AD = A(\lambda_x,t) - A(\lambda_x,t_0)$ at different wavelengths (*Figure 4-13*). The course of the resulting graph provides information about the uniformity of the photoreaction, where a non-linear function indicates two or more independent reactions.[127]

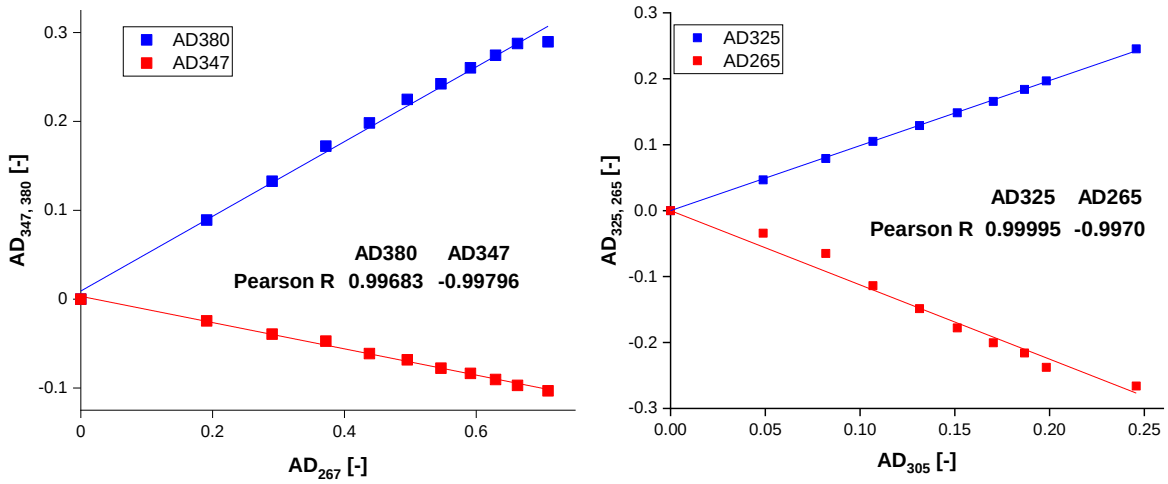

*Figure 4-13: AD diagrams for polymers **35** (left) and **21** (right)*

Overall, good accordance of the linear fit and the measured data can be observed for polymer **35**. A slight deviation of the fit observed at t = 10 s is probably due to superposition with the degradation product absorbance in the UV/Vis spectrum (*Figure 4-12*). In contrast, the results of polymer **21** revealed significantly higher deviation from a linear function, indicating a non-uniform photoreaction process. The reason for this is further reactions of the reactive *o*-nitrosobenzaldehyde derivatives formed as degradation products. However, since all these reactions depend on the initial concentration of **21**, first order kinetics can be assumed for the photodegradation process. For the novel polymer **35**, a reaction pathway based on literature reports was proposed leading to the formation of an *o*-nitrosobenzoketone derivative,[85] which is in line with the UV/Vis results (*Scheme 4-27*).

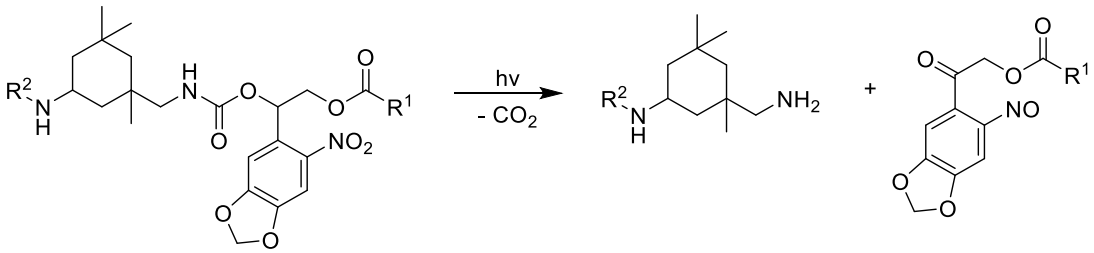

*Scheme 4-27: Proposed degradation route of polymer **35** upon irradiation with UV light.*

According to the literature, these ketone photo degradation products are significantly less reactive than the corresponding aldehydes, which could explain the higher uniformity found. As a second route, degradation at the primary carbamate unit under

formation of an *o*-nitrostyrene derivative could be possible (*Scheme 4-28*).

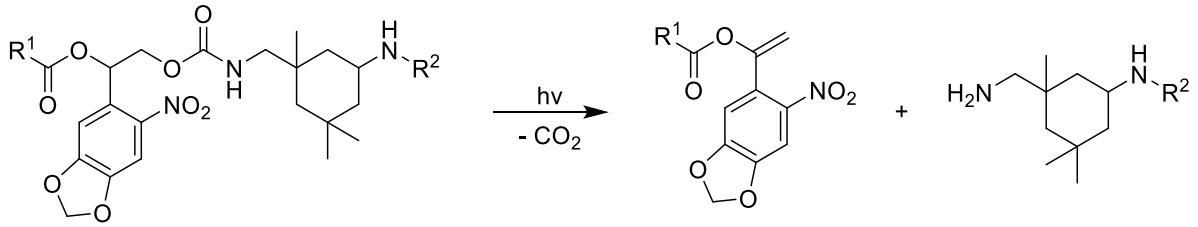

*Scheme 4-28: Alternative degradation route of polymer **35** upon irradiation with UV light.*

However, comparison of the UV/Vis spectra of nitrostyrene derivative **8** and polymer **35** after irradiation showed a significantly higher λ_{max} of compound **8**. In contrast, the λ_{max} value of **35** after degradation and the λ_{max} values of nitrosobenzoketone compounds with similar structure were in good agreement, underlining the route proposed in *Scheme 4-27*.[85]

The analysis of *o*-nitrobenzylacetal-based polymers **32a** and **32b** was carried out analogously to the previous samples in DCM solution. For sample **35**, shorter irradiation intervals had to be used, due to a rapid variation of absorbance with a full decrease of the initial λ_{max} after 25 s (*Figure 4-14*).

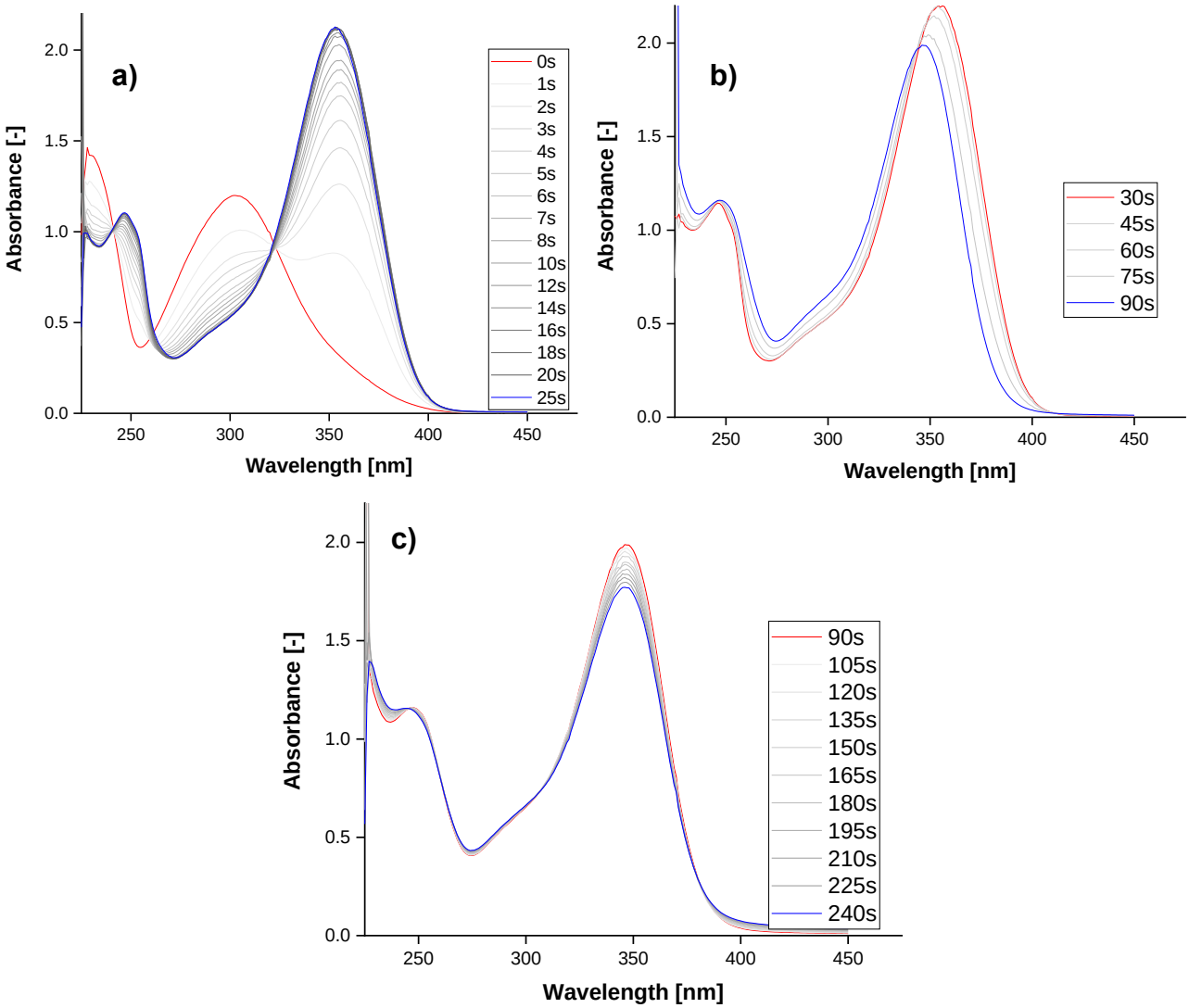

*Figure 4-14: Absorbance variation of polyurethane **32a** in DCM solution upon irradiation with UV light divided into phases 1 (a), 2 (b) and 3 (c).*

Interestingly, the results showed significant further changes in absorbance with on-going illumination, which could be divided into three phases. In the first phase, a typical course of the photoreaction with shrinking of the initial λ_{max} as well as rising of a new λ_{max} at approximately 354 nm could be observed until 25 s of irradiation (*Figure 4-14a*). Further irradiation led to a moderate decrease of the new maximum in both, absorbance and λ_{max} until an irradiation time of 90 s (*Figure 4-14b*). In the last phase, a small absorbance decrease of the final λ_{max} at 347 nm was visible until 240 s. According to the literature, similar low molecular weight compounds show only the formation of a corresponding nitrosobenzoic acid ester derivative upon irradiation, which is then deprotected by acidic or basic hydrolysis for full release.[129] In contrast, especially the λ_{max} decrease from 354 nm to 347 nm in the second phase indicated

another photoreaction dependent from the photodegradation product of the first phase. Thus, SEC should be employed to investigate the molar mass reduction or chain cleavage, respectively.

4.5.2. SEC Polymer Degradation Experiments

SEC is a very essential method of polymer characterization in both, industry and academic research. SEC typically yields the molecular weight (M_n, M_w, etc.) and Đ (= M_w/M_n) of a polymer sample based on its hydrodynamic volume. Dependent on the used detectors and calibration, an absolute value or a relative value is obtained for the molecular weight. Especially for the characterization of polymer degradation it is a very convenient method due to the direct proof of molar mass reduction.

SEC Analysis of Light-Induced Polymer Degradation in Solution

In addition to the UV/Vis analysis, further investigations on the light-responsive behavior of the synthesized polymers were carried out using SEC. Therefore, stock solutions of each polymer in DCM were prepared and irradiated with UV light for certain periods of time. The only exception was polymer **35**, which had to be dissolved in a DCM/DMSO mixture (24/1; v/v). After the samples were dried, SEC measurements in THF were carried out using PS calibration to investigate the molar mass reduction. Though the SEC experiments were performed analogously to the UV/Vis measurements, much higher concentrations were needed for the SEC measurements. At first, homo-polycarbonate **21**, homo-polyurethane **27**, BHED co-polyurethanes **28a**-**c** and PEG400 co-polyurethanes **29a**-**c** were investigated, revealing a significant shift of the initial SEC trace to higher elution volumes for all polymers confirming a decrease in molar mass (*Table 4-15*, *Figure 4-15*).

*Table 4-15: Results of the SEC degradation kinetics of polymers based on **2**.*

	21	**27**	**29a**	**29b**	**29c**	**28a**	**28b**	**28c**
$k_{app,SEC}$ [s^{-1}]	0.0114	0.0103	0.0180	0.0268	0.0541	0.0095	0.0124	0.0253
σ_k [s^{-1}]	±0.0032	±0.0036	±0.0018	±0.0090	±0.0137	±0.0013	±0.0017	±0.0081
$R^2_{corr.}$	0.97431	0.96342	0.9957	0.94362	0.97404	0.99515	0.99355	0.94841

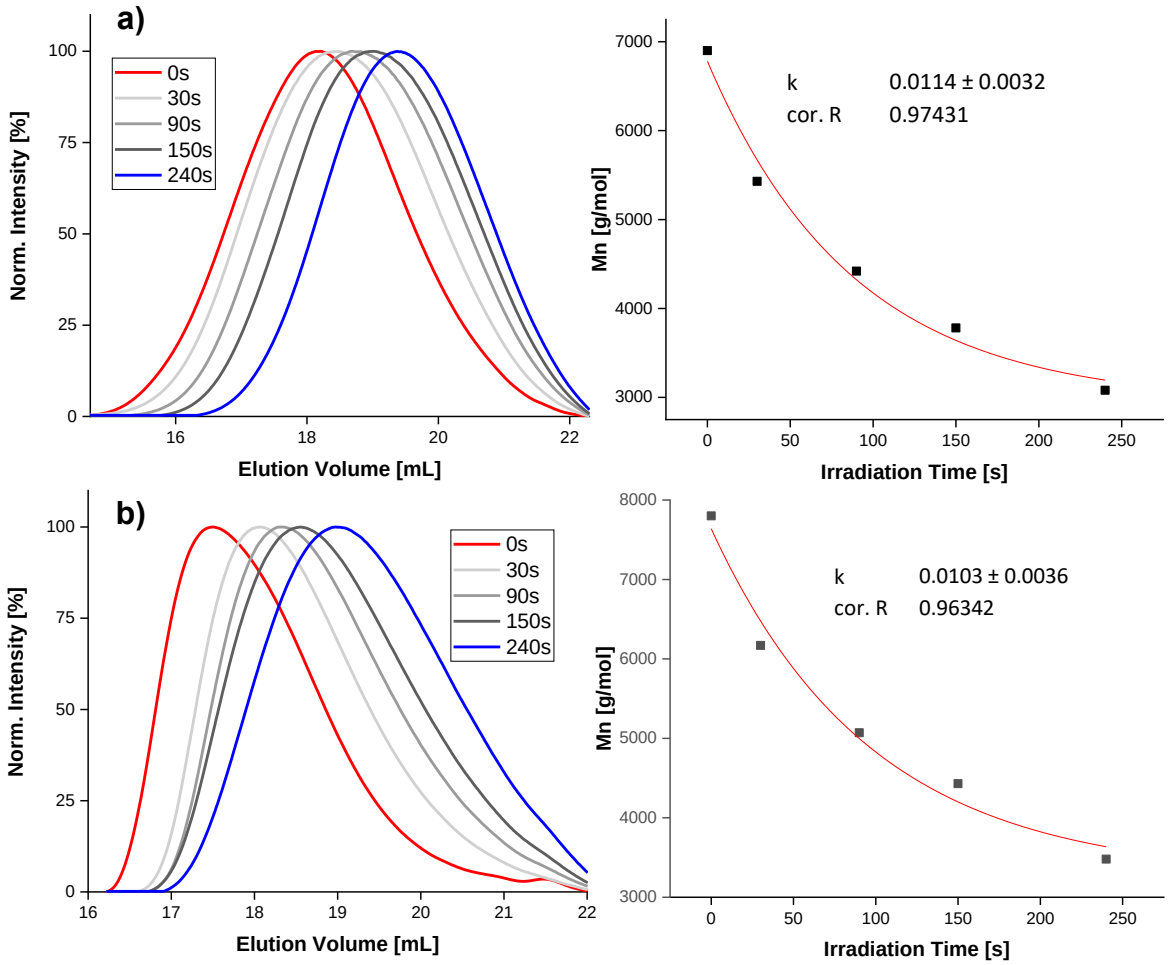

*Figure 4-15: Normalized elugram (left) as well as the corresponding M_n values (right) of homopolymers **21** (a) and **27** (b) upon irradiation with UV light for certain amounts of time.*

In addition to the molar mass decrease, the SEC traces of all samples showed significantly decreasing peak areas with increasing irradiation times, also indicating the degradation of macromolecular compounds (*Figure 4-16*). The peak area of an SEC trace is proportional to the sample concentration, which can be reduced apparently by formation of low molecular weight or oligomeric compounds that surpass the exclusion limit of the SEC system.

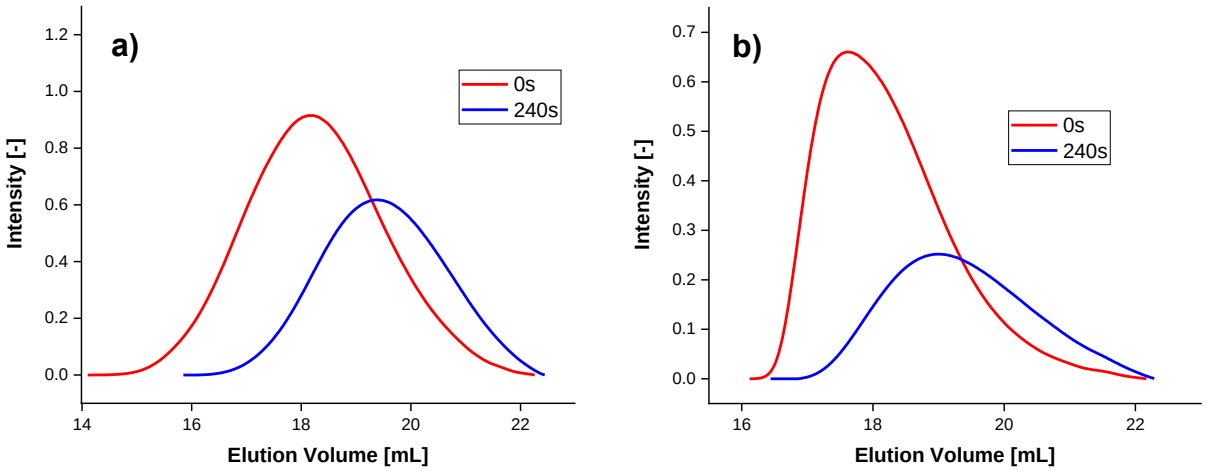

*Figure 4-16: Elugrams with relative intensity of polymers **21** (a) and **27** (b) before and after exposure to UV light.*

Interestingly, the copolymer samples showed a faster shift to higher elution volumes compared to the homopolymer. This contrasts with the results of the UV/Vis analysis, which revealed very similar apparent rate constants for the photoreaction of all polymers. However, due to the backbone-degradation, the introduction of a non-light-responsive comonomer leads to an enhanced loss of molar mass per photoreaction, while the molar mass of the degradation product is increased. The obtained M_n values were plotted versus the irradiation time (*Table 4-15*, *Figure 4-15*) revealing a course of a first order process for the molar mass reduction upon UV irradiation, which is in line with the UV/Vis analysis. Analogously to the UV/Vis analysis, a non-linear fit was applied in order to obtain $k_{app,SEC}$ values for the molar mass degradation. Polycarbonate **21** and polyurethane **27** showed very similar rate constants of 0.0114 ± 0.0032 s^{-1} and 0.0103 ± 0.0036 s^{-1}, which are in the same order of magnitude as the values obtained by UV/Vis analysis. The similarities of the $k_{app,UV/Vis}$ and $k_{app,SEC}$ values for both polymers give proof of chain cleavage by reaction of the photoresponsive unit upon irradiation. As expected, the copolymer samples revealed increasing $k_{app,SEC}$ with higher fractions of the non-light-responsive comonomers. While $k_{app,SEC}$ values of up to 0.0252 ± 0.0081 s^{-1} (**28c**) can be observed for BHED as a comonomer, the PEG400 copolymers show major increased $k_{app,SEC}$ values of up to 0.0541 ± 0.0137 s^{-1} (**29c**). This significant difference in apparent rate constants is due to the higher molar mass of PEG400 compared to BHED leading to an enhanced mass loss per photoreaction of the resulting copolymers. The results prove the successful tunability of the molar mass degradation by copolymerization with non-light-responsive comonomers.

Degradation analysis of polymers **30**, **31a** and **31b** via SEC showed very similar behavior to the samples based on monomer **2**. Upon illumination, all samples revealed a significant shift to higher elution volumes. Again, plotting of the M_n values over the irradiation time revealed a course of first order kinetics for the molar mass decrease (*Figure 4-17*).

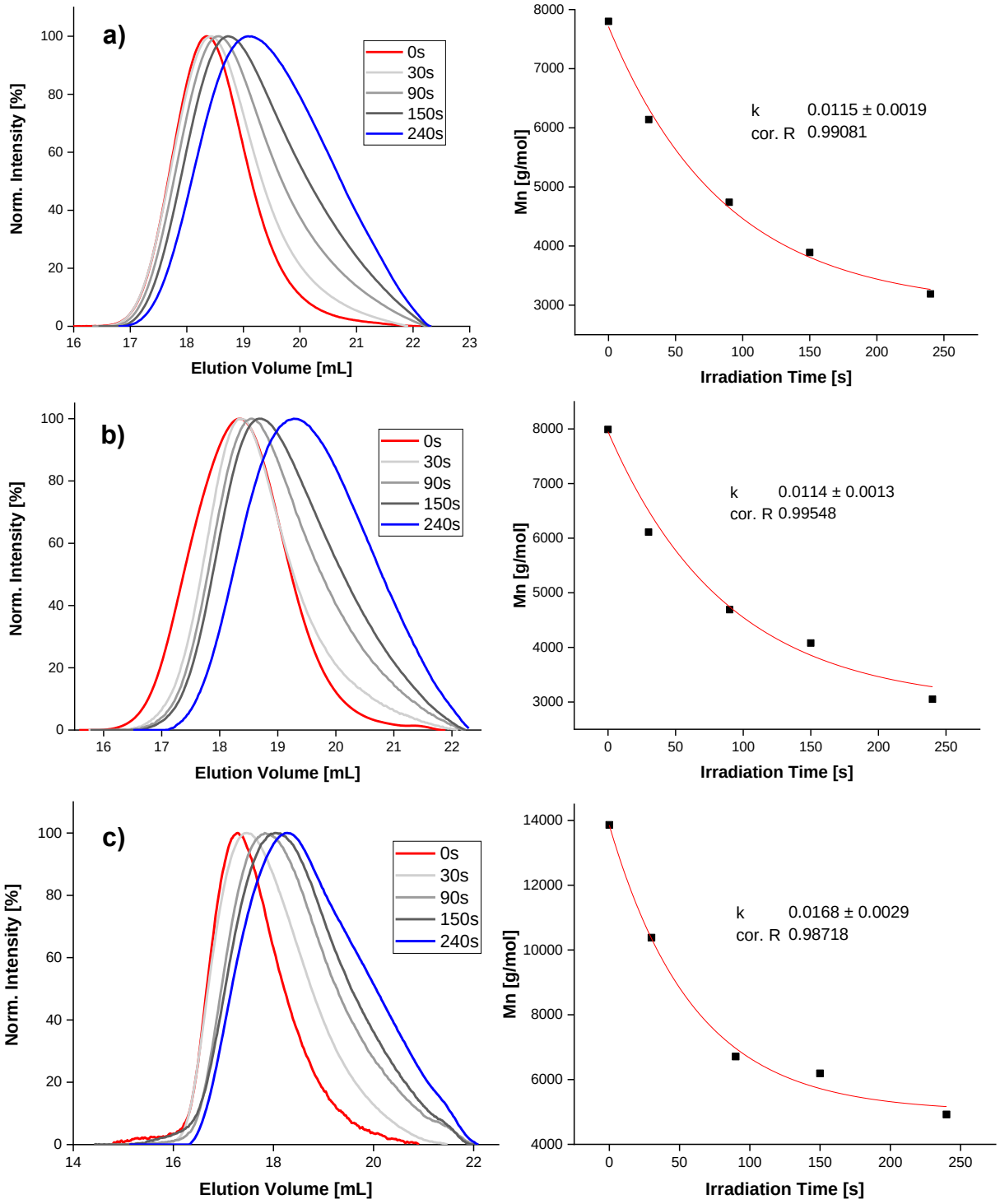

*Figure 4-17: Normalized elugram (left) as well as the corresponding M_n values (right) of homopolymers **30** (a), **31a** (b) and **31b** (c) upon irradiation with UV light for certain amounts of time.*

In contrast to the previous results, polymer **30** showed a significantly lowered $k_{app,SEC}$ value of 0.0115 ± 0.0019 s^{-1} compared to the UV/Vis results, indicating different rates of photoreaction and chain cleavage. On the other hand, samples **31a** and **31b** revealed good agreement of the SEC results with the respective $k_{app,UV/Vis}$ values of both polymers. It appears that the formation of block copolymers has less impact on the molar mass degradation compared to random copolymers. A reason for this could be that block cleavage is a one-time event, while for random copolymers the average molar mass of the degradation product is increased, which leads to higher loss of molar mass for each photoreaction. Though comparison of the $k_{app,SEC}$ values with those obtained for the polymers based on **2** revealed high similarity, compounds **30**, **31a** and **31b** enable usage of UV light at longer wavelengths.

Based on the rapid reaction observed in the UV/Vis experiment of polymer **35**, a first sample was irradiated for only 10 s revealing a significant shift of the elution volume (*Figure 4-18*).

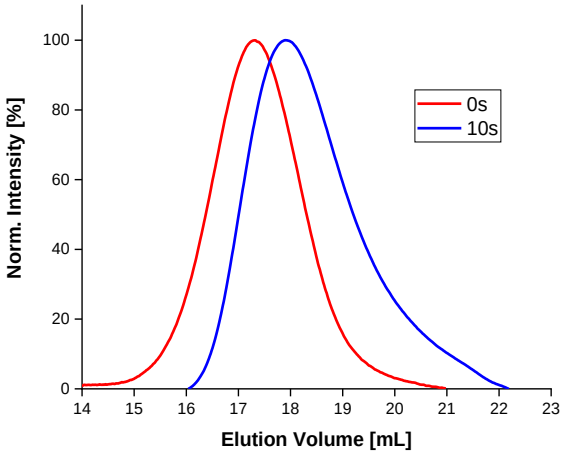

*Figure 4-18: Normalized elugram of polymer **35** before and after 10 s of UV irradiation.*

Though a major decrease in M_n from 15810 g/mol to 6590 g/mol was observed, further irradiation steps were undertaken in the same intervals as for the previous samples. In addition, the M_n values were plotted over each corresponding irradiation time analogously to the previous investigations to evaluate the reaction kinetics (*Figure 4-19*).

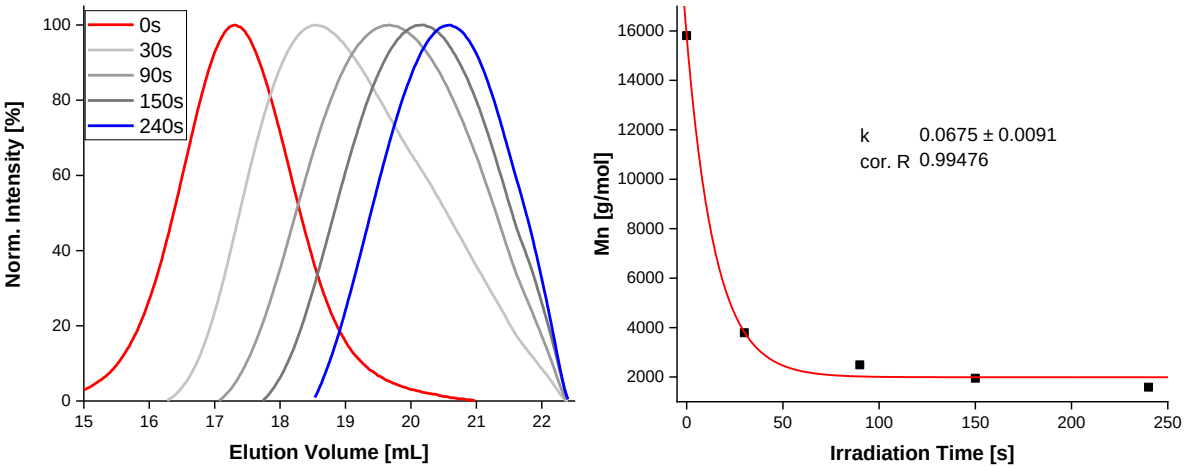

*Figure 4-19: Normalized elugram (left) as well as the corresponding M_n values (right) of homopolymer **35** upon irradiation with UV light for certain amounts of time.*

In line with the UV/Vis results, sample **35** also showed the most rapid molar mass decrease with a $k_{app,SEC}$ of 0.0675 ± 0.0009 s^{-1} confirming the increased quantum yield by functionalization of the benzylic C atom. Similar to polymer **30**, a significant difference between $k_{app,UV/Vis}$ and $k_{app,SEC}$ was observed indicating the photoreaction to be faster than the chain cleavage, which is in line with the literature that suggests the photoisomerization can be considerably faster than the substrate release.[85]

To evaluate the light-induced chain degradation of polymers based on **17**, SEC experiments were carried out for polymers **32a** and **32b** using the same irradiation intervals as for the previous samples (*Figure 4-20*).

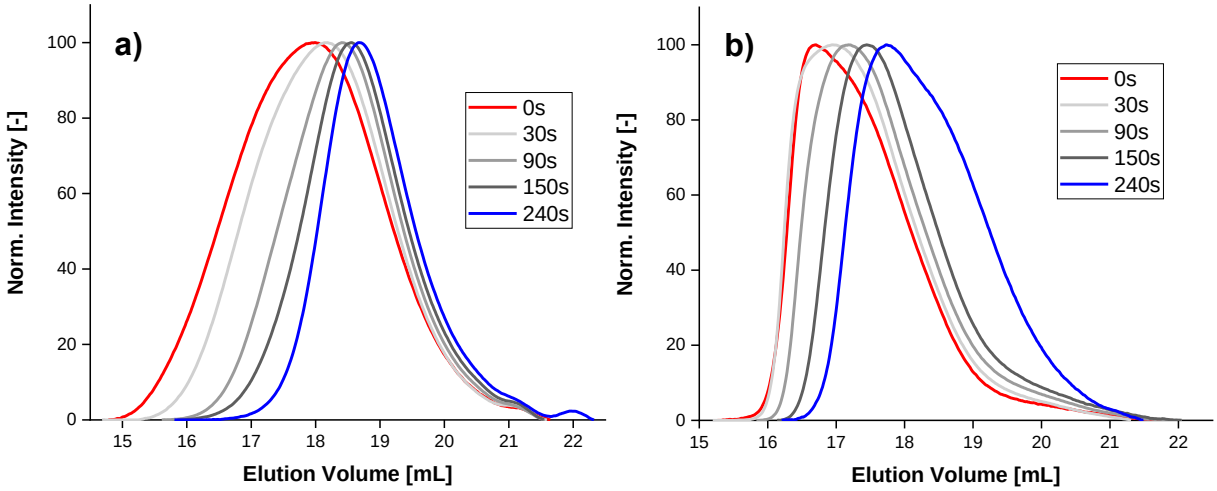

*Figure 4-20: Normalized elugrams of polymers **32a** (a) and **32b** (b) upon irradiation with UV light for certain amounts of time.*

As is known from the UV/Vis experiments, the photoreaction kinetics differs from the previous samples, preventing comparison of $k_{app,SEC}$ values. However, both samples showed a significant shift to higher elution volumes after 240 s of irradiation with UV light, indicating a light-induced M_n decrease. But in sharp contrast to the previous results, the obtained elugrams showed only a slight shift after 30 s of irradiation, which corresponds to minor M_n losses of 900 g/mol for **32a** and 600 g/mol for **32b**. Considering the first phase of the UV/Vis results, which indicated a rapid, light-induced reaction during the first 30 s of irradiation, these results could imply a decoupling of photoreaction and chain cleavage. Thus, further investigations have to be carried out employing other measurements.

SEC Analysis of Stimuli-Induced Polymer Degradation in Aqueous Suspension

For an application as a nanoparticular DDS, the polymer degradability in aqueous environment is essential, as the human body can be considered as an aqueous system. Thus, the light-induced degradability of polymers **21** and **27** in water was tested as a proof-of-concept. Aliquots of THF solutions of both polymers (10 mg/mL) were precipitated into water and stirred at room temperature until complete evaporation of the organic solvent. The obtained white dispersions were filled into a quartz cuvette and irradiated with UV light for 240 s. After isolation and drying of the yellow-colored precipitate, SEC measurements in THF were performed (*Figure 4-21*).

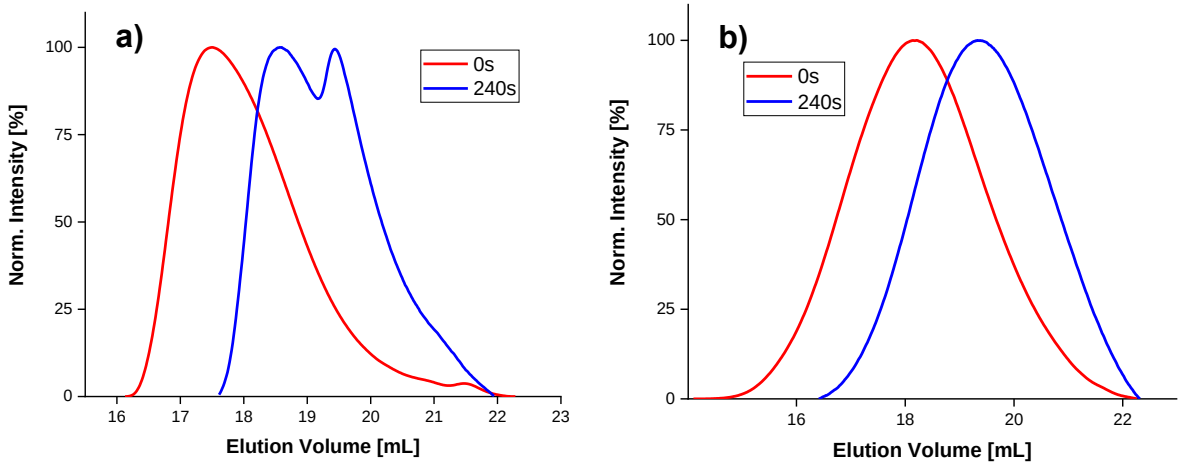

*Figure 4-21: SEC traces of polyurethane **27** (a) and polycarbonate **21** (b) before (red) and after (blue) irradiation with UV light for 240 s in water.*

The elugrams of both polymers reveal a significant shift of the initial SEC trace to higher

elution volumes indicating a decrease of M_n. Furthermore, the SEC trace of polymer **27** after irradiation also shows a strong shoulder at higher elution volumes proving the formation of oligomeric compounds. The observed shifts of the SEC traces align with the shifts obtained by irradiation of the polymer samples in DCM solution confirming the degradability in both, solution and suspension.

Besides light-degradable compounds, acid- as well as redox-labile functions could be implemented into the polymers, either by copolymerization or monomer functionalization. Thus, the degradability of these functions was tested to guarantee the dual-responsiveness. On this behalf, redox-induced degradability of the disulfide containing copolymers **28a-28c** was investigated. In short, the polymers were dissolved in THF and each solution was added dropwise to aqueous DTT solution under stirring and nitrogen atmosphere. DTT is a typical reducing agent which is used, e.g., for the cleavage of disulfide bonds in proteins. The resulting dispersions were stirred overnight and the solid residues were isolated afterwards. SEC measurements confirmed the successful degradation of the polymers (*Figure 4-22*).

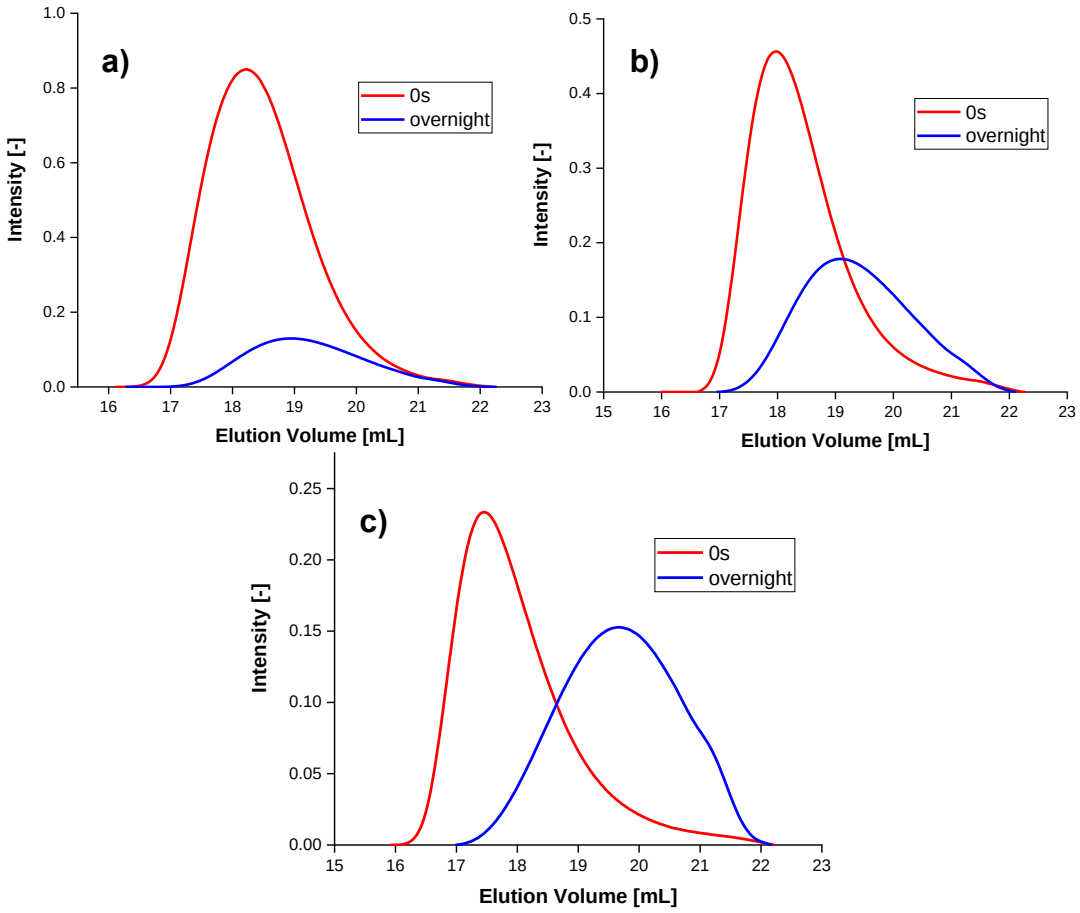

*Figure 4-22: SEC traces of the redox-responsive copolymers **28a** (a), **28b** (b) and **28c** (c) before (red) and after (blue) treatment with aqueous DTT solution.*

A significant drop of the peak areas can be observed for all samples, implying a decreased polymer concentration. Interestingly, sample **28a** showed the highest drop of peak area, while smaller changes can be observed for higher BHED amounts. Furthermore, the results reveal a shift of the SEC trace to higher elution volumes, indicating a decrease of the M_n of all samples and thus proving the successful redox induced degradation. In contrast to the peak areas, a lower M_n was observed for samples with higher amounts of redox-responsive BHED after degradation. The *Đ* of all samples increased to a value of approximately 1.6. An explanation for these findings could be that DTT reduces disulfide bonds by a thiol-disulfide interchange reaction in which the free thiol functions of DTT cleave the disulfide bond of the polymer by nucleophilic attack.[103] During this process DTT is consumed by formation of a cyclic intramolecular disulfide, while the released polymer thiol groups can participate in both, thiol-disulfide interchange reactions and thiol combination. With increasing concentration of thiol groups, the probability of such reactions increases, too. However, all investigated samples showed degradation upon contact with a reductive environment enabling potentially the release of cargo.

Investigation of the acid-induced hydrolysis of acetal-containing polymers **32a** and **32b** was carried out similarly to the redox-induced degradation of polymers **28a**-**28c**. Regarding the later application, only a moderately acidic aqueous environment is of interest as a degradation medium. Thus, instead of aqueous DTT solution, buffered solutions of pH 5 and pH 7.4 were used as degradation medium and reference medium, respectively, for incubating the polymers. It is known that acid-induced hydrolysis of acetal-containing polymers is considerably slower than the previously investigated light-induced degradation. Therefore, the polymers were incubated for 72 h and subsequently measured after isolation (*Figure 4-23*).

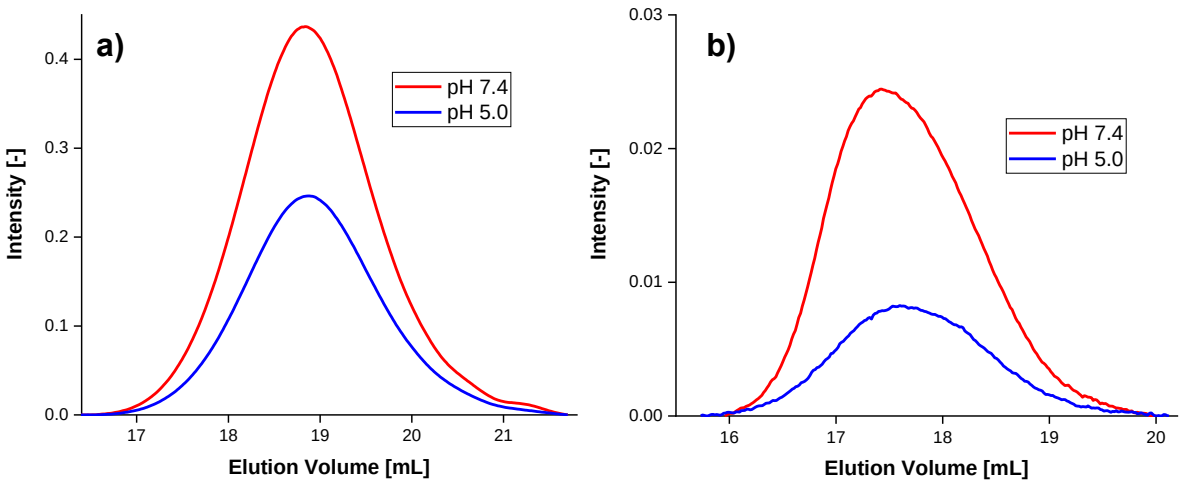

*Figure 4-23: SEC traces of polymers **32a** (a) and **32b** (b) upon treatment with buffered solutions of pH 7.4 (red) and pH 5 (blue).*

While the SEC measurements revealed no change in M_n after being incubated for 72 h in both media, incubation in pH 5 buffered solution led to significantly decreased peak areas compared to incubation in neutral buffer for both samples. In line with the literature, block copolymer **32b** showed a much higher difference of approximately 64% than homopolymer **32a** with approximately 43%. The reason for this could be the increased hydrophilicity of **32b** due to the mPEG5000 blocks, which is known to enhance the hydrolysis even at neutral pH.[100] This also explains the peak area difference at neutral pH between samples **32a** and **32b**, which were prepared with equal amounts of polymer. A reason why the peak areas decreased but no change of M_n was observed could be the increasing hydrophilicity of the degradation products due to the release of hydroxy groups, which further accelerates the hydrolysis of the remaining degradation products. In addition, a second experiment was performed dissolving polymer **32a** in HCl/1,4-dioxan solution instead of preparing an aqueous suspension. After stirring overnight, the solvent was removed *in vacuo* and the residue analyzed via SEC. No polymer signal was obtained, confirming the complete degradation of the sample under acidic conditions and supporting the results in aqueous suspension.

4.5.3. MS Analysis of Light-Induced Degradation

In order to further investigate the photo degradation process as well as the formed degradation products, MS analysis was employed. MS analysis is a powerful and versatile tool for structure determination of both, low and high molecular weight

compounds. Furthermore, only small amounts of substance are needed for the measurements, enabling settings similar to the previous analyses. ESI-ToF mass spectrometry was used to investigate the products formed during the degradation of model compound **20** (*Figure 4-24*), based on the proposed mechanism of the photoisomerization of oNB derivatives. The experiment was performed analogously to the SEC investigations of the polymers with an irradiation time of 150 s.

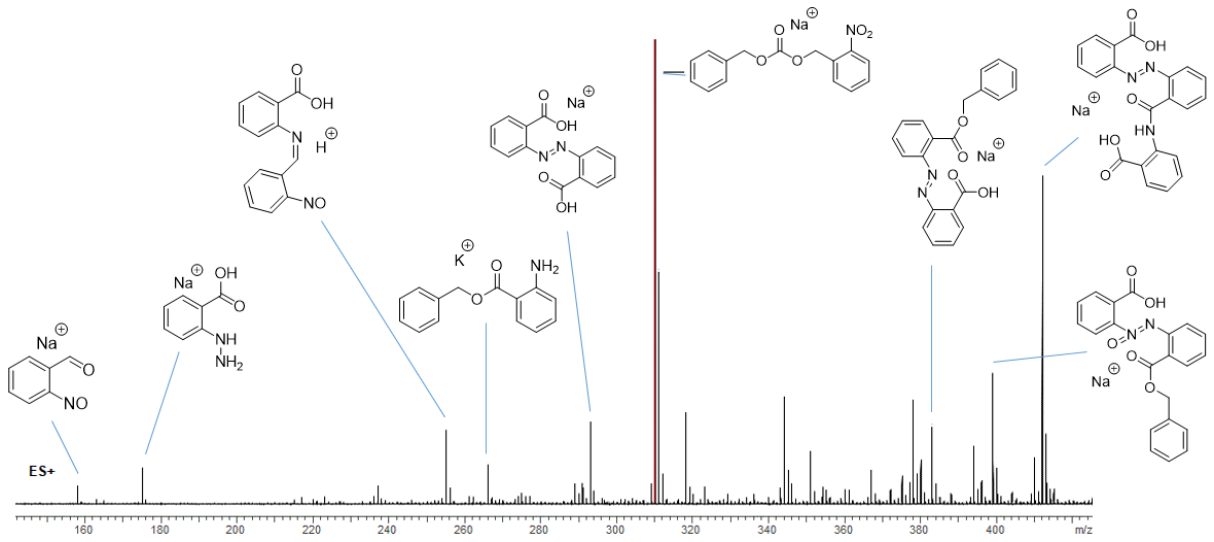

*Figure 4-24: ESI-ToF mass spectrum of model compound **20** and the assigned degradation products after irradiation with UV light.*

Sodium adducts of *ortho*-nitroso benzaldehyde as well as azo- and diazoxy-compounds were obtained as products of the photoreaction confirming the proposed degradation mechanism. In addition, no alterations of the benzyl alcohol moiety were observed, supporting the concept of degradation product variations via the non-light-responsive hydroxyl group of **2**. Interestingly, the data also revealed the formation of hydrazine, imine, ester and amide compounds which appeared to be formed after the photoreaction by reaction of different photodegradation products. However, since all further reactions depend on the initial concentration of model compound **20**, first order kinetics can be assumed for the photodegradation process.
Based on these results, the same method was used to investigate the degradation products of light-responsive monomers **9** and **17** only adjusting the irradiation times according to the corresponding polymer analysis. While for monomer **9** the anticipated diazoxy-dimer of the ketone degradation product was found in good intensity after 10 s of irradiation, no other signal in the obtained spectrum could be assigned to any of the

structures proposed as educts or products of the photodegradation. In fact, various common adducts were subtracted and the resulting exact masses were compared to numerous compositions of carbon-, hydrogen-, nitrogen- and oxygen-atoms, but no structure matching the molecular formulas could be identified. Elongating the irradiation times also did not yield any results. One reason for this could be a different photoreaction pathway than the proposed one, which is quite unlikely since all other results as well as the literature imply the stated route. Another reason could be fragmentation during the ESI process altering the structures of the analyte. Though ESI is considered a very soft ionization technique, fragmentation during the process cannot be ruled out. In case of monomer **17**, educt and the proposed ester product of the photoreaction exhibit the same molecular formula and can thus not be distinguished. However, the typical azo-/azoxy-dimers formed from the nitroso compounds should still be detectable. Unfortunately, identical to monomer **9** no other structures could be identified among the obtained mass peaks supporting the suspected fragmentation.

4.5.4. Analysis of Light-Induced Polycarbonate Film Degradation

In addition to the degradation analysis in solution, the degradability of the polymer as a solid was tested. Consequently, films of polycarbonate **21** were prepared and investigated before and after irradiation with UV light. For the UV/Vis analysis of the polymer film a DCM solution was prepared, and one droplet was casted on the surface of a quartz cuvette. After evaporation of the solvent, the film was irradiated with UV light for certain periods of time and, subsequently, UV/Vis measurements were performed revealing a similar absorbance pattern compared to the polymer in solution (*Figure 4-25*).

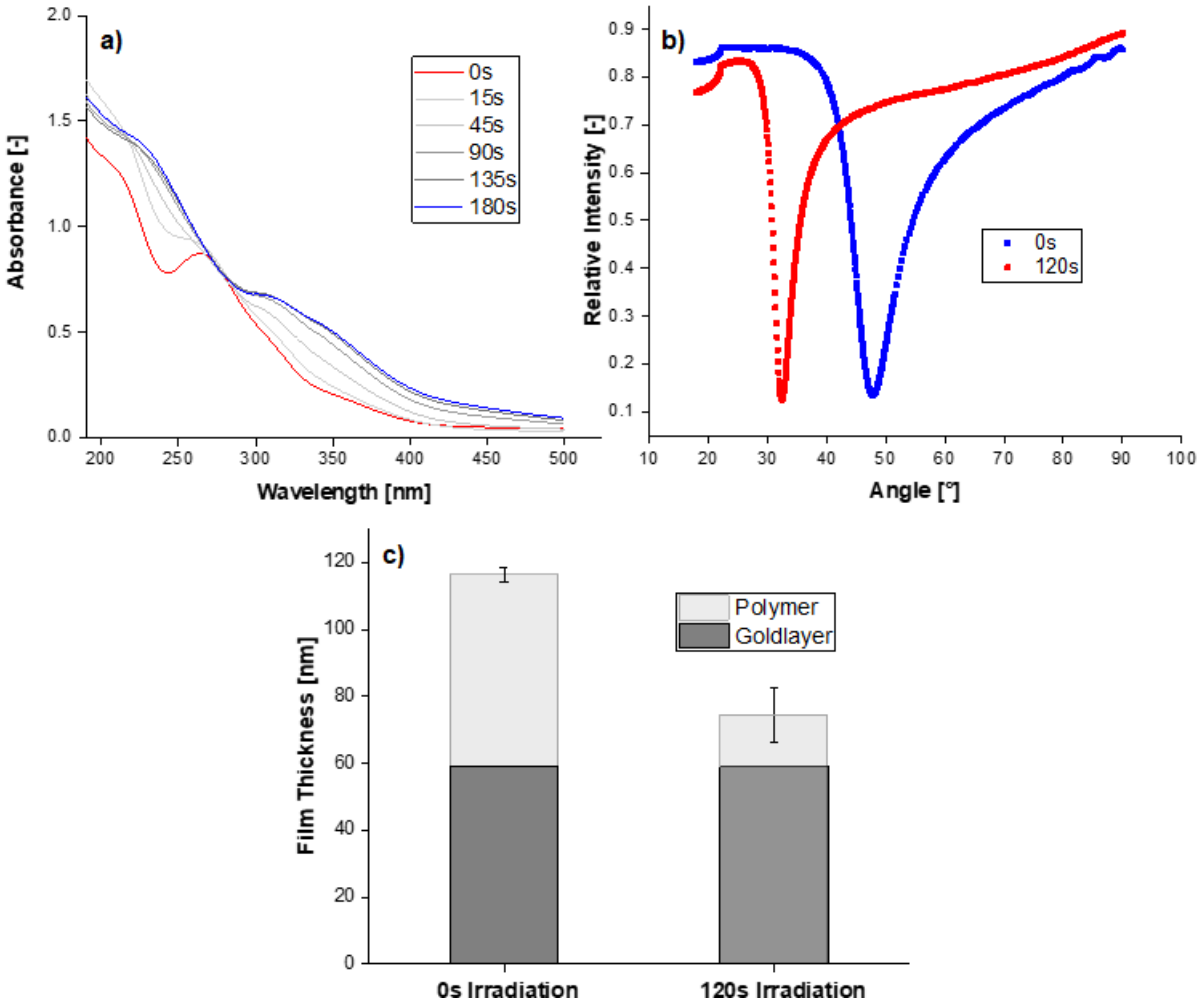

*Figure 4-25: UV/Vis absorbance variations of the polycarbonate film upon irradiation with UV light (a) as well as the change in film thickness of polymer **21** upon irradiation with UV light measured via SPR (b) and profilometry (c).*

Upon irradiation the characteristic vanishing of the maximum at 260 nm as well as rising of the new maximum at 310 nm could be observed, which indicates that the photoisomerization takes place in bulk as well as in solution. For further investigations of the polymer film degradation, SPR analysis and profilometry measurements were employed. Thus, a film of polycarbonate **21** was prepared on a gold-coated wafer via spin coating from a DCM solution (5 wt%). After complete drying of the film, SPR measurements were carried out showing a resonance angle θ of 47.7° (*Figure 4-25*). The film was partly covered applying a photomask and irradiated with UV light for 120 s. Subsequently, the wafer was kept in the dark and placed in a holder containing absolute ethanol. Prior investigations proved the polymer to be insoluble in ethanol and methanol, therefore non-degraded material is not removed during the cleaning process. After complete drying, SPR measurements of the irradiated film were

performed revealing a significant shift of θ to 32.5° while no notable change was observed for the edge of total internal reflection. The SPR resonance angle is linked to thickness and RI of the investigated film thus a shift of θ proves thickness and RI variations of the sample. In addition to SPR analysis, profilometry measurements were carried out revealing a film thickness of 116 ± 2 nm before irradiation including the gold layer of 59 nm. After irradiation, the film thickness decreased significantly by 42 nm to 74 ± 8 nm, confirming the successful film degradation. Based on the thickness of the polymer film obtained by profilometry, the angular reflectivity spectrum of the SPR was fitted yielding RI values before and after irradiation of 1.54 and 2.07.Additionally, IR measurements of the polycarbonate film before and after irradiation with UV light were carried out (*Figure 4-26*) to investigate the transformation of functional groups due to photodegradation.

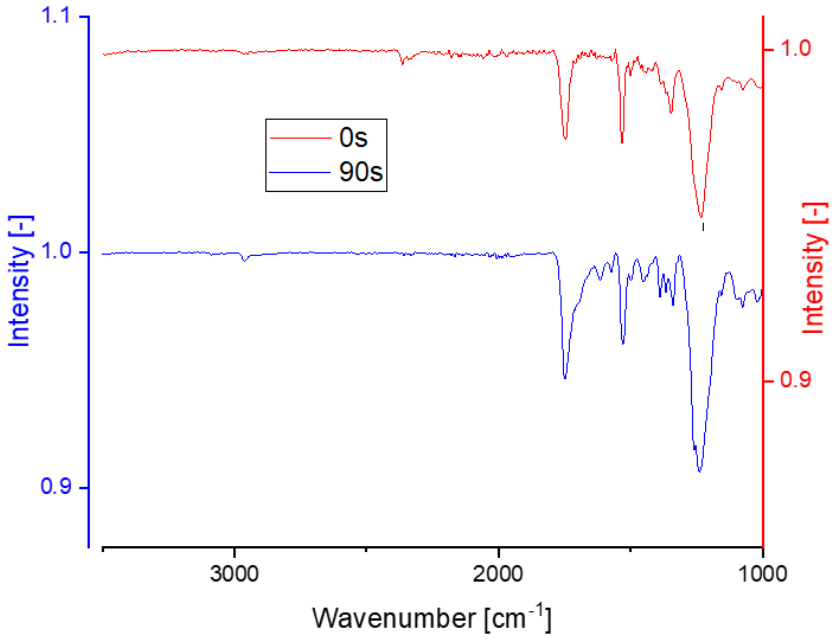

*Figure 4-26: ATR IR spectrum of a film prepared from polymer **21** before (upper) and after (lower) illumination.*

The spectrum of the non-irradiated polymer shows carbonyl bands at 1745 cm^{-1} and 1240 cm^{-1} which is in the typical region of carbonate functions. Furthermore, nitro absorptions at 1530 cm^{-1} and 1350 cm^{-1} can be observed, which is in line with the structure of polycarbonate **21**. After irradiation, the spectrum exhibits a band at 1570 cm^{-1} that is in the typical range of nitroso functions. The bands at 1695 cm^{-1}, 1390 cm^{-1}, and 1365 cm^{-1} are in the region of benzaldehyde and thus indicate the formation of the expected nitroso-benzaldehyde degradation product. Combination of

the IR results with the decrease in film thickness as observed by SPR and profilometry as well as the increase of the characteristic absorbance maximum at 310 nm confirms the successful photodegradation of films based on polymer **21**.

4.5.5. Polymer Degradation in Solution Using Higher Wavelength Light Sources

Especially for biomedical applications, the use of higher wavelength light is desirable due to lesser interaction with, e.g., the human tissue. Thus, two photon absorption induced degradation utilizing lasers of approximately twice the wavelength of the polymer λ_{max} is of high interest. It is known that the quantum yield of oNB compounds for such processes is significantly smaller compared to one photon absorption using UV light sources. Unfortunately, various results and experimental setups are reported in the literature without a clear trend.[85],[93] Nevertheless, the principle applicability should be tested by irradiation of polymer **27** in solution with a 20 mW laser at 515-525 nm. The same experimental procedure as for the UV/Vis analysis of UV light-induced degradation of the polymer in solution was used, only elongating the irradiation time to up to 48 h. The results showed a significant decrease in absorbance at 260 nm accompanied by a moderate relative increase at 305 nm indicating degradation of the polymer (*Figure 4-27*).

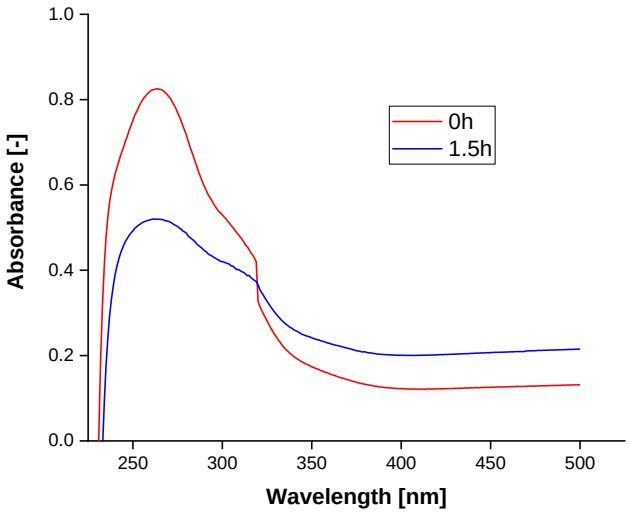

*Figure 4-27: UV/Vis results of polymer **27** before (red) and after (blue) irradiation with a laser at 515-525 nm.*

However, though the experiment was repeated several times, no clear and

reproducible results could be obtained, indicating the need for further elaboration of the experimental setup. The main problems were probably the small beam diameter in comparison to the cuvette size as well as the high volume of polymer solution needed.

4.6. Particle Formation and Degradation Analysis

4.6.1. Formation and Degradation of Polymeric Nanoparticles

Nanoparticles are a promising platform for the therapy of numerous diseases such as cancer due to, e.g., size-dependent passive targeting by the EPR effect. Thus, the applicability of backbone-degradable polymers as material for polymeric nanoparticles was tested. A nanoprecipitation method was used to prepare nanoparticles from light-responsive polymers **21** (**21-NP**) and **27** (**27-NP**) as well as redox-responsive **26** (**26-NP**). In short, the polymers were dissolved in a water miscible organic solvent and slowly added to a vigorously stirred aqueous PVA solution. After stirring overnight, the particles were purified by centrifugation, removal of the PVA solution and redispersion in water. DLS analysis of the aqueous dispersions (0.1 mg/mL) showed Z-average diameters of 184 nm for sample **21-NP**, 147 nm for sample **26-NP**, and 152 nm for sample **27-NP**. Due to comprehensive reasons the term diameter will be used for the obtained Z-average diameters. Furthermore, narrow PDIs of 0.065 for **21-NP**, 0.093 for sample **26-NP** and 0.055 for **27-NP** were achieved. At first the light-induced degradation of **21-NP** was investigated, thus one aliquot was filled into a quartz cuvette, irradiated for 300 s, 600 s as well as 900 s and subsequently analyzed by DLS (*Figure 4-28*).

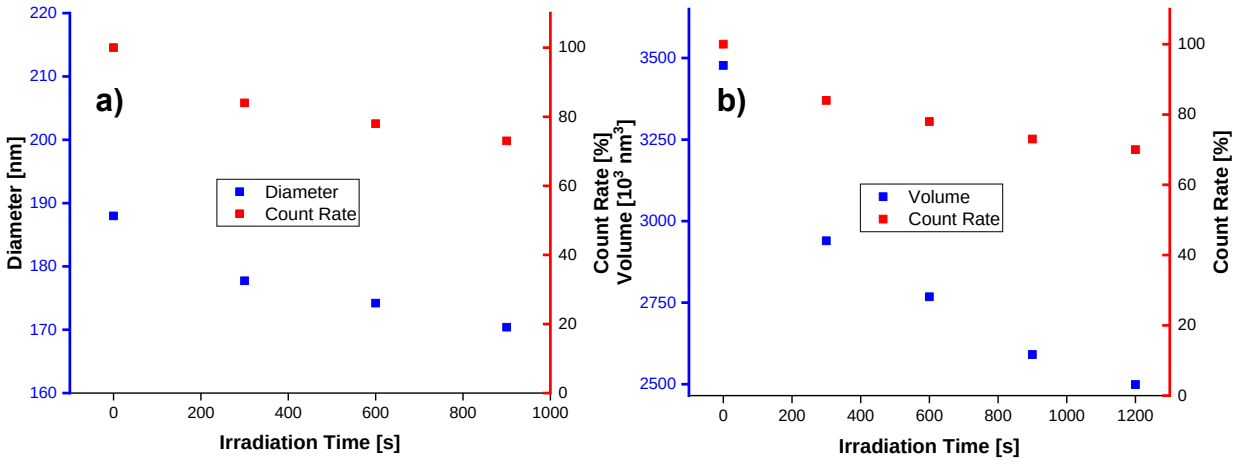

*Figure 4-28: Count rate and diameter (a) as well as count rate and volume (b) variations of **21-NP** upon irradiation with UV light for 300 s, 600 s and 900 s.*

The results revealed continuous decrease in diameter as well as count rate with a final loss of 18 nm and 30%, confirming the light-induced particle decomposition. Although both values decreased, the count rate remained relatively high, which indicates surface degradation of the particles due to the hydrophobicity of both, matrix polymer and degradation products. Based on these results, one aliquot of **27-NP** was irradiated for 900 s in the same fashion as **21-NP**. Again, a significant decrease in count rate as well as diameter was observed proving the successful particle degradation. However, the obtained values of 56% for the count rate drop and 33 nm for the decrease in diameter were considerably higher than those for **21-NP**. A reason for this could be the enhanced hydrophilicity of the lysine derivatives formed as degradation products of **27**. In addition, SEM images of both nanoparticle samples dried on a wafer were recorded before and after irradiation (*Figure 4-29*).

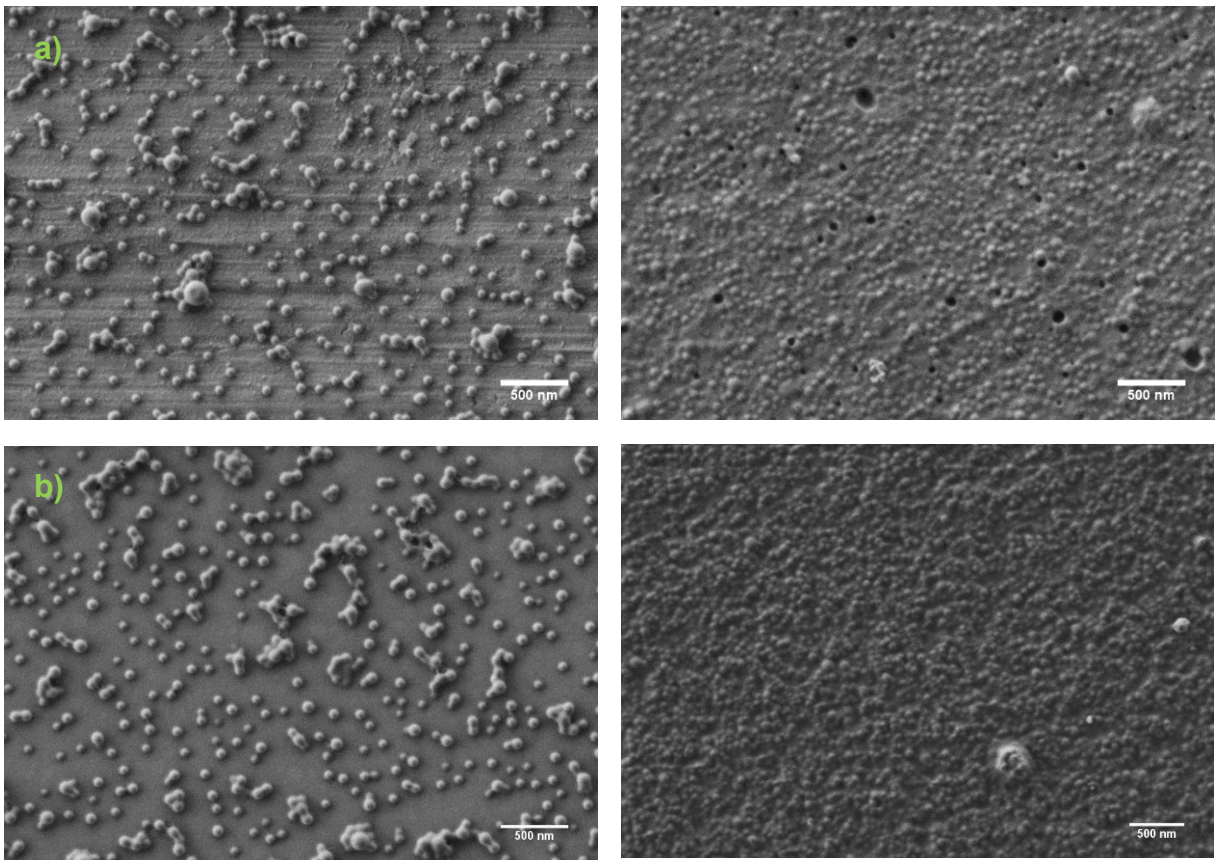

*Figure 4-29: SEM images of **21-NP** (a) and **27-NP** (b) before (left) as well as after (right) irradiation with UV light.*

While the images before irradiation clearly show quite homogeneous, spherical shaped nanoparticles for both samples, after irradiation the degradation of the particles as well as formation of a film is visible underlining the DLS results. Employing the same

method as for the blank **21-NP**, nile red loaded **21-NP** were formulated with a similar size and PDI. In hydrophobic environment, nile red shows fluorescence emission in the red wavelength area, which is quenched when encountering aqueous environment.[7] Thus, the release of nile red by degradation of hydrophobic particles in aqueous dispersion can be monitored by fluorescence intensity decrease (*Figure 4-30*).

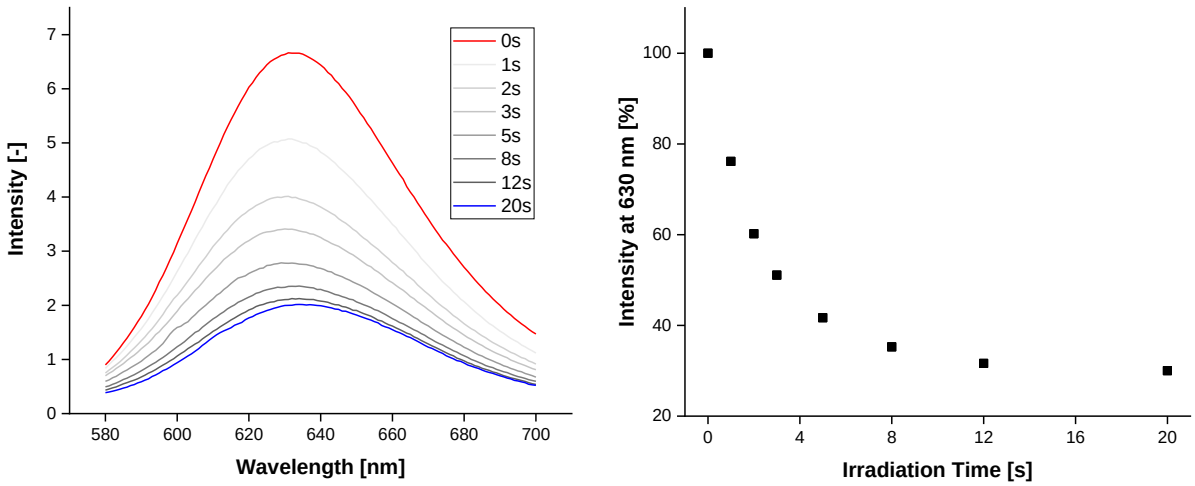

*Figure 4-30: Fluorescence spectra (left) and release kinetics (right) of nile red loaded **21-NP** upon irradiation with UV light.*

After 1 s of illumination, an intensity drop of approximately 25% was observed, indicating rapid release of the model compound nile red. After 20 s an overall intensity decrease of 70% was visible, proving an on-demand cargo release by irradiation.

In line with the SEC analysis, the redox-induced degradability of disulfide containing **26-NP** was investigated using DTT as a reducing agent. Upon addition of aqueous DTT solution to the particle dispersion, a continuous decrease in count rate was observed, proving the particle degradation (*Figure 4-31*).

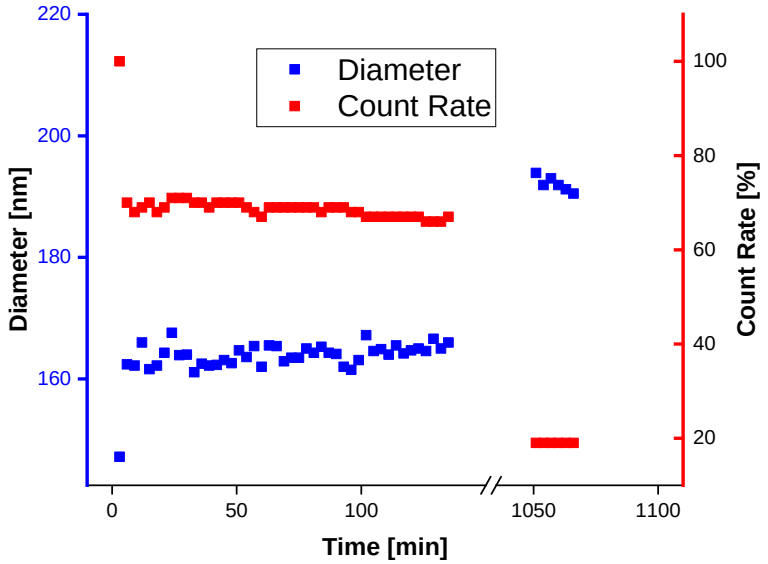

*Figure 4-31: Count rate (red) and diameter (blue) variations of **26-NP** upon DTT addition.*

Furthermore, an increase in particle diameter was visible, which is probably due to the higher hydrophilicity of the thiol degradation products compared to the corresponding disulfides. With increasing hydrophilic character water is taken up by the particles, which leads to swelling of the particle matrix.

4.6.2. Formation and Degradation of Polymeric Microparticles

In order to get a better insight into the applicability as a particulate triggered release system as well as into the degradation after processing, microparticles were formed employing a typical single emulsion solvent evaporation process.[114] Different concentrations of PVA (2.5%, 5%, and 7.5%) were used to form blank microparticles of polymer **27**. Microscopy analysis of the particles revealed spherical shape and an increasing size with decreasing PVA concentration (*Figure 4-32*). Furthermore, the size distribution of the observed particles appears to be narrower using lower PVA concentrations.

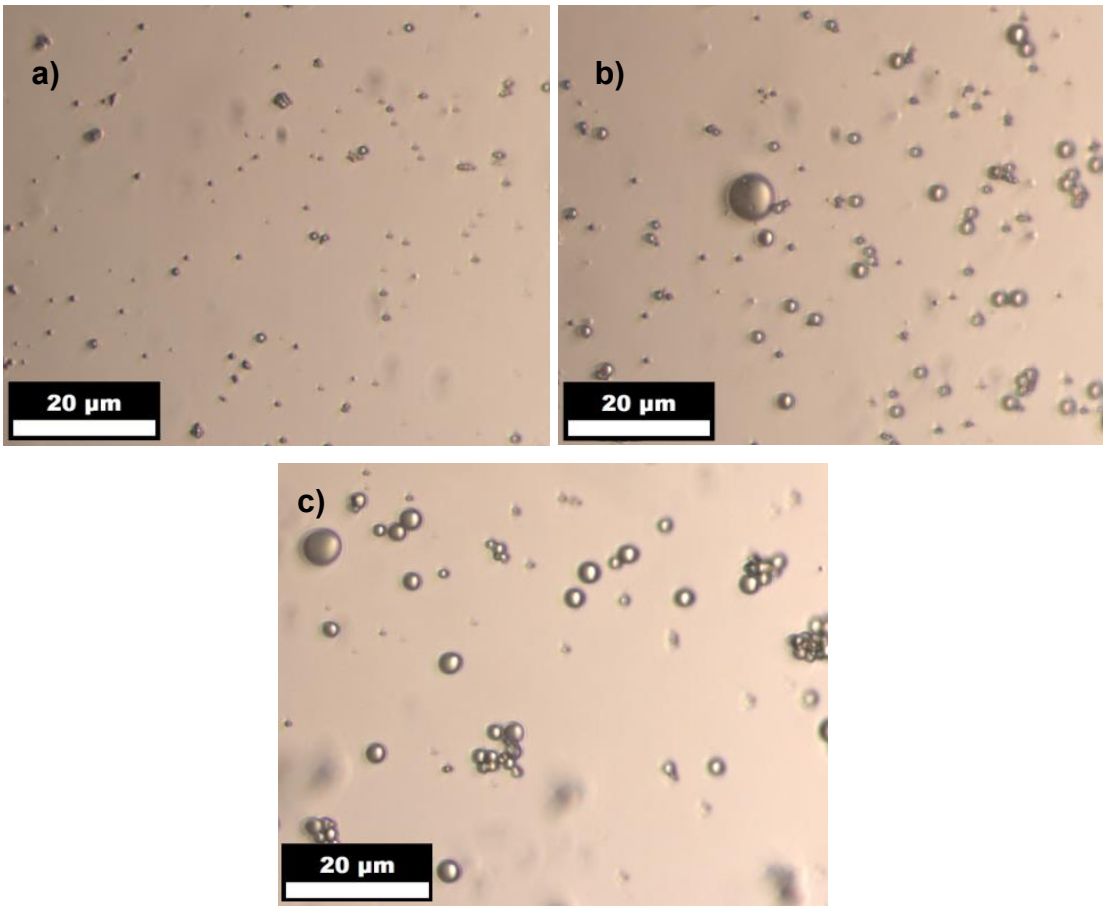

Figure 4-32: Microscopy images of blank microparticles using 7.5% PVA (a), 5% PVA (b) or 2.5% PVA (c).

Microparticles loaded with the fluorescent model compound nile red were obtained using the same method as described for the blank particles. Based on the results of the blank microparticles a PVA concentration of 2.5% was chosen in order to obtain particles in the micrometer range for this proof-of-concept test. As expected, microscopy analysis of the particles revealed spherical shape and a purple color due to the nile red fluorescence (*Figure 4-33a*).

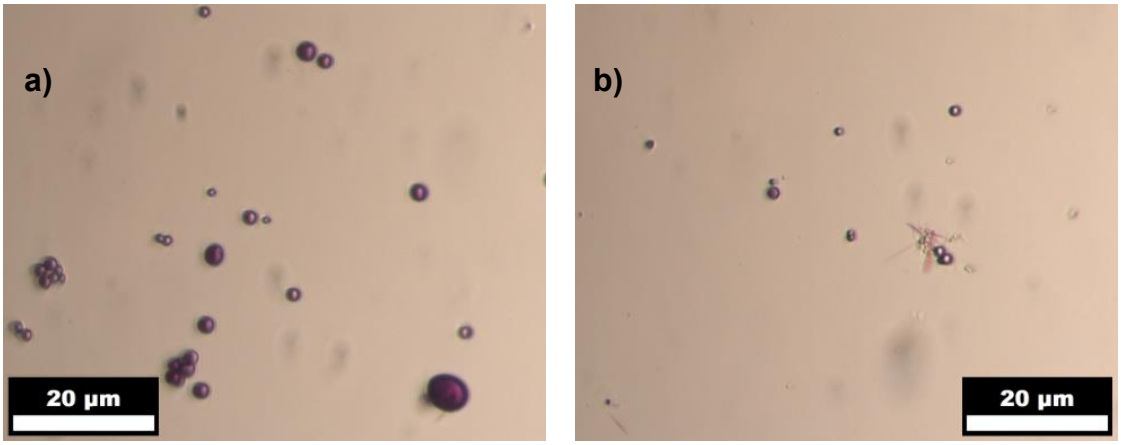

Figure 4-33: Microscopy images of nile red loaded microparticles before (a) and after (b) 1 s of irradiation.

Size and size distribution of the nile red loaded microparticles were similar to the results of the blank particles. For the degradation analysis one aliquot of the particle dispersion was filled into a quartz cuvette, irradiated for 1 s and analyzed subsequently. The analysis via microscopy showed fading of the particle color as well as an increased appearance of red needle like compounds, indicating the release of nile red (*Figure 4-33b*). Fluorescence spectroscopy measurements of the microparticles revealed a significant decrease of fluorescence intensity upon irradiation with UV light (*Figure 4-34*).

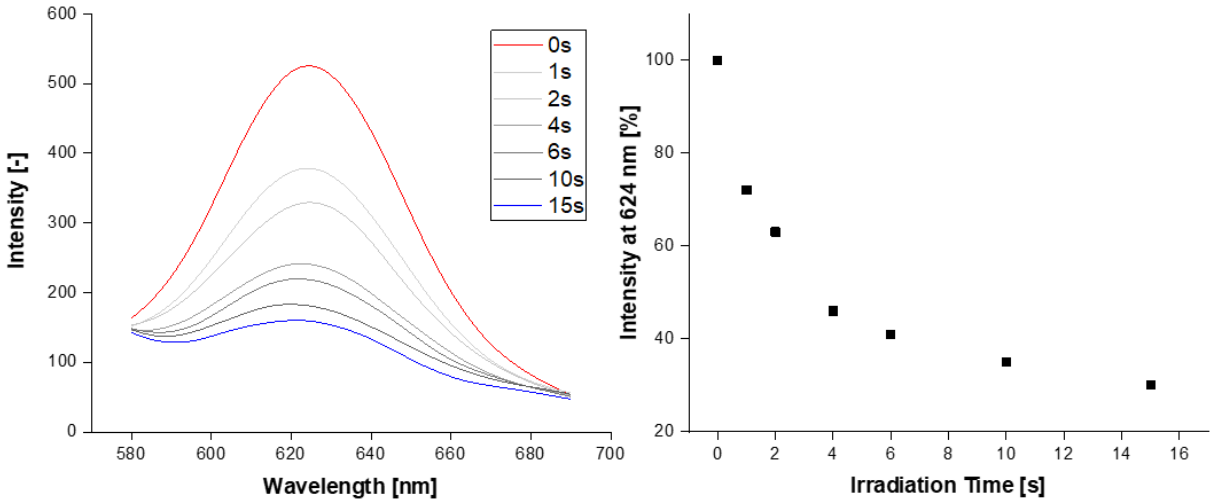

Figure 4-34: Fluorescence spectra (left) and release kinetics (right) of nile red loaded microparticles upon irradiation with UV light.

After 1 s, an intensity drop of nearly 30% could be observed, which indicates a burst

release behavior. Furthermore, after only 15 s of irradiation, 70% of the cargo was released compared to the initial fluorescence intensity. Without irradiation, no significant change of the fluorescence intensity was observed over 24 h, proving a rapid on-demand cargo release by light-triggered degradation.

4.6.3. Formation and Degradation of Polymeric Micellar Nanoparticles

Due to comprehensive reasons, in the following chapter the term micelles will be used for micellar particles or micelle-like structures, respectively. Micelles with a diameter of 54.6 nm and a PDI of 0.19, as obtained by DLS, were formed by addition of PBS (pH 7.4) to a solution of block copolymer **31b** and nile red in THF. After filtration, the clear mixture showed a deep purple color indicating the successful encapsulation of the model compound in contrast to the colorless samples prepared in the same fashion without a model cargo. To investigate the degradability of the micelles DLS, UV/Vis and fluorescence spectroscopy measurements were carried out before and after illumination. Therefore, one aliquot of the mixture was added to pH 7.4 PBS, filled into a quartz cuvette and analyzed using DLS and UV/Vis. Afterwards, the sample was irradiated with UV light for 300 s and immediately measured again under fixed attenuator and detector position. The results revealed a significant count rate decrease of 60%, while maintaining a very similar average diameter (*Figure 4-35*), proving micelle degradation upon illumination.

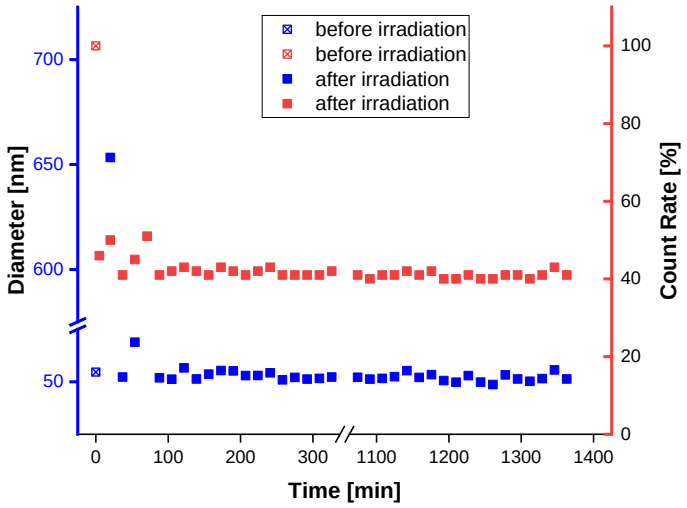

*Figure 4-35: Count rate (red) and diameter (blue) variations of aqueous micelle dispersions of **31b** upon irradiation with UV light.*

Though the diameter was mainly constant, directly after irradiation a major increase of 600 nm was observed, further highlighting the rupture of the micelles. One reason for this increase could be swelling due to higher hydrophilicity of the micelles since the degradation only affects the hydrophobic core. Another possibility is aggregation of the cleaved micelle fragments prior to the dissolution in water. However, DLS measurements apparently showed a rearrangement of the non-degraded material to form micelles of the same diameter as before irradiation and no further variations were observed afterwards. In order to investigate the release of nile red from the micelles, fluorescence spectroscopy measurements were carried out similar to the microparticles (*Figure 4-36*).

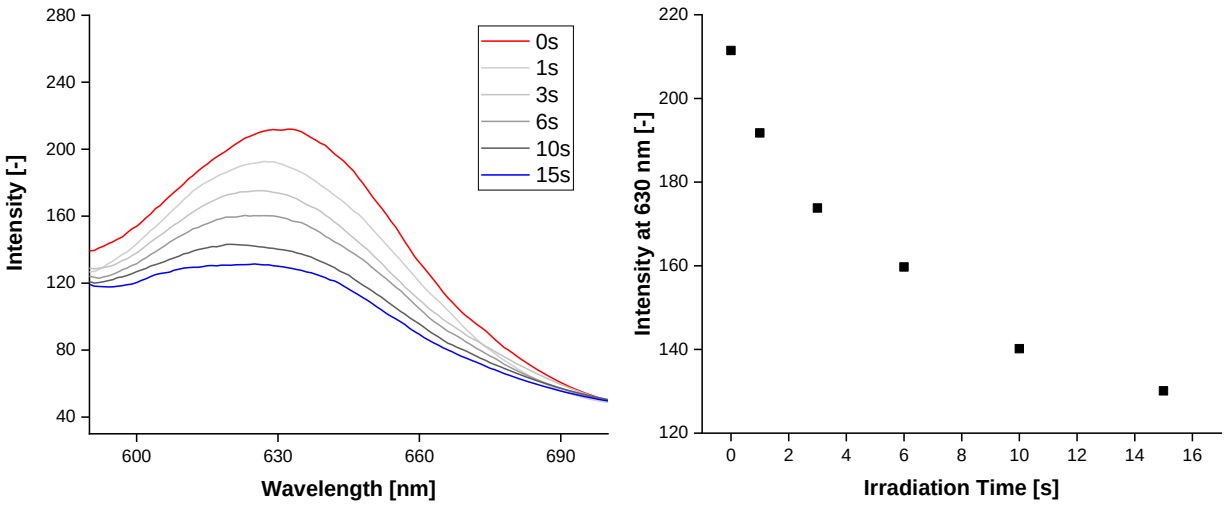

Figure 4-36: Fluorescence spectra (left) and release kinetics (right) of nile red loaded micelles upon irradiation with UV light.

Compared to the microparticles a much lower initial fluorescence intensity was observed for the micelles, which is in line with the smaller diameter. Nevertheless, light-induced release of nile red was proven by decreasing fluorescence intensity. Furthermore, the obtained kinetics were also very similar to the microparticles underlining the similarities in degradation of both polymers. Due to the low turbidity of the micelle sample, UV/Vis measurements were possible before and after irradiation (*Figure 4-37*).

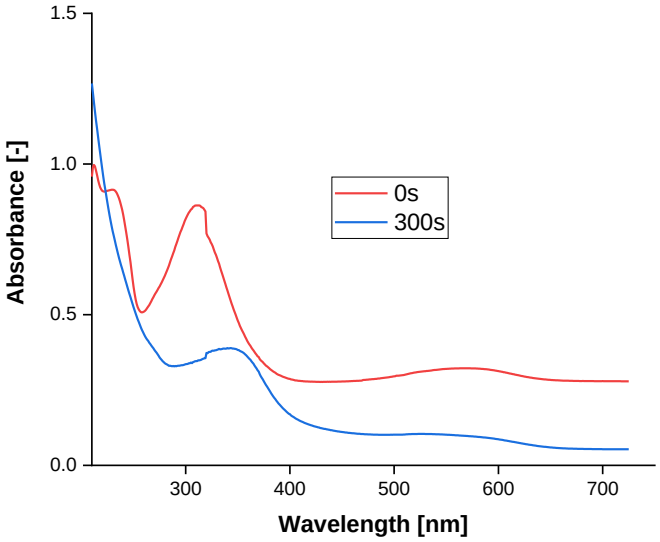

*Figure 4-37: UV/Vis measurement of micelles from polymer **31b** before (red) and after (blue) irradiation.*

The results showed the same peaks as found for the polymer in solution confirming successful degradation. In addition, the nile red absorbance peak at 580 nm as well as the overall absorbance of the sample were also clearly reduced after irradiation, which further proved the release. Using the same approach, micelles with a diameter of 68.1 nm and a PDI of 0.13 were prepared from pH- and light-degradable polymer **32b**, as observed by DLS. Upon irradiation with UV light for 300 s, a count rate decrease of approximately 30% was observed confirming the photo-induced degradation of the micelles (*Figure 4-38*).

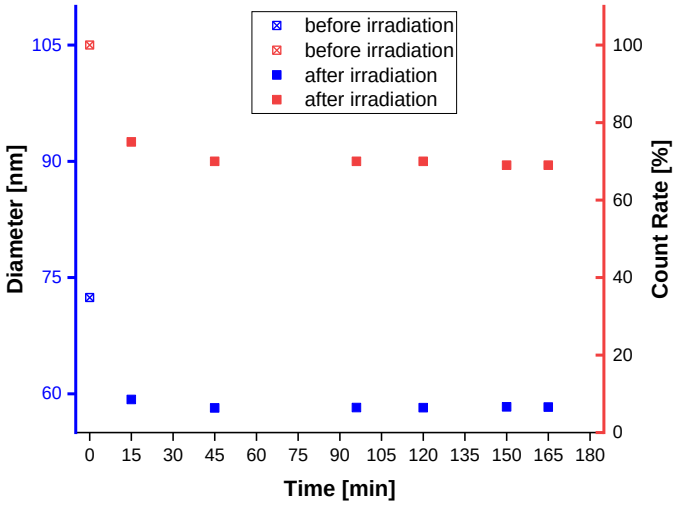

*Figure 4-38: Count rate (red) and diameter (blue) variations of aqueous micelle dispersions of **32b** upon irradiation with UV light.*

Though the count rate drop is significantly lower than observed for sample **31b**, the results also exhibit a decrease in diameter of approximately 10 nm, which further underlines the successful degradation. Interestingly, while unlike sample **31b** no initial increase in diameter was observed, the same dependency on illumination was observed, as no further changes were visible afterwards.

In addition to the light-induced degradation, the acid-induced decomposition of the micelles should be investigated. Therefore, one aliquot of the micelle mixture was added to buffered solutions at pH 7.4 and pH 5, respectively. Subsequently, DLS measurements were carried out to analyze the variation of count rate and diameter (*Figure 4-39*).

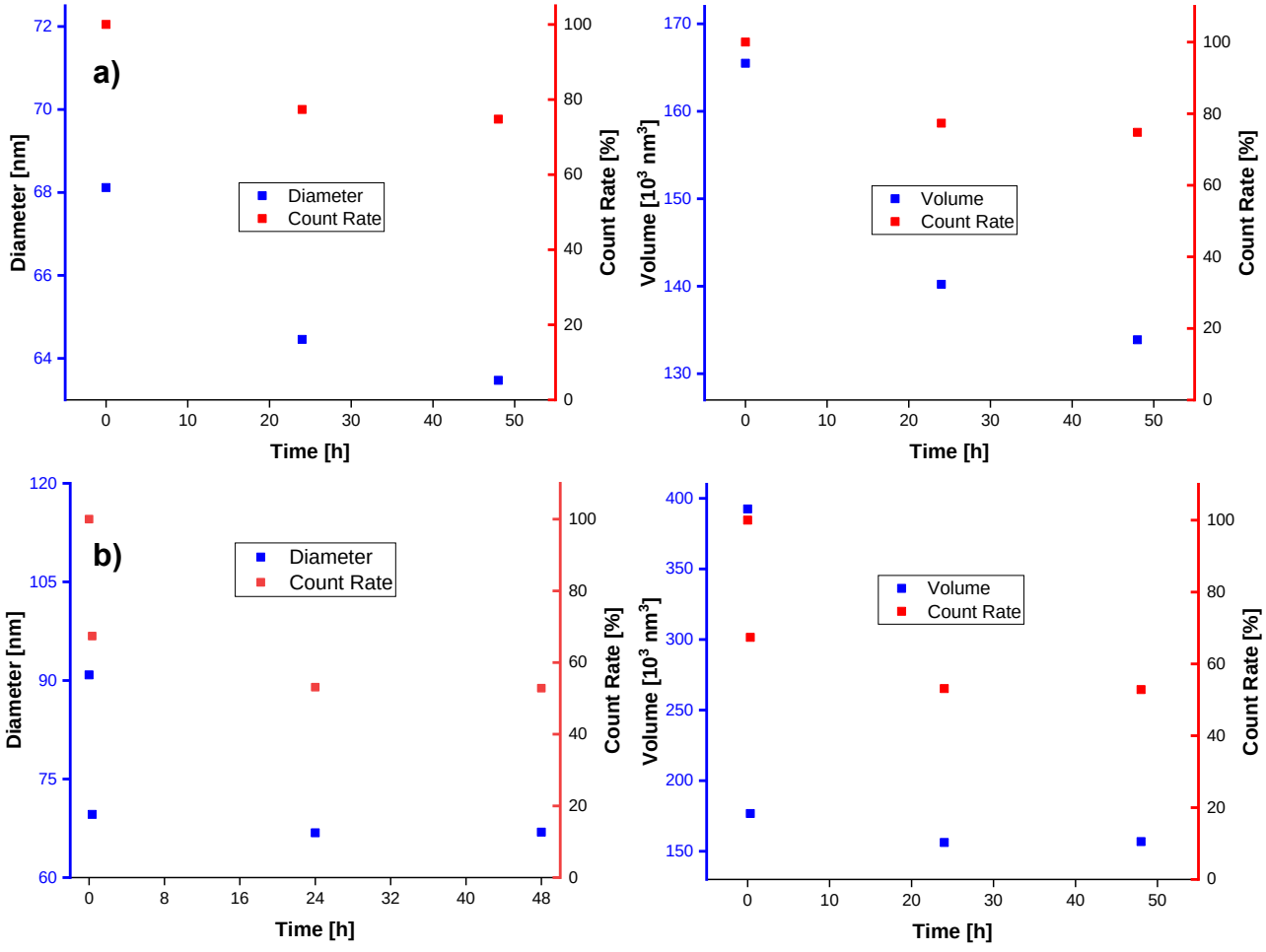

*Figure 4-39: Count rate and diameter (left) as well as count rate and volume (right) variations of aqueous micelle dispersions of **32b** in buffered solutions of pH 7.4 (a) and pH 5 (b).*

While the results showed count rate as well as diameter decrease in both, acidic and neutral media, a much stronger variation could be observed at pH 5. Furthermore, a

considerably higher diameter of approximately 90 nm was obtained in the first measurement after addition to the pH 5 buffer, accompanied by a significant drop in count rate. Since both investigated samples were prepared from the same stock mixture with micelles of a diameter of 68.1 nm, this variation implied rapid hydrolysis upon contact with moderately acidic media. However, the decomposition in neutral media limits the applicability as a triggered release system, due to cargo leakage before reaching the target site. To overcome this drawback, a lower ratio of hydrophilic/hydrophobic units could be desirable to decrease the overall interaction with water.

5. Conclusion and Outlook

Overall, several light-responsive diols with various maximum absorbance wavelengths could be successfully synthesized yielding suitable monomers for the preparation of light-responsive backbone-degradable polymers. Reproducible reaction pathways were established as a platform for the synthesis of monomers with adjusted properties, like dual-responsiveness, enabling fine-tuning of the polymers and tailoring their degradation behavior. Especially the route to monomer **13** revealed high versatility, e.g., by further modification of the aldehyde group as was shown by the acetalization employed for preparation of pH-responsive monomer **17**. Furthermore, alteration of the electrophile used for etherification of **10** appears as a facile way for future works to, e.g., introduce additional stimuli-responsiveness or enhance solubility of the polymers and their degradation products. Based on the method of Kang *et al.*,[130] tosylation of functional diols such as hydrophilic PEG400 or redox-responsive bis(2-hydroxyethyl)disulfide appears to be a promising strategy to obtain electrophiles that could be used instead of halocarbons like methyl bromoacetate. While only monomer **2** led to the formation of polycarbonates by polycondensation in the melt, polyurethanes could be obtained from all synthesized monomers by polyaddition employing suitable diisocyanates. However, it is known that monomers can degrade during the DPC-based polycondensation process due to the much higher temperatures needed compared to the mild polyaddition conditions. Besides numerous homo-polyurethanes, also light-degradable random co-polyurethanes from functional comonomers in different ratios as well as amphiphilic block co-polyurethanes from mPEG5000 were synthesized. In contrast, the formation of polyesters by polycondensation with adipoyl chloride was not successful independent of the used light-responsive monomers. Degradation analysis of the light-responsive polymers employing various methods, e.g., UV/Vis and SEC, revealed fast photoreaction as well as molar mass decrease upon illumination. Including MS measurements, multiple different approaches for the degradation characterization of polycarbonate **21** as well as model compound **20** confirmed the proposed process for backbone-degradable polymers based on primary oNB moieties. In addition, dual-responsive polymers **28** and **32** showed redox- as well as acid-induced decomposition, respectively. Nevertheless, more effort must still be invested in future works to elucidate the degradation products, and thus the process, of polymers **32** and **35**, since explicit

results could not be obtained by the used methods like MS or UV/Vis. Several of the synthesized polymers were tested on their applicability as particulate controlled release systems in proof-of-concept experiments. Therefore, blank as well as loaded micro- and nanoparticles including micelles were prepared based on different formulation platforms. While a typical nanoprecipitation method was used for the hydrophobic polymeric nanoparticles yielding diameters of 150-200 nm and low PDIs, a single emulsion solvent evaporation technique was used to obtain microparticles. In both cases, PVA was added to the aqueous phase as a stabilizing surfactant, which was not necessary for the formation of micellar nanoparticles from amphiphilic block copolymers **31** and **32**. Upon contact with the trigger, all particles revealed decomposition as well as release of the encapsulated model compound, as could be observed by DLS, fluorescence spectroscopy and microscopy. Interestingly, particles formulated from polymers that give more hydrophobic degradation products showed a significant decrease in diameter and only smaller count rate drop. Particles made from polymers that degrade into more hydrophilic compounds, on the other hand, showed a much higher count rate drop, probably due to less degraded fragments remaining in the particle matrix. Micelles based on acid-degradable block copolymer also revealed significantly enhanced degradation in mildly acidic aqueous environment. However, the system lacked specificity as hydrolysis at neutral pH could also be observed, which could be optimized in future works by varying the hydrophilic compound or block length to adjust the interaction with water. Nevertheless, the general applicability of the concept was confirmed and in particular the thorough studies on light as a trigger confirmed the dependency of triggered reaction, chain cleavage and carrier decomposition, respectively. Besides establishing the basis, several trends were identified by comparing homopolymers prepared from different light-responsive monomers as well as by incorporation of functional comonomers and their effect on polymer degradation.

6. Acknowledgment

Financial support from the Deutsche Forschungsgemeinschaft (Paderborn University: 397670170) is gratefully acknowledged.

Parts of this work have already been pre-published:

T. Rust, D. Jung, A. Hoppe, T. Schoppa, K. Langer, D. Kuckling, ACS Applied Polymer Materials (accepted)

D. Jung[a], T. Rust[a], K. Völlmecke, T. Schoppa, K. Langer, D. Kuckling, Polymer Chemistry (accepted)

[a]These authors contributed equally

7. Abbreviations

Acac	Acetylacetonate
ADP	Adipoyl chloride
ATR	Attenuated total reflection
BD	1,4-Butanediol
BHED	Bis(2-hydroxyethyl)disulfide
BHT	2,6-Di-*tert*-butyl-4-methylphenol
BPA	Bisphenol-A
Đ	Dispersity
DBuSnDL	Dibutyltin dilaurate
DCM	Dichloromethane
DDS	Drug Delivery System
DI	Diisocyanate
DLS	Dynamic light scattering
DMAP	4-Dimethylaminopyridine
DSC	Differential scanning calorimetry
DTT	Dithiothreitol
DMF	*N,N*-dimethylformamide
DMSO	Dimethyl sulfoxide
DMC	Dimethylcarbonate
DPC	Diphenylcarbonate
EPR	Enhanced permeability and retention
ESI	Electrospray Ionization
EtOAc	Ethyl acetate
EtOH	Ethanol
Et_2O	Diethyl ether
HDI	1,6-Hexamethylene diisocyanate
HFIP	Hexafluoroisopropanol
HRMS	High resolution mass spectrometry
IPDA	Isophorone diamine
IPDI	Isophorone diisocyanate
IR	Infrared
KOtBu	Potassium *tert*-butoxide

LCST	Lower critical solution temperature
LDI	L-Lysine ethyl ester diisocyanate
mCPBA	*meta*-Chloroperoxybenzoic acid
MDI	Diphenylmethane-4,4'-diisocyanate
MeCN	Acetonitrile
MeOH	Methanol
mPEG	Polyethylene glycol monomethylether
MS	Mass spectrometry
M_n	Number average molecular weight
M_w	Weight average molecular weight
NMR	Nuclear magnetic resonance
NP	Nanoparticle
oNB	*ortho*-Nitrobenzyl
p	Conversion
PC	Polycarbonate
PDT	Photodynamic therapy
PEG	Polyethylene glycol
PLGA	Polylactic-*co*-glycolic acid
PLLA	Poly(L-lactide)
PS	Polystyrene
pTSA	*para*-Toluenesulfonic acid monohydrate
PU	Polyurethane
PVA	Polyvinyl alcohol
P_n	Degree of polymerization
RI	Refractive index
ROP	Ring-opening polymerization
SEC	Size exclusion chromatography
SEM	Scanning electron microscopy
SPR	Surface plasmon resonance
t-BuOH	*tert*-Butyl alcohol
TDI	Toluenediisocyanate
TEM	Transmission electron microscopy
THF	Tetrahydrofuran
ToF	Time of flight

T_g	Glass transition temperature
T_m	Melting point
UV	Ultraviolet
UV/Vis	Wavelength range of ultraviolet/visible Light

8. References

[1] F. Huang, R. Cheng, F. Meng, C. Deng, Z. Zhong, *Biomacromolecules* **2015**, *16*, 2228.

[2] J. Li, X. Zhang, M. Zhao, L. Wu, K. Luo, Y. Pu, B. He, *Biomacromolecules* **2018**, *19*, 3140.

[3] L. I. Ronco, A. Basterretxea, D. Mantione, R. H. Aguirresarobe, R. J. Minari, L. M. Gugliotta, D. Mecerreyes, H. Sardon, *Polymer* **2017**, *122*, 117.

[4] Y. Wang, L. Zhu, Y. Wang, L. Li, Y. Lu, L. Shen, L. W. Zhang, *ACS Appl. Mater. Interfaces* **2016**, *8*, 35106.

[5] H. Sun, R. Cheng, C. Deng, F. Meng, A. A. Dias, M. Hendriks, J. Feijen, Z. Zhong, *Biomacromolecules* **2015**, *16*, 597.

[6] J. Sun, D. Jung, T. Schoppa, J. Anderski, M.-T. Picker, Y. Ren, D. Mulac, N. Stein, K. Langer, D. Kuckling, *ACS Appl. Bio Mater.* **2019**, *2*, 3038.

[7] J. Sun, T. Rust, D. Kuckling, *Macromol. Rapid Commun.* **2019**, *40*, e1900348.

[8] C. de Gracia Lux, C. L. McFearin, S. Joshi-Barr, J. Sankaranarayanan, N. Fomina, A. Almutairi, *ACS Macro Lett.* **2012**, *1*, 922.

[9] A. Herberg, X. Yu, D. Kuckling in *Smart Polymer Catalysts and Tunable Catalysis* (Eds.: S. Li, P. A. Lieberzeit, S. Piletsky, A. P. F. Turner), Elsevier, Amsterdam, Netherlands, **2019**, pp. 115–147.

[10] T. Zhang, G.-Q. Liu, W.-H. Leong, C.-F. Liu, M.-H. Kwok, T. Ngai, R.-B. Liu, Q. Li, *Nat. Commun.* **2018**, *9*, 3188.

[11]W. Li, L. Hu, J. Zhu, D. Li, Y. Luan, W. Xu, M. J. Serpe, *ACS Appl. Mater. Interfaces* **2017**, *9*, 26539.

[12] C. Xue, D. Y. Wong, A. M. Kasko, *Adv. Mater.* **2014**, *26*, 1577.

[13] A. H. Gelebart, D. J. Mulder, G. Vantomme, A. P. H. J. Schenning, D. J. Broer, *Angew. Chem. Int. Ed. Engl.* **2017**, *56*, 13436.

[14] M. Omidi, A. Yadegari, L. Tayebi, *RSC Adv.* **2017**, *7*, 10638.

[15] E. Käpylä, S. M. Delgado, A. M. Kasko, *ACS Appl. Mater. Interfaces* **2016**, *8*, 17885.

[16] M. Gisbert-Garzaran, D. Lozano, M. Vallet-Regí, M. Manzano, *RSC Adv.* **2017**, *7*, 132.

[17] J. Sun, J. Anderski, M.-T. Picker, K. Langer, D. Kuckling, *Macromol. Chem. Phys.* **2019**, *220*, 1800539.

[18] P. Wang, J. Wang, H. Tan, S. Weng, L. Cheng, Z. Zhou, S. Wen, *Biomater. Sci.* **2018**, *6*, 1262.

[19] L. Chen, Z. Xie, T. Gan, Y. Wang, G. Zhang, C. A. Mirkin, Z. Zheng, *Small* **2016**, *12*, 3400.

[20] J. P. Chesterman, F. Chen, A. J. Brissenden, B. G. Amsden, *Polym. Chem.* **2017**, *8*, 7515.

[21] A. M. Kloxin, M. W. Tibbitt, A. M. Kasko, J. A. Fairbairn, K. S. Anseth, *Adv. Mater.* **2010**, *22*, 61.

[22] M. Karimi, A. Ghasemi, P. Sahandi Zangabad, R. Rahighi, S. M. Moosavi Basri, H. Mirshekari, M. Amiri, Z. Shafaei Pishabad, A. Aslani, M. Bozorgomid et al., *Chem. Soc. Rev.* **2016**, *45*, 1457.

[23] N. Kamaly, B. Yameen, J. Wu, O. C. Farokhzad, *Chem. Rev.* **2016**, *116*, 2602.

[24] C. Benoit, S. Talitha, F. David, S. Michel, S.-J. Anna, A.-V. Rachel, W. Patrice, *Polym. Chem.* **2017**, *8*, 4512.

[25] A.-K. Müller, D. Jung, J. Sun, D. Kuckling, *Polym. Chem.* **2020**, *11*, 721.

[26] J. Sun, W. Birnbaum, J. Anderski, M.-T. Picker, D. Mulac, K. Langer, D. Kuckling, *Biomacromolecules* **2018**, *19*, 4677.

[27] L. Yang, H. Sun, Y. Liu, W. Hou, Y. Yang, R. Cai, C. Cui, P. Zhang, X. Pan, X. Li et al., *Angew. Chem. Int. Ed. Engl.* **2018**, *57*, 17048.

[28] S. Nisar, A. H. Pandit, L.-F. Wang, S. Rattan, *RSC Adv.* **2020**, *10*, 14694.

[29] R. Cheng, F. Meng, C. Deng, H.-A. Klok, Z. Zhong, *Biomaterials* **2013**, *34*, 3647.

[30] X. An, A. Zhu, H. Luo, H. Ke, H. Chen, Y. Zhao, *ACS Nano* **2016**, *10*, 5947.

[31] P. Schattling, F. D. Jochum, P. Theato, *Polym. Chem.* **2014**, *5*, 25.

[32] N. Kalva, S. Uthaman, R. Augustine, S. H. Jeon, K. M. Huh, I.-K. Park, I. Kim, *Macromol. Biosci.* **2020**, e2000118.

[33] S. Lappe, D. Mulac, K. Langer, *Int. J. Pharm.* **2017**, *517*, 338.

[34] Y. Matsumura, H. Maeda, *Cancer Res.* **1986**, *46*, 6387.

[35] E. Blanco, H. Shen, M. Ferrari, *Nat. Biotechnol.* **2015**, *33*, 941.

[36] S. Tempelaar, L. Mespouille, O. Coulembier, P. Dubois, A. P. Dove, *Chem. Soc. Rev.* **2013**, *42*, 1312.

[37] J. Sun, K. I. Aly, D. Kuckling, *J. Polym. Sci. A Polym. Chem.* **2017**, *55*, 2104.

[38] J. Liu, W. Liu, I. Weitzhandler, J. Bhattacharyya, X. Li, J. Wang, Y. Qi, S.

Bhattacharjee, A. Chilkoti, *Angew. Chem. Int. Ed. Engl.* **2015**, *54*, 1002.

[39] H. Daemi, S. Rajabi-Zeleti, H. Sardon, M. Barikani, A. Khademhosseini, H. Baharvand, *Biomaterials* **2016**, *84*, 54.

[40] S. Sartori, V. Chiono, C. Tonda-Turo, C. Mattu, C. Gianluca, *J. Mater. Chem. B* **2014**, *2*, 5128.

[41] S. Kim, S. Liu, *ACS Biomater. Sci. Eng.* **2018**, *4*, 1479.

[42] L. Zhou, L. Yu, M. Ding, J. Li, H. Tan, Z. Wang, Q. Fu, *Macromolecules* **2011**, *44*, 857.

[43] G. Becker, F. R. Wurm, *Chem. Soc. Rev.* **2018**, *47*, 7739.

[44] L. Meabe, N. Lago, L. Rubatat, C. Li, A. J. Müller, H. Sardon, M. Armand, D. Mecerreyes, *Electrochim. Acta* **2017**, *237*, 259.

[45] J. H. Park, J. Y. Jeon, J. J. Lee, Y. Jang, J. K. Varghese, B. Y. Lee, *Macromolecules* **2013**, *46*, 3301.

[46] J. Sun, D. Kuckling, *Polym. Chem.* **2016**, *7*, 1642.

[47] J. Anderski, L. Mahlert, J. Sun, W. Birnbaum, D. Mulac, S. Schreiber, F. Herrmann, D. Kuckling, K. Langer, *Int. J. Pharm.* **2019**, *557*, 182.

[48] L. Mahlert, J. Anderski, T. Schoppa, D. Mulac, J. Sun, D. Kuckling, K. Langer, *Int. J. Pharm.* **2019**, *565*, 199.

[49] S. Koltzenburg, M. Maskos, O. Nuyken, *Polymere: Synthese, Eigenschaften und Anwendungen*, Springer Berlin Heidelberg, Berlin, Heidelberg, **2014**.

[50] M. D. Lechner, K. Gehrke, E. Nordmeier, *Makromolekulare Chemie*. *Ein Lehrbuch für Chemiker, Physiker, Materialwissenschaftler und Verfahrenstechniker*, Birkhäuser, Basel, Boston, Mass., Berlin, **2010**.

[51] D. Braun, H. Cherdron, M. Rehahn, H. Ritter, B. Voit, *Polymer synthesis: theory and practice*. *Fundamentals, methods, experiments*, Springer, Berlin, Heidelberg, New York, **2005**.

[52] E. R. Baral, J. H. Lee, J. G. Kim, *J. Org. Chem.* **2018**, *83*, 11768.

[53] M. Lancaster, *Green Chemistry: An Introductory Text*, The Royal Society of Chemistry, Cambridge, **2016**.

[54] D. J. Brunelle, *Advances in Polycarbonates*, American Chemical Society, **2005**.

[55] J. T. Bendler, *Handbook of Polycarbonate Science and Technology*, Chapman and Hall/CRC, Boca Raton, **1999**.

[56] J. Xu, E. Feng, J. Song, *J. Appl. Polym. Sci.* **2014**, *131*.

[57] W. B. Kim, U. A. Joshi, J. S. Lee, *Ind. Eng. Chem. Res.* **2004**, *43*, 1897.

[58] Jyh-Ping Hsu, Jinn-Jong Wong, *Ind. Eng. Chem. Res.* **2006**, *45*, 2672.

[59] V. N. Ignatov, V. Tartari, C. Carraro, R. Pippa, G. Nadali, C. Berti, M. Fiorini, *Macromol. Chem. Phys.* **2001**, *202*, 1941.

[60] Q. Li, W. Zhu, C. Li, G. Guan, D. Zhang, Y. Xiao, L. Zheng, *J. Polym. Sci. A Polym. Chem.* **2013**, *51*, 1387.

[61] W. Zhu, X. Huang, C. Li, Y. Xiao, D. Zhang, G. Guan, *Polym. Int.* **2011**, *60*, 1060.

[62] Z. Jiang, C. Liu, W. Xie, R. A. Gross, *Macromolecules* **2007**, *40*, 7934.

[63] J. O. Akindoyo, M. D. H. Beg, S. Ghazali, M. R. Islam, N. Jeyaratnam, A. R. Yuvaraj, *RSC Adv.* **2016**, *6*, 114453.

[64] S. L. Reegen, K. C. Frisch, *J. Polym. Sci. A1.* **1970**, *8*, 2883.

[65] S.-G. Luo, H.-M. Tan, J.-G. Zhang, Y.-J. Wu, F.-K. Pei, X.-H. Meng, *J. Appl. Polym. Sci.* **1997**, *65*, 1217.

[66] H. Sugimoto, S. Inoue, *Pure Appl. Chem.* **2006**, *78*, 1823.

[67] G. Luinstra, *Polym. Rev. (Phila Pa)* **2008**, *48*, 192.

[68] D. M. D'Alessandro, B. Smit, J. R. Long, *Angew. Chem. Int. Ed. Engl.* **2010**, *49*, 6058.

[69] S. Cui, J. Borgemenke, Y. Qin, Z. Liu, Y. Li in *Advances in Bioenergy*, Elsevier, **2019**, pp. 183–208.

[70] H. Seyednejad, A. H. Ghassemi, C. F. van Nostrum, T. Vermonden, W. E. Hennink, *J. Control. Release* **2011**, *152*, 168.

[71] J. Sun, S. Fransen, X. Yu, D. Kuckling, *Polym. Chem.* **2018**, *9*, 3287.

[72] M. E. Rogers, T. E. Long (Eds.) *Synthetic methods in step-growth polymers*, Wiley, Hoboken NJ, **2003**.

[73] L. Jiang, Z. Ren, W. Zhao, W. Liu, H. Liu, C. Zhu, *R. Soc. Open Sci.* **2018**, *5*, 180536.

[74] S. Wendels, L. Avérous, *Bioact. Mater.* **2021**, *6*, 1083.

[75] M. V. de Paz, F. Zamora, B. Begines, C. Ferris, J. A. Galbis, *Biomacromolecules* **2010**, *11*, 269.

[76] M. Bil, J. Ryszkowska, P. Woźniak, K. J. Kurzydłowski, M. Lewandowska-Szumieł, *Acta Biomater.* **2010**, *6*, 2501.

[77] J. Dey, H. Xu, K. T. Nguyen, J. Yang, *J. Biomed. Mater. Res. A* **2010**, *95*, 361.

[78] A. Wang, H. Gao, Y. Sun, Y.-l. Sun, Y.-W. Yang, G. Wu, Y. Wang, Y. Fan, J.

Ma, *Int. J. Pharm.* **2013**, *441*, 30.

[79] C. Mattu, R. M. Pabari, M. Boffito, S. Sartori, G. Ciardelli, Z. Ramtoola, *Eur. J. Pharm. Biopharm.* **2013**, *85*, 463.

[80] I. Sanzari, E. Buratti, R. Huang, C. G. Tusan, F. Dinelli, N. D. Evans, T. Prodromakis, M. Bertoldo, *Sci. Rep.* **2020**, *10*, 6126.

[81] S. Mura, J. Nicolas, P. Couvreur, *Nat. Mater.* **2013**, *12*, 991.

[82] T. Schoppa, D. Jung, T. Rust, D. Mulac, D. Kuckling, K. Langer, *Int. J. Pharm.* **2021**, *597*, 120326.

[83] S. Kaur, C. Prasad, B. Balakrishnan, R. Banerjee, *Biomater. Sci.* **2015**, *3*, 955.

[84] D. Steinhilber, M. Witting, X. Zhang, M. Staegemann, F. Paulus, W. Friess, S. Küchler, R. Haag, *J. Control. Release* **2013**, *169*, 289.

[85] P. Klán, T. Šolomek, C. G. Bochet, A. Blanc, R. Givens, M. Rubina, V. Popik, A. Kostikov, J. Wirz, *Chem. Rev.* **2012**, *113*, 119.

[86] C. Englert, I. Nischang, C. Bader, P. Borchers, J. Alex, M. Pröhl, M. Hentschel, M. Hartlieb, A. Traeger, G. Pohnert et al., *Angew. Chem. Int. Ed. Engl.* **2018**, *57*, 2479.

[87] S. Barman, S. K. Mukhopadhyay, S. Biswas, S. Nandi, M. Gangopadhyay, S. Dey, A. Anoop, N. D. Pradeep Singh, *Angew. Chem. Int. Ed.* **2016**, *55*, 4194.

[88] J. H. Kaplan, B. Forbush, J. F. Hoffman, *Biochemistry* **1978**, *17*, 1929.

[89] J. W. Walker, G. P. Reid, J. A. McCray, D. R. Trentham, *J. Am. Chem. Soc.* **1988**, *110*, 7170.

[90] H. Zhao, E. S. Sterner, E. B. Coughlin, P. Theato, *Macromolecules* **2012**, *45*, 1723.

[91] T. Schmierer, S. Laimgruber, K. Haiser, K. Kiewisch, J. Neugebauer, P. Gilch, *Phys. Chem. Chem. Phys.* **2010**, *12*, 15653.

[92] E. Reichmanis, B. C. Smith, R. Gooden, *J. Polym. Sci. Polym. Chem. Ed.* **1985**, *23*, 1.

[93] M. Rumi, J. W. Perry, *Adv. Opt. Photonics* **2010**, *2*, 451.

[94] D. Klinger, K. Landfester, *Soft Matter* **2011**, *7*, 1426.

[95] N. Kongkatigumjorn, S. A. Smith, M. Chen, K. Fang, S. Yang, E. R. Gillies, A. P. R. Johnston, G. K. Such, *ACS Appl. Nano Mater.* **2018**, *1*, 3164.

[96] A. Abe, A.-C. Albertsson, H.-J. Cantow, K. Dušek, S. Edwards, H. Höcker, J.-F. Joanny, H.-H. Kausch, K.-S. Lee, J. E. McGrath et al. (Eds.) *Advances in*

Polymer Science, *Vol. 157*, Springer, Berlin, Heidelberg, **2002**.

[97] W. Gao, J. M. Chan, O. C. Farokhzad, *Mol. Pharm.* **2010**, *7*, 1913.

[98] L. Feng, Z. Dong, D. Tao, Y. Zhang, Z. Liu, *Natl. Sci. Rev.* **2018**, *5*, 269.

[99] A. A. Deschamps, D. W. Grijpma, J. Feijen, *Polymer* **2001**, *42*, 9335.

[100] J. Olejniczak, V. A. Nguyen Huu, J. Lux, M. Grossman, S. He, A. Almutairi, *Chem. Commun. (Camb)* **2015**, *51*, 16980.

[101] X. Zhang, L. Han, M. Liu, K. Wang, L. Tao, Q. Wan, Y. Wei, *Mater. Chem. Front.* **2017**, *1*, 807.

[102] S. Mollazadeh, M. Mackiewicz, M. Yazdimamaghani, *Mater. Sci. Eng. C Mater. Biol. Appl.* **2021**, *118*, 111536.

[103] P. Nagy, *Antioxid. Redox Signal.* **2013**, *18*, 1623.

[104] X. Duan, T. Bai, J. Du, J. Kong, *J. Mater. Chem. B* **2018**, *6*, 39.

[105] N. Ma, Y. Li, H. Xu, Z. Wang, X. Zhang, *J. Am. Chem. Soc.* **2010**, *132*, 442.

[106] R. Gref, A. Domb, P. Quellec, T. Blunk, R. H. Müller, J. M. Verbavatz, R. Langer, *Adv. Drug Deliv. Rev.* **1995**, *16*, 215.

[107] C. D. Ochoa, T. Stevens, *Am. J. Physiol. Lung Cell. Mol. Physiol.* **2012**, *302*, L275-86.

[108] L. K. Prasad, H. O'Mary, Z. Cui, *Nanomedicine (Lond)* **2015**, *10*, 2063.

[109] P. L. Rodriguez, T. Harada, D. A. Christian, D. A. Pantano, R. K. Tsai, D. E. Discher, *Science* **2013**, *339*, 971.

[110] C.-M. J. Hu, L. Zhang, S. Aryal, C. Cheung, R. H. Fang, L. Zhang, *Proc. Natl. Acad. Sci. U. S. A.* **2011**, *108*, 10980.

[111] K. S. Soppimath, T. M. Aminabhavi, A. R. Kulkarni, W. E. Rudzinski, *J. Control. Release* **2001**, *70*, 1.

[112] M. J. Mitchell, M. M. Billingsley, R. M. Haley, M. E. Wechsler, N. A. Peppas, R. Langer, *Nat. Rev. Drug Discov.* **2021**, *20*, 101.

[113] V. Lassalle, M. L. Ferreira, *Macromol. Biosci.* **2007**, *7*, 767.

[114] I. D. Rosca, F. Watari, M. Uo, *J. Control. Release* **2004**, *99*, 271.

[115] J.G.J.L. Lebouille, R. Stepanyan, J.J.M. Slot, M. A. Cohen Stuart, R. Tuinier, *Colloids Surf. A Physicochem. Eng. Asp.* **2014**, *460*, 225.

[116] J. Vandervoort, A. Ludwig, *Int. J. Pharm.* **2002**, *238*, 77.

[117] S. K. Sahoo, J. Panyam, S. Prabha, V. Labhasetwar, *J. Control. Release* **2002**, *82*, 105.

[118] S. Chen, X. Zhao, J. Chen, J. Chen, L. Kuznetsova, S. S. Wong, I. Ojima,

Bioconjug. Chem. **2010**, *21*, 979.

[119] J. I. Jin, Y. H. Lee, H. K. Shim, *Macromolecules* **1993**, *26*, 1805.

[120] R. Reinhard, B. F. Schmidt, *J. Org. Chem.* **1998**, *63*, 2434.

[121] K. Yamamoto, A. M. Kiyan, J. C. Bagio, K. A. B. Rossi, F. Delabio Berezuk, M. E. Berezuk, *Green Process. Synth.* **2019**, *8*, 183.

[122] D. W. van Krevelen, K. t. Nijenhuis, *Properties of polymers*. *Their correlation with chemical structure; their numerical estimation and prediction from additive group contributions*, Elsevier, Amsterdam, **2009**.

[123] B. Trathnigg, S. Feichtenhofer, M. Kollroser, *J. Chromatogr. A* **1997**, *786*, 75.

[124] Y. Mai, A. Eisenberg, *Chem. Soc. Rev.* **2012**, *41*, 5969.

[125] N. Rapoport, *Prog. Polym. Sci.* **2007**, *32*, 962.

[126] B. Neises, W. Steglich, *Angew. Chem. Int. Ed. Engl.* **1978**, *17*, 522.

[127] M. Hesse, H. Meier, B. Zeeh, *Spektroskopische Methoden in der organischen Chemie*, Thieme, Stuttgart, New York, **2005**.

[128] I. Aujard, C. Benbrahim, M. Gouget, O. Ruel, J.-B. Baudin, P. Neveu, L. Jullien, *Chemistry* **2006**, *12*, 6865.

[129] P. Sebej, T. Solomek, L.'u. Hroudná, P. Brancová, P. Klán, *J. Org. Chem.* **2009**, *74*, 8647.

[130] M. Kang, B. Moon, *Macromolecules* **2009**, *42*, 455.

Danksagung

An dieser Stelle möchte ich mich bei allen Menschen bedanken, die mich beim Erstellen dieser Arbeit unterstützt und begleitet haben.

Zunächst möchte ich mich besonders bei Prof. Dr. Dirk Kuckling bedanken, in dessen Arbeitskreis ich an zahlreichen spannenden Projekten arbeiten durfte. Vielen Dank für das Bereitstellen dieses interessanten Themas sowie die langjährige Förderung und nicht zuletzt das große Vertrauen.

Bei unserem Projektpartner Prof. Dr. Klaus Langer und seinen Mitarbeitern, insbesondere Timo Schoppa, möchte ich mich für die wertvolle Zusammenarbeit sowie die vielen spannenden Gespräche und gegenseitigen Anregungen bedanken.

Natürlich möchte ich mich auch bei der gesamten zentralen Analytik der Universität Paderborn für die unzähligen unterschiedlichen Messungen und Beratungen bedanken.

Auch bei allen Mitgliedern der Arbeitskreise von Prof. Dr. Heinz-Siegfried Kitzerow, Prof. Dr. Thomas Zentgraf, Prof. Dr. Matthias Bauer, Prof. Dr. Wolfgang Bremser und Prof. Dr. Guido Grundmeier möchte ich mich noch mal für die Möglichkeit bedanken, zahlreiche Messungen und Experimente durchgeführt haben zu können.

Mein ausdrücklicher Dank gilt natürlich auch allen Freunden, aktiven und ehemaligen Kollegen im Department Chemie, besonders den Mitgliedern der Arbeitskreise von Prof. Dr. Kuckling und Prof. Dr. Paradies für die freundliche und produktive Arbeitsatmosphäre sowie für die gegenseitige moralische Unterstützung – auch dann, wenn im Labor mal nicht alles funktioniert wie geplant. An dieser Stelle möchte ich mich auch bei meinen Abschlussstudenten bedanken, die meinen Laboralltag bereichert haben und deren Betreuung mir eine große Freude war.

Abschließend gilt mein grenzenloser Dank noch meiner Familie, meinen engen Freunden und nicht zuletzt meiner Freundin Lavinia für ihre fortwährende immense Unterstützung. Ohne diesen Rückhalt wäre diese Arbeit so nicht möglich gewesen, danke!

Eidesstattliche Erklärung

Hiermit versichere ich, Tarik Rust, die vorliegende Arbeit selbstständig, ohne Hilfe Dritter und nur mit den angegebenen Quellen sowie Hilfsmitteln angefertigt zu haben. Alle Stellen, die ganz oder in Teilen anderen Quellen entnommen wurden, sind als solche kenntlich gemacht worden. Diese Arbeit wurde weder in dieser noch in ähnlicher Form einer Prüfungsbehörde des In- oder Auslands vorgelegt.

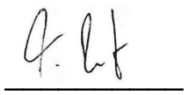

Paderborn, 16.04.2021

Tarik Rust

Anerkennung der Promotionsordnung

Hiermit erkenne ich, Tarik Rust, die Promotionsordnung der Fakultät für Naturwissenschaften der Universität Paderborn, welche am 12. November 2012 durch die Universität erlassen und zuletzt mit der Satzung vom 20. Februar 2020 geändert wurde, an. Bisher wurde weder an der Universität Paderborn noch an einer anderen Hochschule im In- oder Ausland ein Promotionsversuch unternommen.

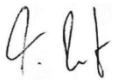

Paderborn, 16.04.2021

Tarik Rust